Department of Science

PhD Program in "BIOMEDICAL SCIENCES AND TECHNOLOGIES"

XXXI CYCLE

Smart Biomaterials for Tissue Engineering: Structural and Biological Properties

Supervisor:

Prof. Chiara Battocchio

PhD Candidate:

Valeria Secchi

Director of the Doctoral program

Prof. Paolo Visca

Riassunto
Biomateriali intelligenti per l'ingegneria tissutale: proprietà strutturali e biologiche

Il termine *"Ingegneria tissutale"* è stato definito come "*un campo multidisciplinare che applica i principi dell'ingegneria e delle scienze della vita per la realizzazione di sostituti biologici che ripristinino, mantengano o migliorino le funzioni di tessuti e organi*".
La ricerca in questo campo ha lo scopo di sviluppare nuovi biomateriali che possano essere impiantati in sostituzione di tessuti/organi danneggiati per ristabilire le loro normali funzioni. I biomateriali sono infatti definiti come dispositivi concepiti per interfacciarsi con i sistemi biologici al fine di valutare, dare supporto o sostituire un qualsiasi tessuto, organo o funzione dell'organismo.
Allo stato dell'arte le tecniche d'ingegneria tissutale permettono, attraverso l'utilizzo combinato di materiali, cellule e segnali biochimici, di produrre *in vitro* tessuti e, in prospettiva futura, permetteranno di ottenere interi organi.
Tutto ciò conferma, e avvalora, gli sforzi profusi dalla ricerca scientifica nel settore dello sviluppo di materiali "biomimetici", cioè di dispositivi che supportino informazioni biologiche specifiche e siano perciò capaci di "dialogare" con il circostante ambiente biologico. Tale capacità di dialogo deve essere espressa, in primo luogo sulla superficie del materiale, sede di una complessa sequenza di fenomeni che, nel loro insieme, possono favorire o ostacolare l'integrazione con il tessuto biologico. Ne consegue che spesso il materiale biomimetico sia in realtà un materiale "tradizionale" (ad esempio titanio), sulla cui superficie, opportunamente trattata, siano ancorate molecole dotate di attività biologica; queste ultime, una volta identificate dalle cellule mediante i recettori di membrana, inducono comportamenti specifici. Le molecole con attività biologica, oggetto delle più attuali ricerche e applicazioni, sono (o derivano da) proteine già presenti o nella matrice extra-cellulare dei tessuti o sulla membrana citoplasmatica delle cellule. Si sta facendo sempre più spesso ricorso a peptidi derivati da queste proteine poiché presentano indubbi vantaggi in termini di stabilità, facilità di reperimento e costi di ottenimento. I peptidi, essendo sequenze amminoacidiche che riproducono un frammento della proteina dalla quale provengono, esibiscono in genere un'attività biologica inferiore rispetto a quella della proteina nativa; cionondimeno, il loro impiego è preferito proprio in ragione della superiore maneggiabilità e del minore costo di produzione. Inoltre, un'altra promettente classe di

molecole utilizzate per la bioattivazione di scaffold per l'ingegneria tissutale è quella dei carboidrati, in virtù della loro biocompatibilità e del loro naturale coinvolgimento in fenomeni di adesione cellula-matrice e cellula-cellula.

In questa tesi sono stati studiati diversi tipi di biomateriali:

- Un modello costituito da una superficie metallica (Au) su cui è stato legato covalentemente un peptide auto-assemblante con un residuo di cisteina terminale.
- Biomateriali basati su titanio (o una sua lega: Ti25Nb10Zr) funzionalizzati con peptidi auto-assemblanti;
- Biomateriali basati su titanio funzionalizzati con chitosano coniugato covalentemente a peptidi auto-assemblanti;
- Un esempio di biomateriale per la medicina rigenerativa: PCL (ε-policaprolattone) funzionalizzato con maltosio.

La progettazione di qualsiasi dispositivo medico destinato al contatto, temporaneo o permanente, con i tessuti, non può prescindere dalla conoscenza dei fenomeni che hanno luogo in ambiente biologico. Sarebbe infatti rischioso esporre un paziente al contatto con un biomateriale del quale non si conoscano appieno le potenzialità e l'interazione con l'organismo: nella migliore delle ipotesi, il livello d'interazione tra il materiale e il tessuto potrebbe essere trascurabile, rendendolo non sufficientemente efficace o del tutto inutile; in altri casi, si potrebbero evocare reazioni avverse pericolose per la salute del paziente o anche solo dannose per la funzionalità del dispositivo. Da questa serie di considerazioni emerge con forza la necessità di conoscere quali siano i complessi meccanismi (fisici, chimici, biochimici) che determinano le interazioni tra biomateriali e tessuti biologici, quali le molecole coinvolte, quali i metodi per favorirle/inibirle. È noto che il livello d'interazione con i tessuti biologici di questi dispositivi sia fortemente condizionato dalle caratteristiche della superficie, non solo in termini di composizione chimica, ma anche in termini morfologici; ciò deriva dal fatto che gli eventi, numerosi e complessi, che hanno luogo all'interfaccia tra il dispositivo ed il tessuto, dipendono sia dalla natura degli atomi e delle molecole che compongono gli strati esterni del materiali, sia dall'eventuale presenza di "difetti" superficiali, dal loro numero, dalla loro estensione e dal loro grado di organizzazione. La natura chimica e fisica della superficie del biomateriale determina il

modo in cui il tessuto dell'ospite interagisce con l'impianto. Per questo motivo devono essere prese in considerazione le proprietà conformazionali, biologiche e meccaniche della superficie e devono essere approfondite le conoscenze delle interazioni chimico-fisiche tra l'ambiente biologico e il biomateriale. Di conseguenza, la caratterizzazione delle interazioni chimiche e la comprensione di come queste siano influenzate dalla natura del substrato acquisiscono grande importanza nella progettazione dei biomateriali.

Per questo motivi i biomateriali oggetto di questa tesi, sono stati caratterizzati in termini di proprietà chimico-fisiche e strutturali mediante diverse tecniche sensibili alla superficie tra cui Spettroscopia di Fotoemissione a raggi X (XPS) e la Spettroscopia di Assorbimento di raggi X vicino soglia NEXAFS.

Abstract

Smart biomaterials for tissue engineering: structural and biological properties

Tissue engineering is a multidisciplinary field involving the "*application of the principles and methods of engineering and life sciences towards the fundamental understanding of structure-function relationships in normal and pathological mammalian tissues and the development of biological substitutes that restore, maintain or improve tissue function*". Research in this field deals with the development of new biomaterials to be implanted into a human body to substitute tissues/organs in a state of deterioration, to restore or establish their normal functions. The main approach of the tissue engineering consists in producing a functional tissue starting from scaffolds: three-dimensional structures made of natural and/or artificial biomaterials and populated by cells, before or after implantation. The chemical, physical and biological properties of the scaffold have to be designed carefully. The generally followed strategy consists in mimicking characteristics and properties of the biological system to be restored or regenerated. This principle is well known as biomimetics. Apart from blood cells, most, if not all other, normal cells in human tissues are anchorage-dependent residing in a solid Extra Cellular Matrix (ECM), a complex network of proteins and polysaccharide chains that are secreted locally and assembled into an organized meshwork in close association with the surfaces of the cells that produce them. The multiple functions, the complex composition and the dynamic nature of ECM in native tissues make it difficult to mimic exactly. Therefore, contemporary concept of scaffolding in tissue engineering is to mimic the functions of native ECM, at least partially. As a result, the important roles played by scaffolds in engineered tissues, are analogous to the functions of ECM in native tissues and are associated with their architectural, biological, and mechanical features.

In this context different type of biomaterials were chemically characterized:

- A model sample made by a metal surface covalently grafted by a self-assembling peptide with a cysteine introduced as a terminal residue. This study opens wide perspectives for chemical modification of surfaces with biomolecules and the proposed functionalization scheme can be extended, with some modification, for different metals used as biomaterials;
- Titanium based biomaterial and titanium Ti25Nb10Zr Alloy biofunctionalized with a

self-assembling peptide;

- Titanium based biomaterial functionalized with chitosan conjugated self-assembling peptide;
- Polycaprolactone functionalized with maltose, with the goal to enhance the cytocompatibility of the polymeric material without altering the bulk and its mechanical properties;

The design of any biomedical device destined to a biological environment must depend on the knowledge of the phenomena that take place in the biological site after the implant's insertion. The specific nature of a biomaterial surface determines how the living tissue and organism interact with the implant and are strongly influenced by the method of surface preparation, handling and storage. During preparation of the implant, the outmost layers of the material are subjected to various chemical processes that will leave residues at the surface. The close connection between surface preparation and resulting characteristics implies that in order to manufacture implants with reproducible structured surfaces, all aspects of the production process and ensuing logistics need to be carefully controlled. For this reason the biomaterials surfaces were characterized by means of surface-sensitive spectroscopic techniques as SR-XPS (Synchrotron Radiation induced X-Ray Photoelectron Spectroscopy) and NEXAFS (Near-Edge X-Ray Absorption Fine Structure), that are very well suited to check the chemical composition of the surface and the stability of the materials.

TABLE OF CONTENTS

Chapter 1

Introduction

1. Introduction

Tissue engineering is a multidisciplinary field involving the "*application of the principles and methods of engineering and life sciences towards the fundamental understanding of structure-function relationships in normal and pathological mammalian tissues and the development of biological substitutes that restore, maintain or improve tissue function*" [1]. Research in this fields deals with the development of new biomaterials to be implanted into a human body to substitute tissues/organs in a state of deterioration, to restore or establish their normal functions. The most accepted definition of biomaterials is currently the one employed by the American National Institute of Health that describes a biomaterial as ‘‘*any substance or combination of substances, other than drugs, synthetic or natural in origin, which can be used for any period of time, which augments or replaces partially or totally any tissue, organ or function of the body, in order to maintain or improve the quality of life of the individual*’’ [2]. The main approach of the tissue engineering consists in producing a functional tissue starting from scaffolds: three-dimensional structures made of natural and/or artificial biomaterials and populated by cells, before or after implantation. The chemical, physical and biological properties of the scaffold have to be designed carefully. The strategy generally followed consists in mimicking characteristics and properties of the biological system to be restored or regenerated. This principle is well known as biomimetics [3]. Intuitively, the best scaffold for an engineered tissue should be the Extra Cellular Matrix (ECM) of the target tissue in its native state.

1.1 The extracellular matrix

Apart from blood cells, most, if not all other, normal cells in human tissues are anchorage-dependent residing in a solid ECM, a complex network of proteins and polysaccharide chains that are secreted locally and assembled into an organized meshwork in close association with the surfaces of the cells that produce them [3, 4]. The classes of macromolecules constituting the extracellular matrix in different animal tissues are broadly similar, but variations in the relative amounts of these different classes of molecules and in the ways in which they are organized give rise to an amazing diversity of materials [3]. For example the matrix can become calcified to form the rock-hard structures of bone or teeth, or it can form the transparent substance of the cornea, or it can adopt the ropelike

organization that gives tendons their tensile strength.

The extracellular matrix is composed of three major classes of macromolecules: glycosaminoglycans (*GAGs*), which are large and highly charged polysaccharides that are usually covalently linked to protein in the form of *proteoglycans*; fibrous proteins, which are primarily members of the *collagen* family; and a large class of non-collagen *glycoproteins*, which carry conventional asparagine-linked oligosaccharides. All three classes of macromolecules have many members and come in a great variety of shapes and size. Mammals are thought to have almost 300 matrix proteins, including about 36 proteoglycans, about 40 collagens, and over 200 glycoproteins, which usually contain multiple subdomains and self-associate to form multimers. Add to this the large number of matrix-associated proteins and enzymes that can modify matrix behavior by cross-linking, degradation, or other mechanisms, and one begins to see that the matrix is an almost infinitely variable material.

The proteoglycan molecules in connective tissue typically form a highly hydrated, gel-like "ground substance" in which collagens and glycoproteins are embedded. The polysaccharide gel resists compressive forces on the matrix while permitting the rapid diffusion of nutrients, metabolites, and hormones between the blood and the tissue cells. The collagen fibers strengthen and help organize the matrix, while other fibrous proteins, such as the *elastin*, give it resilience. Finally, the many matrix glycoproteins help cells migrate, settle, and differentiate in the appropriate locations.

Each tissue contains its own unique blend of matrix components, resulting in an extracellular matrix that is specialized for the needs of that tissue.

The macromolecules that constitute the ECM are mainly produced locally by cells in the matrix. These cells also help to organize the matrix: the orientation of the cytoskeleton inside the cell can control the orientation of the matrix produced outside. In most connective tissues, the matrix macromolecules are secreted by cells called *fibroblasts*. In certain specialized types of connective tissues, such as cartilage and bone, however, they are secreted by cells of the fibroblast family that have more specific names: *chondroblasts*, for example, form cartilage, and *osteoblasts* form bone.

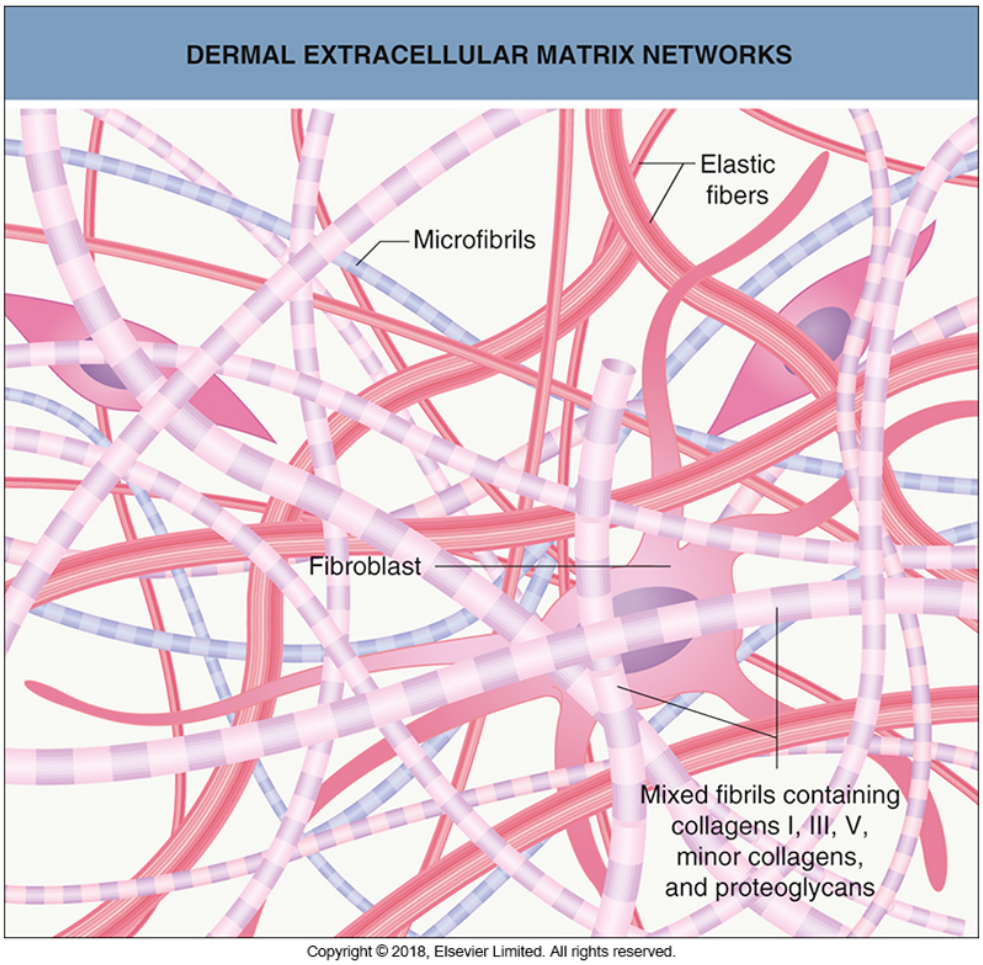

Figure 1.1.: Dermal Extracellular Matrix networks
[J. L. Bolognia et al., Dermatology: 2-Volume Set, 4th Edition, 2018]

The extracellular matrix is more than a passive scaffold able to provide physical support. It has an active and complex role in regulating the behavior of the cells that touch it, inhabit it, or crawl through its meshes, influencing their survival, development, migration, proliferation, shape, and function. The ability of cells to degrade and destroy extracellular matrix is as important as their ability to make it and bind to it. Rapid matrix degradation is required in processes such as tissue repair, and even in the seemingly static extracellular matrix of adult animals there is a slow, continuous turnover, with matrix macromolecules being degraded and resynthesized. This allows bone, for example, to be remodeled so as to adapt to changes in the stresses on it. From the point of view of individual cells, the ability to cut through matrix is crucial in two ways: it enables them to divide while embedded in matrix, and it enables them to travel through it. Cells in connective tissues generally need to

be able to stretch out in order to divide. If a cell lacks the enzymes needed to degrade the surrounding matrix, it is strongly inhibited from dividing, as well as being hindered from migrating. [4].

The numerous types of ECM in human tissues have multiple components and tissue-specific composition. The functions of ECM in tissues can be generally classified into five categories:

- ECM provides structural support and physical environment for cells residing in that tissue to attach, grow, migrate and respond to signals.
- Gives the tissue its structural and therefore mechanical properties, such as rigidity and elasticity that is associated with the tissue functions. For example, well-organized thick bundles of collagen type I in tendons are highly resistant to stretching and are responsible for the high tensile strength of them. On the other hand, randomly distributed collagen fibrils and elastin fibers of skin are responsible for its toughness and elasticity.
- It may actively provide bioactive cues to the residing cells for the regulation of their activities
- It may act as reservoir of growth factors and potentiate their bioactivities
- It provides a degradable physical environment so as to allow neovascularization and remodelling in response to developmental, physiological and pathological challenges during tissue dynamic processes namely morphogenesis, homeostasis and wound healing, respectively [3].

1.2 Scaffolds for tissue engineering

The multiple functions, the complex composition and the dynamic nature of ECM in native tissues make it difficult to mimic exactly. Therefore, contemporary concept of scaffolding in tissue engineering is to mimic the functions of native ECM, at least partially. As a result, the important roles played by scaffolds in engineered tissues, are analogous to the functions of ECM in native tissues and are associated with their architectural, biological, and mechanical features.

1. Architecture: scaffolds should be designed to have a high reproducibility and appropriate characteristics such as porosity, interconnected geometry, elasticity and chemical composition and should provide void volume for vascularization, new tissue formation and remodelling so as to facilitate host tissue integration upon implantation. The biomaterials should be processed to give a porous enough structure for efficient nutrient and metabolite transport without significantly compromising the mechanical stability of the scaffold. Moreover, the biomaterials could also be degradable upon implantation at a rate matching that of the new matrix production by the developing tissue [3].
2. Mechanical properties: scaffolds should provide mechanical and shape stability to the tissue defect. The intrinsic mechanical properties of the biomaterials used for scaffolding or their post-processing properties should match that of the host tissue. Recent studies on mechano-biology have highlighted the importance of mechanical properties of a scaffold to replace normal functions. The mechanical properties of the culturing microenvironment, and more specifically its stiffness, are known to potently regulate cells differentiation [5].

   Exerting traction forces on a substrate, many mature cell types, such as epithelial cells, fibroblasts, muscle cells, and neurons, sense the stiffness of the substrate and show dissimilar morphology and adhesive characteristics [6]. Several research groups are currently focusing their attention on the cell–material interface, with the aim of unravelling the intricate and unidentified principles that regulate cell-material crosstalk, leading to a rapid increase in the basic knowledge of the different stages and phases that occur across the cell membrane as a result of different material properties and distribution density of biological sites. Recent literature has described the phenomenon of crosstalk at the cell– material interface as being mostly influenced by the dynamics of large macromolecular complexes across the cell membrane whose formation and extension depend on material properties. Advancements in materials engineering, functionalization methods and most importantly micro- and nano-fabrication technologies provided researchers with "artificial" alternatives to conventional rigid plates or glass, which more closely mimic the native microenvironment [5].

3. Biocompatibility: a scaffold should be also developed by modulating different properties which in turn determine its biocompatibility, defined exhaustively by Williams [7] "*Biocompatibility refers to the ability of a biomaterial to perform its desired function with respect to a medical therapy, without eliciting any undesirable local or systemic effects in the recipient or beneficiary of that therapy, but generating the most appropriate beneficial cellular or tissue response in that specific situation, and optimizing the clinically relevant performance of that therapy*".
4. Bioactivity: scaffolds may interact with the cellular components of the engineered tissues actively to facilitate and regulate their activities. In this context, to improve tissue development, specific signals can be conjugated to the scaffold to bio-activate the construct. These signals can be chemical (i.e. growth factors) or mechanical (i.e. hydrostatic pressure or compressive stimulation). Moreover the chemistry used to produce biomolecule-biomaterial conjugates is an important aspect of biomaterial design and plays a key role in influencing bioactivity and construct performance. There is no single optimal method for conjugation (chemical-, enzymatic-, photo-, and noncovalent conjugations) [8] and their aim is to help processes such as cell adhesion, ECM functional distribution throughout the scaffold and cell differentiation [9]. The scaffold may also serve as a delivery vehicle or reservoir for exogenous growth-stimulating signals such as growth factors to speed up regeneration. In this regard, the biomaterials need to be compatible with the biomolecules and amenable to an encapsulation technique for controlled release of the biomolecules with retained bioactivity. For example, hydrogels synthesized by covalent or ionic crosslinking can entrap proteins and release them by a mechanism controlled by swelling of the hydrogels [10].

The bioactive material surface characteristics are strongly influenced by the method of surface preparation, handling and storage. During preparation of the implant, the outmost layers of the material are subjected to various chemical processes that will leave residues at the surface. The close connection between surface preparation and resulting characteristics implies that in order to manufacture implants with reproducible structured surfaces, all aspects of the production process and ensuing logistics need to be carefully controlled [11].

After all these considerations, the complexity of the tissue engineering approach appears evident.

1.3 Proposed biomaterials

To fabricate a scaffold, several promising candidates for biomaterials have been proposed and tested:

- Biomaterials based on titanium (or titanium alloy) are commonly and successfully used for orthopaedic and dental applications because of its good mechano-chemical properties. Commercially pure titanium is the gold standard, because it is a bioinert material that does not induce allergic reactions or hypersensitivity in surrounding tissues. When the titanium surface is exposed to air it reacts rapidly with oxygen to form a thin layer of surface oxide, usually of TiO_2. The surface oxide is chemically stable and corrosion-resistant, preventing the diffusion of environmental oxygen toward the bulk of the prosthesis [11], which makes titanium surfaces quite stable under normal physiological conditions. The surface oxide may also contain varying amounts of other intentional or non-intentional (impurity) substances [12]. However, a potential problem is the unpredictability of implant integration with the host bone, and in clinical practice the osseointegration of orthopaedic implants is often incomplete, resulting in the risk of implant loosening over time. A possible strategy to enhance the biological acceptance of orthopaedic implants and promote osseointegration is the functionalization of the titanium surface with bioactive molecules (as for example osteogenic growth factors or cell adhesion sequences), that can be grafted on the metal surface and establish a “molecular dialogue” with host's cells [13].

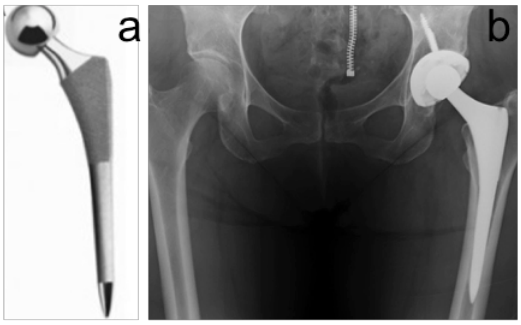

Figure 1.2.: Images of the Summit triple-tapered stem (a) Sixty-year-old female with total hip arthroplasty performed for osteoarthritis after 5 years of surgery (b)
[S.W. Carlson et al. / The Journal of Arthroplasty 31, 2016 fig. 1a, 2b]

- For bone tissue engineering, commonly used materials to fabricate a scaffold are also natural and synthetic polymers, due to their degradation properties; in some other bone applications, ceramic materials (i.e. calcium phosphate, glass ceramic, chalk calcium carbonate, coralline hydroxyapatite) are also used, especially combined with polymers as composites, due to their mechanical properties. Synthetic polymers are generally less biocompatible than the natural polymers and it is necessary to evaluate the possible toxicity of the released monomers. On the other hand they have high and tunable properties, they are easily processed and adapted and the results are usually more reproducible; For example, poly(ε-caprolactone) (PCL) is a well known biocompatible and biodegradable [14, 15] material with low cytotoxicity that is widely adopted as synthetic polymer for several medical applications [16, 17], due to its several desirable features, such as good stability under ambient conditions and ease of processability with different techniques and morphologies. However, PCL is a hydrophobic polymer, limiting its suitability for cell adhesion and growth. In order to improve hydrophilicity and cellular compatibility, PCL surface can be modified with appropriates chemical groups, biomolecules, or by physical treatments, improving hydrophilicity and/or eliciting a desired cellular response. For example several techniques can be exploited, such as laser [18] or plasma treatments [19], followed by covalent immobilization of collagen or other ECM proteins such as gelatin, and laminin [20, 21]. At the same time different bio-conjugation strategies have been developed in order to graft material surface

with a specific bioactive compound. The covalent grafting of selected (bio)molecules on PCL can be obtained by controlled polyester hydrolysis using NaOH or aminolysis, promoting the generation of specific functional groups on the scaffolds, useful for subsequent functionalization [22].

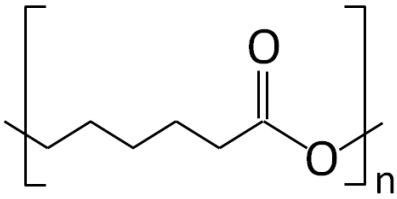

Figure 1.3.: chemical structure of poly(ε-caprolactone) (PCL)

As explained before, specific signals can be conjugated to the scaffold to bio-activate the construct in order to improve tissue development:

- Self-assembling peptides (SAPs) are an appealing class of synthetic materials suitable for this purpose, since they are capable to self-organize in nanostructures both in solution and as thin/thick films and adhere on biocompatible materials surfaces as a scaffold coating [23]. Scaffolding SAPs could be designed with the purpose to mimic the structure of the extra-cellular matrix (ECM), offering tridimensional support for cells, promoting their adhesion, proliferation and differentiation for new tissue formation [24,25].

- Natural derived polymers are obtained by extraction from living organisms and include: agarose, chitosan, collagen, glycosaminoglycans (GAGs), hyaluronic acid, silk fibroin. They possess usually a good interaction cell-material, low toxicity, low chronic inflammatory response and an ideal environment for cell growth but exhibit poor engineering properties and are characterized by certain variability. Moreover, the main problem is to understand which are the induced stimuli. In fact, cell response may not be what expected or desired.

In particular, carbohydrate backbone-based polysaccharide biomaterials have been the current research target in the field of material science and engineering. Polysaccharides constitute an important component of life matter and exhibit excellent characteristics such as bio-degradability and biocompatibility, which are the typical features of polymers application as biomaterials. The interest toward polysaccharides as biomaterials is increasing continuously during the past decade owing to their applications in pharmaceuticals, biomedical use, food supplements, and cosmetics [26].

The biomaterials proposed in this research work were functionalized with two different polysaccarides: chitosan and maltose.

- Chitosan: Chitosan, the most important derivative of chitin in term of applications, is obtained by partial deacetylation under alkaline conditions. The presence of amine groups makes chitosan cationic in nature. Chitosan has been reported to have excellent biocompatibility, biodegradability, antimicrobial activity, and wound-healing capability. Hence, it is considered as one of the potential biomaterials for regeneration of different tissues, namely, bone, cartilage, skin cardiovascular tissue [26].

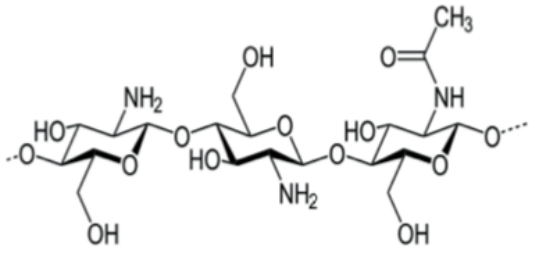

. *Figure 1.4.:chemical structure of chitosan. Chitosan is a partially and randomly de-acetylated form of chitin, constituted by N-acetylglucosamine units linked to glucosamine units*

- In the field of regenerative medicine glycans are an appealing class of bioactive molecules for the scaffold's functionalization. In particular, disaccharides have been shown to have pivotal roles in nervous system development, regeneration and synaptic plasticity. The glycoengineering of materials with functionally active glycans might add another dimension to neural tissue regeneration [27].

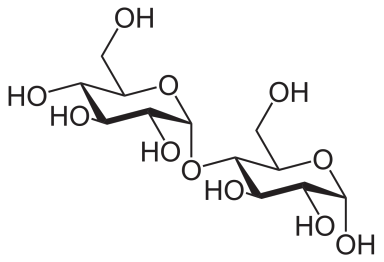

Figure 1.5.: chemical structure of maltose.

1.4 Biomaterials surface characterization

The design of any biomedical device destined to a biological environment must depend on the knowledge of the phenomena that take place in the same biological site after the implant. The specific nature of a biomaterial surface determines how the living tissue and organism interact with the implant [28]. For this reason the biomaterials surfaces were characterized by means of surface-sensitive spectroscopic techniques as SR-XPS (Synchrotron Radiation induced X-Ray Photoelectron Spectroscopy) and NEXAFS (Near-Edge X-Ray Absorption Fine Structure), that are very well suited to check the chemical composition of the surface and the stability of the materials:

1. SR-XPS measurements were performed to obtain qualitative and quantitative information about the chemical composition of the samples surface. SR-XPS was used to determine what chemical elements were present on the surface of the samples and their relative amount [29]. The main advantages of using synchrotron radiation instead of the conventional source (supplied with aluminium and magnesium anodes) are: the high

brilliance of this kind of radiation, which is orders of magnitude more intense and better collimated than the one produced by anode-based sources, allowing to detect extremely diluted atoms (as for example sulfur in peptides) and to obtain high resolution signals in very small times, avoiding sample damage; the tunability of synchrotron radiation over a wide frequency range, allowing to maximize signals arising by specific atoms; the high photon flux and the possibility of producing extremely short pulses at a frequency as high as a MHz [30]. SR-XPS measurements were performed at the Beamline "Material Science" at the Elettra Synchrotron Radiation Facility in Trieste, and at the Beamline "PM4 Low Dose PES" at the Bessy II Synchrotron Radiation Facility in Berlin; both Beamlines are ideally suited to perform measurements on biomolecules, thanks to the "low dose" of x-rays arising by the Bending Magnet devices [31].

2. NEXAFS is sensitive to fine details of the electronic structure of organic molecules and gives complementary information about the occupied and unoccupied valence states [32]. By selecting the transition energy, it is possible to focus on a specific valence orbital, projected onto a specific atom in a well- defined oxidation state. In addition, the orientation of the orbital can be determined by the polarization dependence of the transition intensity using optical-dipole selection rules [33].

Synchrotron radiation has a natural polarization that can be exploited for NEXAFS studies. The commonly studied molecular adsorbates have s and p bonds that may have a particular orientation on a surface. The angle dependence of the X-Ray absorption tracks the orientation of resonant bonds due to dipole selection rules [34].

References

[1] Shalak R., Fox C.F., Preface, in: A.R. Liss (Ed*.), Tissue Engineering* (**1988**); 22–29 New York.

[2] Bergmann C.P., Stumpf A., Biomaterials, *Dental Ceramics. Topics in Mining, Metallurgy and Materials Engineering.* Springer, Berlin, Heidelberg (**2013**);

[3] Chan B.P., Leong K.W., Scaffolding in tissue engineering: general approaches and tissue-specific considerations, *European Spine Journal* (**2008**); 4: 467–479.
DOI: 10.1007/s00586-008-0745-3

[4]Alberts B., Johnson A., Lewis J., Raff M., Roberts K., Walter P., Molecular biology of the cell, *Galrand Science* **(2014)**; 19:1035-1090.

[5] Cimmino C., Rossano L., Netti P.A., Ventre M., Spatio-Temporal Control of Cell Adhesion: Toward Programmable Platforms to Manipulate Cell Functions and Fate**,** *Frontiers in Bioengineering and Biotechnology* (**2018**); 6:190.

[6] Discher D.E., Janmey P., Wang Y.L., Tissue cells feel and respond to the stiffness of their substrate, *Science* (**2005**); 310:1139–1143.
DOI: 10.1126/science.1116995

[7] Williams D. F., On the mechanisms of biocompatibility, *Biomaterials* (**2008**); 29: 2941–53.

[8] Spicer C.D., Pashuck E.T., Stevens M.M., Achieving controlled Biomolecule-Biomaterial Conjugation, *Chemical Reviews* (**2018**); 118 (16): 7702-7743.
DOI: 10.1021/acs.chemrev.8b00253

[9] Langer R., Vacanti, J. P.,Tissue engineering, *Science* (**1993**); 260: 920–926.

[10] Berger J., Reist M., Mayer J.M., Felt O., Peppas N.A., Gurny R., Structure and interactions in covalently and ionically crosslinked chitosan hydrogels for biomedical applications, *European Journal of Pharmaceutics and Biopharm*aceutics (**2004**); 57(1):19–34.
DOI: 10.1016/S0939-6411(03)00161-9

[11] Bakacova L., Filova E., Parizek M., Ruml, T., Svorcik V., Modulation of cell adhesion, proliferation and differentiation on materials designed for body implants, *Biotechnology Advances* (**2011)**; 29: 739–767.
DOI:10.1016/j.biotechadv. 2011.06.004.

[12] Palmquist A., Omar O.M., Esposito M., Lausmaa J., Thomsen P., Titanium oral implants: surface characteristics, interface biology and clinical outcome, *Journal of the Royal Society Interface* (**2010**); 7 (5): 515–S527.

[13] Nayak S., Dey T., Naskar D., Kundu S.C., The promotion of osseointegration of titanium surfaces by coating with silk protein sericin, *Biomaterials* (**2013)**; 34:2855–2864.

[14] Chandra R:, Rustgi R., Recent advances in the synthesis, degradation and stabilization of poly (phenylene oxides), *Progress in Polymer Science,* **(1998)**; 23:1273-1335.

[15] Pena J., Corrales T., Izquierdo-Barba I., Doadrio A.L., Vallet-Regi M., Long term degradation of poly (3-caprolactone) films in biologically related fluids, Polymer Degradation and Stability **(2006);** 91:1424-1432.

[16] Lancuski A., Bossard F., Fort S., Carbohydrate-decorated PCL fibers for specific protein adhesion, *Biomacromolecules* **(2013)**; 14 (6):1877-1884.

[17] Mondal D., Griffith M., Venkatraman S.S.,Polycaprolactone-basedbiomaterials for tissue engineering and drug delivery: current scenario and challenges, *International Journal of Polymeric Materials and Polymeric Biomateraterials* **(2016);** 65:255-265.

[18] Kurella A., Dahotre N.B., Surface modification for bioimplants: the role of laser surface engineering, *Journal of Biomaterials Applications*, **(2005);** 20:5-50.

[19] Taraballi F., Zanini S., Lupo C., Panseri S., Cunha C., Riccardi C., Marcacci M., Campione M., Cipolla L., Amino and carboxyl plasma functionalization of collagen films for tissue engineering applications, *Journal of Colloid Interface Science* **(2013);** 394: 590-597.

[20] Abedalwafa M., Wang F., Wang L., Li C., Biodegradable poly-ε- caprolactone (PCL) for tissue engineering applications: a review, Review on Advanced Material Science **(2013);** 34 (2):123-140.

[21] Chen F., Lee C.N., Teoh S.H., Nanofibrous modification on ultra-thin poly (e-caprolactone) membrane via electrospinning, *Matererial Science and Engineering C* **(2007);** 325-332.

[22]Yoo H.S., Kim T.G., Park T.G., Surface-functionalized electrospun Nanofibers for tissue engineering and drug delivery, *Advanced Drug Delivery Review* **(2009);** 61 (12): 1033-1042.

[23] Zhang S., Holmes T.C., Lockshin C., Rich A., Spontaneous assembly of a self-complementary oligopeptide to form a stable macroscopic membrane, *Procedings of the National Academy of Sciences* (**1993**); 90: 3334-3338.

[24] Moscarelli P., Boraldi F., Bochicchio B., Pepe A., Salvi A.M., Quaglino D., Structural characterization and biological properties of the amyloidogenic elastin peptide $(VGGVG)_3$, *Matrix Biol.* (**2014);** 36:15–27.
DOI:10.1016/j.matbio. 2014.03.004.

[25] Dettin M., Zamuner A., Iucci G., Messina G.M.L., Battocchio C., Picariello G., Gallina G., Marletta G., Castagliuolo I., Brun P., Driving h-osteoblast adhesion and proliferation on titania: peptide hydrogels decorated with growth factors and adhesive conjugate, *Journal of Peptide Science* (**2014**); 20:585–594.
DOI:10.1002/psc. 2652.

[26] Wasupalli G. K., Verma, D., Polysaccharides as biomaterials, *Fundamental Biomaterials: Polymers* **(2018);** 37–70.
DOI: 10.1016/b978-0-08-102194-1.00003-7

[27] Russo L., Cipolla L., Glycomics: New Challenges and Opportunities in Regenerative Medicine, *Chemistry* **(2016)**; 22 (38):13380-13388.

[28] Owen, G.R., Jackson J., Chehroudi B., Burt H., Brunette D.M., A PLGA membrane controlling cell behaviour for promoting tissue regeneration**,** *Biomaterials **(2005);*** 26:7447.

[29] Swift P., Practical Surface Analysis by Auger and X-ray Photoelectron Spectroscopy, **(1983);** 201-251.

[30] Italian Society of Physics, Conference Acts: Synchrotron Radiation: Fundamentals, Methodologies and Applications, S. Mobilio and G. Vlaic eds. **(2003);** 82.

[31] Erika, G., Ruslan, O., Florian, S., Hikmet, S., Alexander, F., LowDosePES: An End-Station for Low-Dose, Angular-Resolved and Time-Resolved Photoelectron Spectroscopy at BESSY II, *Proceedings of the Scientific Opportunities with Electron Spectroscopy and RIXS, HZB/BESSY II, Berlin, Germany* **(2017)**

[32] Feyer V., Plekan O., Richter R., Coreno M., Prince K. C., Carravetta V., Photoemission and Photoabsorption Spectroscopy of Glycyl-Glycine in the Gas Phase, *Journal of Physical Chemistry* **(2009);** 113:10726–10733.

[33] Liu X., Jang C.H., Zheng F., Jürgensen A., Denlinger J.D., Dickson K.A., Raines R.T., Abbott N.L., Himpsel F.J., Characterization of protein immobilization at silver surfaces by near edge X-ray absorption fine structure spectroscopy, *Langmuir* **(2006);** 22 (18): 7719-7725..

[34] Stöhr J., NEXAFS Spectroscopy, Springer Series in Surface Sciences, R. Geomer (Ed.), Springer-Verlag (**1991**); 9.4.3

.

Chapter 2

Aims

2. Aims

The general aim of my PhD research was the study of smart biomaterials for tissue engineering applications.

Different type of biomaterials were chemically characterized:

- A model sample made by a metal surface covalently grafted by a self-assembling peptide (SAP) with a cysteine (Cys) introduced as a terminal residue. This study opens wide perspectives for chemical modification of surfaces with biomolecules and the proposed functionalization scheme can be extended, with some modification, for different metals used as biomaterials;
- Titanium based biomaterial and titanium Ti25Nb10Zr Alloy biofunctionalized with a SAP. The increase interest in commercially pure titanium and its alloys for dental and prosthesis application derives from their exceptional mechanical properties. However a potential problem is the unpredictability of implant integration with the host bone. A possible strategy to promote osteointegration is the biofunctionalization of the titanium (and of the titanium alloy) surface with SAPs.
- Titanium based biomaterial coated with chitosan covalently functionalized with SAP, with the aim to obtain a biomaterial that is at the same time: bioactive, biomimetic and able to prevent bacterial adhesion and colonization.
- Polycaprolactone (PCL) functionalized with maltose. PCL is a biocompatible material with low cytotoxicity that is widely adopted as synthetic polymer in several applications. However, it is hydrophobic, which limits its use in tissue engineering. In order to improve its hydrophilicity and cellular compatibility, PCL surface was grafted with maltose without altering the bulk and its mechanical properties;

The proposed biomaterials surfaces were characterized by means of surface-sensitive spectroscopic techniques as SR-XPS (Synchrotron Radiation induced X-Ray Photoelectron Spectroscopy) and NEXAFS (Near-Edge X-Ray Absorption Fine Structure), that are very well suited to check the chemical composition of the surface and the stability of the materials. SR-XPS measurements were performed at the Beamline "Material Science" at the Elettra Synchrotron Radiation Facility in Trieste, and at the Beamline "PM4 Low Dose PES" at the Bessy II Synchrotron Radiation Facility in Berlin; NEXAFS measurements were performed at the Beamline "BEAR" at the Elettra Synchrotron Radiation Facility in Trieste.

Chapter 3

Self-Assembling Behavior of Cysteine-Modified Oligopeptides: An XPS and NEXAFS Study

V. Secchi,[a] S. Franchi,[b] M. Santi,[a] M. Dettin,[c] A. Zamuner,[c] G. Iucci,[a] C. Battocchio[a]

[a] Department of Science, Roma Tre University of Rome, Via della Vasca Navale 79, 00146 Rome, Italy

[b]Elettra-Sincrotrone Trieste S.c.p.A., Strada statale 14, km 163.5, Basovizza, Trieste 34149, Italy

[c] Department of Industrial Engineering, University of Padua, Via Marzolo, 9, Padua 35131, Italy

J. Phys. Chem. C 2018, 122, 6236−6239

DOI: 10.1021/acs.jpcc.8b0079

3. Self-Assembling Behavior of Cysteine-Modified Oligopeptides: An XPS and NEXAFS Study

Achieving rigorous control over the procedures aiming at modifying surfaces by selective and covalent anchoring of bioactive molecules is a mandatory step in view of the realistic applicability of bioengineered materials in the fields of tissue engineering and nanomedicine. From the point of view of the chemical synthesis, covalent linkage of the active biomolecule on a material surface should allow obtaining bioactive materials by exposing a stable surface to the aqueous medium, thanks to the strong chemical bond at the biomolecule/biomaterial interface. Among others, self-assembling peptides (SAPs) are an appealing class of biomolecules for this purpose because of their ability to organize in nanostructures both in solution and as thin/thick films on biocompatible material surfaces as well as to give rise to porous gels. In this context, one of the aim of my PhD project was to design and test innovative but simple chemical strategies to efficiently modify surfaces by exploiting minor modifications in the bioactive molecule functionalities, as for example, introducing cysteine (Cys) as a terminal residue in SAPs. The Cys thiol functional group is able to covalently graft metal surfaces, inducing the formation of a stable and well-organized coverage on the metal substrate, as extensively investigated for small molecule self-assembled monolayers (SAMs) in the literature. Here, the specific objective was to demonstrate that a Cys residue positioned in the end of a SAP chain is able to grant the formation of a stable and well-organized layer of bioactive molecules on a metal surface, preserving at the same time the ability of the SAP to self-assemble in antiparallel β-sheet structures. The effectiveness of the surface functionalization in a monolayer regime and the molecular stability of SAP-Cys were probed by X-ray photoelectron spectroscopy; the highly ordered self-organization attained by the grafting molecules was assessed by means of angular-dependent near edge X- ray absorption spectroscopy studies. This study opens wide perspectives for efficient chemical modification of surfaces with biomolecules to include bioactive motifs and/or to add nanometric fibrous patterns.

THE JOURNAL OF PHYSICAL CHEMISTRY C

Article

Cite This: J. Phys. Chem. C 2018, 122, 6236−6239

pubs.acs.org/JPCC

Self-Assembling Behavior of Cysteine-Modified Oligopeptides: An XPS and NEXAFS Study

Valeria Secchi,[†] Stefano Franchi,[‡] Marta Santi,[†] Monica Dettin,[§] Annj Zamuner,[§] Giovanna Iucci,[†] and Chiara Battocchio[†,*]

[†]Department of Science, Roma Tre University of Rome, Via della Vasca Navale 79, 00146 Rome, Italy

[‡]Elettra-Sincrotrone Trieste S.c.p.A., Strada statale 14, km 163.5, Basovizza, Trieste 34149, Italy

[§]Department of Industrial Engineering, University of Padua, Via Marzolo, 9, Padua 35131, Italy

Supporting Information

ABSTRACT: Achieving rigorous control over the procedures aiming at modifying surfaces by selective and covalent anchoring of bioactive molecules is a mandatory step in view of the realistic applicability of bioengineered materials in the field of tissue engineering, biosensing, and nanomedicine. In this context, we report here a proof-of-concept study carried out on a self-assembling peptide (SAP) functionalized with cysteine (Cys), as to ideally grant molecule grafting to gold surfaces. The effectiveness of the surface functionalization in a monolayer regime and the molecular stability of SAP-Cys were probed by X-ray photoelectron spectroscopy; the highly ordered self-organization attained by the grafting molecules was assessed by means of angular-dependent near edge X-ray absorption spectroscopy studies. This study opens wide perspectives for efficient chemical modification of surfaces with biomolecules to include bioactive motifs and/or to add nanometric fibrous patterns.

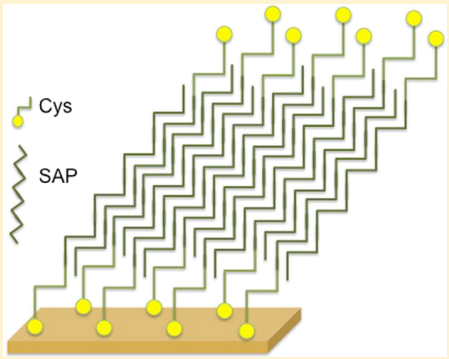

INTRODUCTION

In the framework of biosensing and nanomedicine, there is a great need for bioactive materials of proved chemical stability in aqueous medium. For this reason, chemical strategies that allow functionalizing a biocompatible material surface with appropriate biomolecules are eliciting great interest in the scientific community.[1] From the point of view of the chemical synthesis, covalent linkage of the active biomolecule on a material surface should allow obtaining bioactive materials by exposing a stable surface to the aqueous medium, thanks to the strong chemical bond at the biomolecule/biomaterial interface. Among others, self-assembling peptides (SAPs) are an appealing class of biomolecules for this purpose because of their ability to organize in nanostructures both in solution and as thin/thick films on biocompatible material surfaces[2−4] as well as to give rise to porous gels.

In this context, the general aim of our project is to design and test innovative but simple chemical strategies to efficiently modify surfaces by exploiting minor modifications in the bioactive molecule functionalities, as for example, introducing cysteine (Cys) as a terminal residue in SAPs. The Cys thiol functional group is able to covalently graft metal surfaces, inducing the formation of a stable and well-organized coverage on the metal substrate, as extensively investigated for small molecule self-assembled monolayers (SAMs) in the literature. Here, our specific objective is to demonstrate that a Cys residue positioned in the end of a SAP chain is able to grant the formation of a stable and well-organized layer of bioactive molecules on a metal surface, preserving at the same time the ability of the SAP to self-assemble in antiparallel β-sheet structures. The effectiveness of the surface functionalization in the monolayer regime and the molecular stability of the SAP-Cys were probed by X-ray photoelectron spectroscopy (XPS); the highly ordered molecular organization attained by the SAP monolayer was investigated by means of angular-dependent near edge X-ray absorption fine structure (AD-NEXAFS) spectroscopy studies. The complementary information acquired by XPS and AD-NEXAFS allowed assessing the formation of a highly ordered molecular layer on the gold surface.

Proper surface orientation of a ligand on a gold surface results in increased antigen detection fundamental in immunosensor design and could represent an advantage in the formulation of gold nanoparticles for biosensing and nanomedicine. Even in the case of SAPs without a bioactive motif (e.g., Arginylglycylaspartic acid (RGD)), the nanofibrous structure of SAPs anchored to the surface can modulate the interaction with molecules and cells. In addition, in the light of interesting properties of the functionalized surface, the functionalization scheme involving the Cys side chain and the Au surface can be extended, with some modification, for different metals used as biomaterials.

Received: January 23, 2018
Revised: February 21, 2018
Published: February 23, 2018

DOI: 10.1021/acs.jpcc.8b00794
J. Phys. Chem. C 2018, 122, 6236−6239

EXPERIMENTAL METHODS

Sample Preparation. The peptide CysEAK (sequence: H-Cys-Ala-Glu-Ala-Glu-Ala-Lys-Ala-Lys-Ala-Glu-Ala-Glu-Ala-Lys-Ala-Lys-OH) was synthesized on a MBHA Rink amide resin using Fmoc chemistry by a Syro I synthesizer (Multisyntech, Witten, Germany). The side-chain protecting groups were OtBu, Glu; Boc, Lys and Acm, and Cys. After Fmoc-deprotection of the last inserted amino acid, the peptide was cleaved from the solid support with the contemporary side-chain deprotection except Acm [95% trifluoroacetic acid, 2.5% H_2O, and 2.5% triethylsilane (v/v/v) for 1, 5 h at room temperature]. The crude peptide was purified by reversed-phase (RP)-chromatography and characterized by matrix-assisted laser desorption ionization mass spectrometry and analytical RP-high-performance liquid chromatography. Finally, the Acm group was removed, and the final product was purified and characterized by mass spectrometry.

Each gold surface was covered with 1 mM peptide solution in Milli-Q water overnight and then washed twice with Milli-Q water.

XPS experiments were carried out at the Surface Physics and Chemistry Laboratory at the University of Linköping, Sweden, using a Scienta ESCA 200 spectrometer in ultrahigh vacuum (UHV) with a base pressure of 1×10^{-10} mbar. The measurement chamber was equipped with a monochromatic Al Kα X-ray source providing photons with energy of 1486.6 eV.

Synchrotron radiation (SR)-induced XPS measurements were performed at the materials science beamline (MSB) at the Elettra synchrotron radiation source (Trieste, Italy). MSB, placed at the left end of the bending magnet 6.1, is equipped with a plane grating monochromator that provides light in the energy range of 21−1000 eV. The UHV endstation, with a base pressure of 1×10^{-8} Pa, is equipped with a SPECS PHOIBOS 150 hemispherical electron analyzer, low-energy electron diffraction optics, a dual-anode Mg/Al X-ray source, an ion gun, and a sample manipulator with a K-type thermocouple attached to the rear side of the sample. Photoelectrons emitted by C 1s, S 2p, Au 4f, and N 1s core levels were detected at normal emission geometry, with an energy step of 0.05 eV and a pass energy of 20 eV, using photon energy of 370 and 586 eV, respectively. Binding energies (BEs) are reported after correction for charging using the aliphatic C 1s as a reference (BE 285.0 eV). Core level spectra were fitted with a Shirley background and Gaussian peak functions.

NEXAFS spectroscopy experiments were performed at the Elettra storage ring at the BEAR (bending magnet for emission absorption and reflectivity) beamline, installed at the left exit of the 8.1 bending magnet. The apparatus is based on a bending magnet as a source, a beamline optics delivering photons from 5 eV up to about 1600 eV with a selectable degree of ellipticity. The nitrogen K-edge spectra were collected at normal (90°), magic (54.7, and grazing (20°) incidence angles of the linearly polarized photon beam with respect to the sample surface. The photon energy and resolution were calibrated and experimentally tested at the K absorption edges of Ar, N_2, and Ne. The spectra were then normalized by subtracting a straight line that fits the part of the spectrum below the edge and assessing to 1 the value at 420.00 eV.

IRRAS (infrared reflection−absorption spectroscopy) measurements were performed by means of a VECTOR 22 (Bruker) FT-IR interferometer equipped with a DTGS detector and with a Specac P/N 19650 series monolayer/grazing angle accessory.

RESULTS AND DISCUSSION

SAP-Cys SAM was obtained by overnight incubation of Au surfaces with 1 mM Cys-EAK aqueous solution, prepared as described in the Experimental Methods section. XPS data analysis was performed at C 1s, O 1s, N 1s, Au 4f, and S 2p core levels, with the aim to ascertain the molecular stability upon anchoring to the gold surface. C 1s, O 1s, and N 1s spectra are reported in the Supporting Information, together with the relevant data analysis results (Figure S1 and Table S1). Briefly, the C1 signal can be resolved by the curve fitting analysis into three components corresponding, respectively, to aliphatic C−C carbons (BE = 285.0 eV), to C−N carbons of the peptide backbone and of the lysine pending groups (BE = 286.6 eV), and to N−C═O peptidic carbons and O−C═O of glutamic acid pending groups (BE = 288.5 eV); N 1s spectrum shows two peaks corresponding to peptidic nitrogen (BE = 400.3 eV) and protonated nitrogens of the lysine pending groups (BE = 402.4 eV) (this BE value is slightly higher than expected from the literature, probably due to the low intensity of the monolayer (ML) spectra, leading to noisy signals, as observable in Figure S1); O 1s spectrum shows two peaks corresponding to organic oxygen (i.e., oxygen atoms belonging to organic molecules, e.g., the peptide) (BE = 533.67 eV) and physisorbed H_2O (BE = 535.34 eV). All these signals are in excellent agreement with the literature data collected on EAK and EAK-like SAPs,[5−7] confirming the successfulness of the adhesion procedure and the overall molecular stability.

XPS data analysis allows for estimating the film thickness. For an overlayer adsorbed onto a substrate, this feature can be estimated by evaluating the attenuation of the substrate signal according to the equation $I = I_0 \exp(-d/\lambda_{Au})$, where I is the intensity of the substrate signal in the presence of the overlayer, I_0 is the intensity of the same signal for the clean surface, d is the overlayer thickness, and λ_{Au} is the inelastic mean free path for gold. λ_{Au} is correlated with the kinetic energy of the photoemitted electron by the equation $\lambda_{Au} = B(KE)^{1/2}$, where B = 0.087 nm$(eV)^{1/2}$ for organic materials.[8] Within the limits of the method and the use of a B factor that is not specifically appropriate, the estimated thickness value is 4.45 nm.

S 2p core level is the most interesting for investigating the interface interaction occurring between the EAK-Cys peptide and the polycrystalline gold surface. In Figure 1, the S 2p core level spectra collected with conventional Mg Kα X-ray source (photon energy = 1253.4 eV) (a) and SR (photon energy = 370 eV) (b) are reported. S 2p XPS data analysis results are summarized in Table 1. It is noteworthy that SR, allowing for choosing a less energetic photon, is here more surface-sensitive than conventional Mg Kα radiation.[8] Both spectra reported in Figure 1 show several spin−orbit pairs (as expected for 2p photoelectrons), four for the "surface-sensitive" SR-induced measurement and three for the "bulk-sensitive" measurement performed with Mg Kα radiation, that are indicative of sulfur atoms in different functional groups. The two signals at lower BE values (S $2p_{3/2}$ components at about 161.3 and 162.3 eV) are attributed to sulfur atoms of Cys covalently bonded to metals in a monolayer or sub-monolayer regime, with the S atom in two different hybridizations: sp (lower BE signal) and sp^3.[9] In detail, the low BE signal (S $2p_{3/2}$ BE = 161.3 eV) is reported in the literature as occurring characteristically in SAMs of extremely low degree of coverage[10,11] and attributed to S

DOI: 10.1021/acs.jpcc.8b00794
J. Phys. Chem. C 2018, 122, 6236−6239

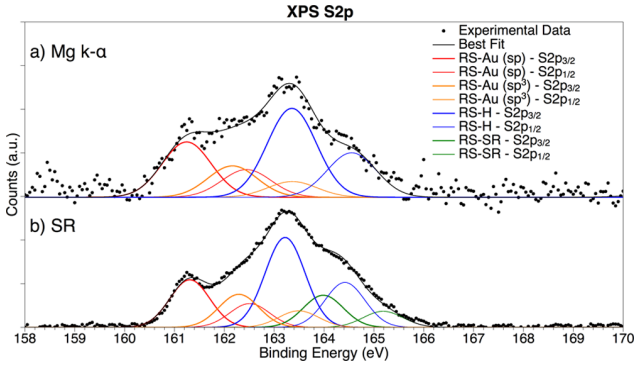

Figure 1. S 2p core level spectra of EAK-Cys as measured with (a) a conventional Mg Kα source (more bulk-sensitive) and (b) SR-induced XPS (more surface-sensitive). The red and orange spectral components are associated with sulfur atoms chemically bonded to Au atoms on the substrate surface, and the blue and green peaks are, respectively, indicative of free −SH terminal groups of cysteine moieties and disulphides at the film surface.

Table 1. S 2p core Level XPS Data, Collected at Different Sampling Depths

sampling depth	BE (eV)	fwhm (eV)	assignments	atomic %[a]
Bulk-sensitive (Mg Kα; $h\nu$ = 1253.4 eV)	161.24	1.16	R−S−Au S $2p_{3/2}$ (sp)	49%
	162.16	1.16	R−S−Au S $2p_{3/2}$ (sp^3)	
	163.35	1.16	R−SH S $2p_{3/2}$	51%
surface-sensitive (SR-XPS; $h\nu$ = 370 eV)	161.30	0.94	R−S−Au S $2p_{3/2}$ (sp)	40%
	162.29	0.94	R−S−Au S $2p_{3/2}$ (sp^3)	
	163.22	0.94	R−SH S $2p_{3/2}$	60%
	163.98	0.94	R−S−S−R or partially oxidized S S $2p_{3/2}$	

[a]The statistic error in semiquantitative XPS analysis is about 5% of the estimated value.[8]

atoms covalently bonded to the metal surface in sp hybridization; on the other hand, the S 2p component at higher BE values (S $2p_{3/2}$ peak found at 162.3 eV BE) is usually associated with sp^3-hybridized S atoms covalently grafting a metal surface.[12] The spin−orbit pair at a higher BE (S $2p_{3/2}$ component at about 163.3 eV) is due to free thiol moieties of Cys.[10,13] The fourth signal, observable in the "surface-sensitive" spectrum only (Figure 1b, green curves) can be associated with a small amount of thiol end groups of Cys giving rise to disulphides (S $2p_{3/2}$ BE = 164.0 eV[14]).

Interestingly, on reducing the sampling depth (i.e., using the lower photon energy allowed from SR, Figure 1b), the intensity of the signal related to thiol moieties that are not chemically bonded to gold atoms increases. Actually, S 2p XPS data suggest that a quote of the Cys amino acids at the end of the EAK chains are not bonded to the gold surface, and looking at the trend observed for the signal intensity and sample depth, such end groups should point out from the thin film surface. A semiquantitative evaluation of this trend is reported in Table 1.

AD-NEXAFS allowed for investigating the molecular orientation of EAK-Cys on the gold surface. N K-edge spectrum collected at normal (90°) and grazing (20°) incidence angles of the impinging radiation on the sample surface is reported in Figure 2, together with the difference signal grazing−normal. The reported spectra evidence a

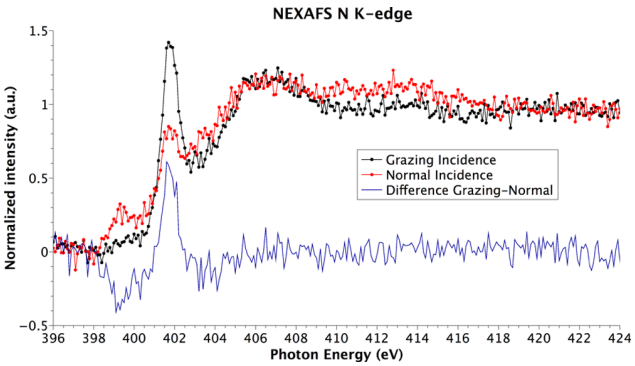

Figure 2. NEXAFS N K-edge spectrum collected at grazing (black) and normal (red) incidence of the impinging radiation on the sample surface. The difference grazing−normal spectrum is also reported (light blue).

dichroic effect for the π^* resonance associated with the peptide bond (402 eV), which is indicative of a preferential orientation of the peptide chains in the film.[5]

N K-edge spectral features are assigned as in[5] N 1s → π^* transition at 402 eV = peptide bond; N 1s → σ^* features above 406 eV and around 413 eV =N−H and N−C signals of amine groups, respectively.

The tilt angle between the π^* vector orbital of the peptide bond and the normal to the plane surface has been calculated using the formula reported by Stohr,[15] with a polarization factor $P = 0.95$ and the intensity ratio $I_{20°}/I_{90°}$ determined by the peak fitting of the experimental data. The resulting tilt angle value is about 20°, leading to an estimate of the mean angle between the peptide bond axis (the axis of the main chain) and the substrate surface of about 60° (see Chart 1). In calculating the molecular orientation, we made the assumption that the secondary structure of the peptide chain is a β-sheet conformation. The secondary structure of peptides can be probed by infrared (IR) spectroscopy; the position of the amide (I) band (C=O stretching) is influenced by the different

Chart 1. Schematic Representation of the EAK-Cys Molecular Orientation on the Gold Surface as Deduced by AD-NEXAFS Measurements

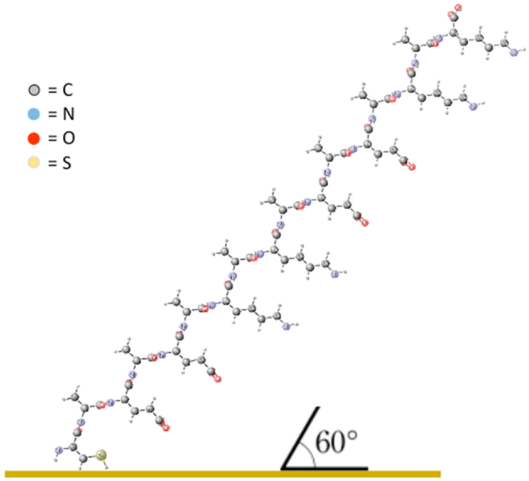

DOI: 10.1021/acs.jpcc.8b00794
J. Phys. Chem. C 2018, 122, 6236−6239

hydrogen bonding in α-helix and β-sheet conformations of the peptide backbone and can be used as a marker.[16] In previous studies, antiparallel β-sheet conformation was evidenced for related SAPs, such as EAK, by means of IRRAS measurements.[5] This structure was confirmed also for EAK-Cys; the IR spectrum (Figure S2 in Supporting Information) shows an amide (I) band located at about 1630 cm^{-1} with a shoulder at about 1690 cm^{-1}, featuring a typical antiparallel β-sheet conformation.

Interestingly, the tilt angle value estimated by AD-NEXAFS is different from the one observed for pure EAK-16 SAPs deposited as thick layers on gold (i.e., 70−80°)[5] because of the different anchoring mechanism allowed by the Cys residue.

Considering the evaluated average tilt angle between the peptide bond axis (the axis of the main chain) and the substrate surface of 60° and the rough molecular dimension esteemed for a 17-unit peptide chain length in a β-sheet conformation of 5.9 nm, the calculated SAP layer thickness is 4.77 nm. This estimated value is in excellent agreement with the SAP film thickness experimentally determined by the attenuation of the substrate XPS signal, which is 4.45 nm.

CONCLUSIONS

In conclusion, the complementary information acquired by XPS and NEXAFS allowed assessing the formation of a highly ordered molecular layer on the gold surface; the proper orientation of a ligand on a gold surface results in increased antigen detection, a property that is of primary importance in immunosensor design, and could represent an advantage in the design of gold nanoparticles for biosensing and nanomedicine. Moreover, in the light of the interesting properties observed for the functionalized surface, the proposed functionalization scheme involving the Cys side chain and Au surface can be extended, with some modification, for different metals used as biomaterials.

ASSOCIATED CONTENT

Supporting Information

The Supporting Information is available free of charge on the ACS Publications website at DOI: 10.1021/acs.jpcc.8b00794.

C 1s, O 1s, and N 1s core level XPS spectra, IR spectrum of SAP-Cys in the 2000−1500 cm^{-1} region, and all XPS data analysis results (PDF)

AUTHOR INFORMATION

Corresponding Author

*E-mail: chiara.battocchio@uniroma3.it. Phone: +39-06-57333400.

ORCID

Valeria Secchi: 0000-0002-3528-1194
Stefano Franchi: 0000-0002-5009-9147
Marta Santi: 0000-0003-2724-3996
Giovanna Iucci: 0000-0002-6478-3759
Chiara Battocchio: 0000-0003-4590-0865

Notes

The authors declare no competing financial interest.

ACKNOWLEDGMENTS

The authors gratefully acknowledge Prof. Mats Fahlman at the Department of Physics, Chemistry, and Biology in the Linköping University, Sweden, for the support in XPS measurements. This work has been partially financially supported by the Department of Science, Roma Tre University. CERIC-ERIC consortium and Czech Ministry of Education (LM2015057) are also acknowledged for the financial support.

REFERENCES

(1) Beutner, R.; Michael, J.; Schwenzer, B.; Scharnweber, D. Biological Nanofunctionalization of Titanium Based Biomaterial Surfaces: a Flexible Toolbox. *J. R. Soc., Interface* **2010**, *7*, S93−S105.

(2) Zhang, S.; Holmes, T.; Lockshin, C.; Rich, A. Spontaneous Assembly of a Self-Complementary Oligopeptide to Form a Stable Macroscopic membrane. *Proc. Natl. Acad. Sci. U.S.A.* **1993**, *90*, 3334−3338.

(3) Zhang, S. Emerging Biological Materials Through Molecular Self-Assembly. *Biotechnol. Adv.* **2002**, *20*, 321−339.

(4) Gelain, F.; Horii, A.; Zhang, S. Designer Self-Assembling Peptide Scaffolds for 3-D Tissue Cell Cultures and Regenerative Medicine. *Macromol. Biosci.* **2007**, *7*, 544−551.

(5) Battocchio, C.; Iucci, G.; Dettin, M.; Carravetta, V.; Monti, S.; Polzonetti, G. Self-assembling Behaviour of Self-Complementary Oligopeptides on Biocompatible Substrates. *Mater. Sci. Eng., B* **2010**, *169*, 36−42.

(6) Moulder, J. F.; Stickle, W. F.; Sobol, P. E.; Bomben, K. D. *Handbook of X-ray Photoelectron Spectroscopy*; Physical Electronics Inc.: Eden Prairie, Minnesota, 1996.

(7) Dettin, M.; Zamuner, A.; Iucci, G.; Messina, G. M. L.; Battocchio, C.; Picariello, G.; Gallina, G.; Marletta, G.; Castagliuolo, I.; Brun, P. Driving h-osteoblast Adhesion and Proliferation on Titania: Peptide Hydrogels Decorated with Growth Factors and Adhesive Conjugates. *J. Pept. Sci.* **2014**, *20*, 585−594.

(8) Swift, P.; Shuttleworth, D.; Seah, M. P. *Practical Surface Analysis by Auger and X-ray Photoelectron Spectroscopy*; Briggs, D.; Seah, M. P. Eds.; J. Wiley & Sons: Chichester, 1983, Chapter 4.

(9) Venditti, I.; Testa, G.; Sciubba, F.; Carlini, L.; Porcaro, F.; Meneghini, C.; Mobilio, S.; Battocchio, C.; Fratoddi, I. Hydrophilic Metal Nanoparticles Functionalized by 2-Diethylaminoethane Thiol: A Close Look on the Metal-ligand Interaction and Interface Chemical Structure. *J. Phys. Chem. C* **2017**, *121*, 8002−8013.

(10) Kim, J. W.; Lee, Y. M.; Lee, S. M.; Son, M. J.; Kang, H.; Park, Y. Surface Reaction of Sulfur-Containing Amino Acids on Cu(110). *Langmuir* **2010**, *26*, 5632−5636.

(11) Ishida, T.; Hara, M.; Kojima, I.; Tsuneda, S.; Nishida, N.; Sasabe, H.; Knoll, W. High Resolution X-ray Photoelectron Spectroscopy Measurements of Octadecanethiol Self-Assembled Monolayers on Au(111). *Langmuir* **1998**, *14*, 2092−2096.

(12) Polzonetti, G.; Iucci, G.; Furlani, C.; Russo, M. V.; Furlani, A.; Infante, G.; Paolucci, G.; Brena, B.; Cocco, D. A Photoelectron Spectroscopic Study of the Interface Formation between Chromium and a Palladium-Intercalated Polymer Film. *Chem. Phys. Lett.* **1997**, *267*, 384−390.

(13) Zhang, S.; Leem, G.; Lee, T. R. Monolayer-Protected Gold Nanoparticles Prepared Using Long-Chain Alkanethioacetates. *Langmuir* **2009**, *25*, 13855−13860.

(14) Lindberg, B. J.; Hamrin, K.; Johansson, G.; Gelius, U.; Fahlman, A.; Nordling, C.; Siegbahn, K. Molecular Spectroscopy by Means of ESCA II. Sulfur compounds. Correlation of electron binding energy with structure. *Phys. Scr.* **1970**, *1*, 286−298.

(15) Stohr, J. NEXAFS Spectroscopy. *Springer Series in Surface Sciences*; Gomer, C. Ed.; Springer Verlag, 1991.

(16) Haris, P. I.; Chapman, D. The Conformational Analysis of Peptides Using Fourier Transform IR Spectroscopy. *Biopolymers* **1995**, *37*, 251−263.

DOI: 10.1021/acs.jpcc.8b00794
J. Phys. Chem. C 2018, 122, 6236−6239

Chapter 4

Biofunctionalization of TiO_2 surfaces with self-assembling oligopeptides in different pH and Ionic Strength conditions: Charge effects and molecular organization

S. Franchi[a], V. Secchi[a,*], M. Santi[a], M. Dettin[b], A. Zamuner[b], C. Battocchio[a], G. Iucci[a]

[a] Department of Science, Roma Tre University of Rome, Via della Vasca Navale 79, 00146 Rome, Italy

[b] Department of Chemical Process Engineering, University of Padova, via Marzolo 9, 35131 Padova, Italy

Materials Science & Engineering C 90 (2018) 651–656

DOI: 10.1016/j.msec.2018.05.006

4. Biofunctionalization of TiO2 surfaces with self-assembling oligopeptides in different pH and Ionic Strength conditions: Charge effects and molecular organization

Biomaterials based on titanium are commonly and successfully used for orthopaedic and dental applications. Commercially pure titanium is the most used metal, because it is a bioinert material that does not induce allergic reactions or hypersensitivity in surrounding tissues. However, a potential problem is the unpredictability of implant integration with the host bone, and in clinical practice the osseointegration of orthopaedic implants is often incomplete, resulting in the risk of implant loosening over time. A possible strategy to enhance the biological acceptance of orthopaedic implants and promote osseointegration is the functionalization of the titanium surface with bioactive molecules as self-assembling peptides (SAPs) that can be grafted on the metal surface and establish a "molecular dialogue" with host's cells. In this framework, we tested different pH and Ionic Strength (I) conditions in the procedure leading to graft SAPs onto TiO_2 surface. The aim was to individuate the experimental conditions allowing to obtain a homogeneous and stable SAP coverage of controlled thickness on TiO_2 substrates. The preparation of an ordered and homogeneous SAP layer is mandatory in order to enhance biocompatibility and osteoblasts adhesion; Self-assembling peptides (SAPs) were investigated by means of XPS and Angular Dependent NEXAFS spectroscopies in order to study surfaces and biomolecule/substrate interfaces and ascertaining that SAPs molecular structure is preserved upon grafting to the titania surface. The objective of the study was to establish a set of methodologies for obtaining arrangements of well-organized biomolecules on scaffolds surfaces as a basic technology to develop and optimize cells adhesion and proliferation for tissue engineering applications.

Materials Science & Engineering C 90 (2018) 651–656

Contents lists available at ScienceDirect

Materials Science & Engineering C

journal homepage: www.elsevier.com/locate/msec

Biofunctionalization of TiO_2 surfaces with self-assembling oligopeptides in different pH and Ionic Strength conditions: Charge effects and molecular organization

S. Franchi[a], V. Secchi[a,*], M. Santi[a], M. Dettin[b], A. Zamuner[b], C. Battocchio[a], G. Iucci[a]

[a] Department of Sciences, University of Roma Tre, Via della Vasca Navale 79, 00146 Rome, Italy
[b] Department of Chemical Process Engineering, University of Padova, via Marzolo 9, 35131 Padova, Italy

ARTICLE INFO

Keywords:
Self-assembling peptides
Surface chemical structure
Tissue engineering
X-ray spectroscopy
Biocompatible materials

ABSTRACT

Self-assembling peptides (SAPs) were investigated by means of XPS and Angular Dependent NEXAFS spectroscopies, with the aim to probe the influence of pH and Ionic Strength conditions on the chemical structure and molecular organization of SAPs anchored on titania surfaces. XPS at the C1s, N1s, O1s core levels allowed to study surfaces and biomolecule/substrate interfaces. NEXAFS data allowed ascertaining that SAPs molecular structure is preserved upon grafting to the titania surface. Angular Dependent NEXAFS was used to investigate the influence of environmental conditions on the molecular organization behaviour. The objective of our study was to establish a set of methodologies for obtaining arrangements of well-organized biomolecules on scaffolds surfaces as a basic technology to develop and optimize cells adhesion and proliferation for tissue engineering applications.

1. Introduction

Tissue engineering is a multidisciplinary field involving the '*application of the principles and methods of engineering and life sciences towards the fundamental understanding of structure - function relationships in normal and pathological mammalian tissues and the development of biological substitutes that restore, maintain or improve tissue function*' [1]. Research in this fields deals with the development of new biomaterials to be implanted into a human body to substitute tissues/organs in a state of deterioration, to restore or establish their normal functions.

In particular, biomaterials based on titanium are commonly and successfully used for orthopaedic and dental applications because of its good mechano-chemical properties. Commercially pure titanium is the most used metal, because it is a bioinert material that does not induce allergic reactions or hypersensitivity in surrounding tissues. When the titanium surface is exposed to air it reacts rapidly with oxygen to form a thin layer of surface oxide, usually of TiO_2. The surface oxide is chemically stable and corrosion-resistant, preventing the diffusion of environmental oxygen toward the bulk of the prosthesis [2], which makes titanium surfaces quite stable under normal physiological conditions. The surface oxide may also contain varying amounts of other intentional or non-intentional (impurity) substances [3]. However, a potential problem is the unpredictability of implant integration with the host bone, and in clinical practice the osseointegration of orthopaedic implants is often incomplete, resulting in the risk of implant loosening over time. A possible strategy to enhance the biological acceptance of orthopaedic implants and promote osseointegration is the functionalization of the titanium surface with bioactive molecules (as for example osteogenic growth factors or cell adhesion sequences), that can be grafted on the metal surface and establish a "molecular dialogue" with host's cells [4].

Self-assembling peptides (SAPs) are an appealing class of synthetic materials suitable for this purpose, since they are capable to self-organize in nanostructures both in solution and as thin/thick films and adhere on biocompatible materials surfaces as a scaffold coating [5]. Scaffolding SAPs could be designed with the purpose to mimic the structure of the extra-cellular matrix (ECM), offering tridimensional support for cells, promoting their adhesion, proliferation and differentiation for new tissue formation [6,7].

The bioactive material surface characteristics are strongly influenced by the method of surface preparation, handling and storage. During preparation of the implant, the outmost layers of the material are subjected to various chemical processes that will leave residues at the surface. The close connection between surface preparation and resulting characteristics implies that in order to manufacture implants with reproducible structured surfaces, all aspects of the production

* Corresponding author.
E-mail address: valeria.secchi@uniroma3.it (V. Secchi).

https://doi.org/10.1016/j.msec.2018.05.006
Received 7 November 2017; Received in revised form 15 April 2018; Accepted 2 May 2018
Available online 03 May 2018

process and ensuing logistics need to be carefully controlled [2].

In this framework, we tested different pH and Ionic Strength (I) conditions in the procedure leading to graft SAPs onto TiO_2 surface. Our goal was to individuate the experimental conditions allowing to obtain a homogeneous and stable SAP coverage of controlled thickness on TiO_2 substrates. According to literature [8,9] the preparation of an ordered and homogeneous SAP layer is mandatory in order to enhance biocompatibility and osteoblasts adhesion; In this context, we here report our investigations on TiO_2 substrates functionalized with the SAP EAbuK16-II (a synthetic peptide analogous of EAK-16-II that spontaneously aggregates in anti-parallel β-sheet conformation in aqueous solution) by finely tuning the pH and I (ionic) conditions. Structural surface information was acquired by surface sensitive methodologies as X-ray Photoelectron Spectroscopy (XPS) and Near Edge X-ray Absorption Fine Structure (NEXAFS) spectroscopy. These techniques strongly contributed to the knowledge of our systems, providing unique data, which characterize both the electronic structure and the chemical interaction at the TiO_2/biomolecule interface. In particular NEXAFS spectroscopy carried out in angular dependent mode is an extremely well suited technique to probe the self-organization properties of the SAPs layer anchored on a titania substrate [10–12]. This paper presents the analysis of the chemical structure, composition, and molecular organization of the EAbuK16-II/TiO_2 interfaces as a function of pH and Ionic Strength parameters.

2. Experimental

2.1. Bioactive material preparation

The complete peptide sequence of EAbuK16-II is H-Abu-Glu-Abu-Glu-Abu-Lys-Abu-Lys-Abu-Glu-Abu-Glu-Abu-Lys-Abu-Lys-NH_2
(Abu = α-aminobutyric acid, hydrophobic residues; E = glutamic acid, negatively charged residue, K = lysine positively charged residue).

The SAP was synthesised as described in [7], while TiO_2 substrates were prepared by growing Ti film 200 nm thick onto Si(111) substrates and subsequent oxidation in air. Immobilization of SAP onto TiO_2 surfaces was carried out as described in [10–12] with minor modifications: Ti/Si wafers were sonicated in acetone for 5 min, then dried and incubated into the peptide aqueous solution containing 1 mg/mL SAP for 18 h, then washed thrice with NaCl 0.100 M at pH 7, and finally thrice with distilled water. The pH and Ionic Strength of the mother peptide solutions were modulated by adding the proper reagents, as described below:

- pH modulation: 0.0100 M HCl (J. T. Baker) (samples “pH 2”), 0.100 mM HCl (“pH 4”), 10 mM NaCl (“pH 7”), 0.100 mM NaOH (Carlo Erba) (“pH 10”), 0.0100 M NaOH (“pH 12”).
- Ionic Strength modulation: 10.0 mM and 100 mM NaCl (Carlo Erba); the corresponding samples will be mentioned as I10 and I100 in the following text.

2.2. Spectroscopic techniques

2.2.1. X-ray photoelectron spectroscopy

XPS analyses were performed in an instrument of our own design consisting of two chambers (preparation and analysis) separated by a gate valve. The analysis chamber is equipped with a manipulator having six degrees of freedom and with a 150-mm mean radius hemispherical electron analyzer with a five lens output system combined with a 16-channel detector. Measurements were performed at normal take-off (θ = 90°). Samples were introduced in the preparation chamber and left outgassing overnight at a base pressure of about 10^{-8} Torr, before introduction in the analysis chamber. Typical vacuum pressure in the analysis chamber during measurements was in the 10^{-9}–10^{-10} Torr range. The investigation was performed on clean TiO_2 surface and TiO_2 surfaces with immobilized peptide using Mg Kα non-monochromatized X-radiation (hν = 1253.6 eV) to record core level excitation of Ti2p, O1s, C1s and N1s lines spectra on the respective samples.

All spectra were energy referenced to the C1s signal of aliphatic carbon (BE = 285.0 eV). Atomic ratios were calculated from peak intensities by using Scofield's cross section values and, for the N1s photoelectrons, by an experimentally determined sensitivity factor of 1.44 based on the spectra of reference peptides used as standards.

Curve-fitting analysis of the C1s, O1s, and N1s spectra was performed using Gaussian curves having full width at half maximum (FWHM) = 1.7–2.2 eV as fitting functions. The thickness of the organic overlayer immobilized on the TiO_2 surface was calculated from the ratio between the intensities of the $Ti2p_{3/2}$ and N1s signals, according to the equation:

$$\frac{N_l(\Theta)}{N_k(\Theta)} = \frac{\Omega_0(E_l)A_0(E_l)D_0(E_l)}{\Omega_0(E_k)A_0(E_k)D_0(E_k)} \bullet \frac{\rho_l\left(\frac{d\sigma_l}{d\Omega}\right)}{\rho_k\left(\frac{d\sigma_k}{d\Omega}\right)} \bullet \frac{\Lambda_l(E_l)}{\Lambda_k(E_k)} \bullet \left[1 - \exp\left(-\frac{t}{\Lambda_l(E_l)\,sin\,\Theta}\right)\right] \bullet \exp\frac{t}{\Lambda_k(E_k)\,sin\,\Theta} \quad (1)$$

where N_l and N_k are the intensity of a signal belonging to the overlayer and the substrate, respectively; Θ is the angle of mean emission direction with respect the sample surface; Ω is the acceptance angle; A_0 is the specimen area; t is the specimen thickness; E is photoelectron kinetic energy, D_0 is the instrumental detection efficiency, ρ is the density of the molecules, Λ is the photoelectron mean free path, ($\Lambda = B\sqrt{E}$, where B = 0.087 nm $(V)^{1/2}$ for organic materials [13]), $d\sigma/d\Omega$ is the differential cross section [14]. Ω, A_0 and D_0 are assumed to be the same for substrate and overlayer; ρ for the substrate was calculated by averaging the molecular density of anatase and rutile, while to estimate peptide density was used the formula (2) reported in [15].

In this case measured overlayer thickness should be considered as an approximate estimate (± 15% experimental error) [13,14].

2.2.2. Near Edge x-ray Absorption Fine Structure (NEXAFS) spectroscopy

Near Edge x-ray Absorption Fine Structure (NEXAFS) spectroscopy experiments were performed at the ELETTRA storage ring at the BEAR beamline (bending magnet for emission absorption and reflectivity). BEAR is installed at the left exit of the 8.1 bending magnet exit. The apparatus is based on a bending magnet as a source and beamline optics delivering photons from 5 eV up to about 1600 eV with selectable degree of ellipticity. The UHV end station has a movable hemispherical electron analyzer and a set of photodiodes to collect angle resolved photoemission spectra, optical reflectivity and fluorescence yield. In these experiments ammeters to measure drain current from the sample for NEXAFS measurements were used. The carbon and nitrogen K-edge spectra were collected at normal (90°), grazing (20°) and magic (54.7°) incidence angles of the linearly polarized photon beam with respect to the sample surface.

The photon energy and resolution were calibrated and experimentally tested at the K absorption edges of Ar, N_2 and Ne. Spectra were then normalized subtracting a straight line that fits the part of the spectrum below the edge and assessing to 1 the value at 320.00 eV and 425.00 eV for carbon and nitrogen, respectively.

3. Results

3.1. XPS

Theoretical simulations show how peptides can bind TiO_2 surface by means of their amino and carboxyl groups [16,17] while other experiments assert they are oriented with respect the surface [10]; in the reported experimental conditions, however, the peptide is expected to bind TiO_2 surface through the carboxyl groups. Binding energies (BE) and atomic ratios determined by XPS measurements are summarized in

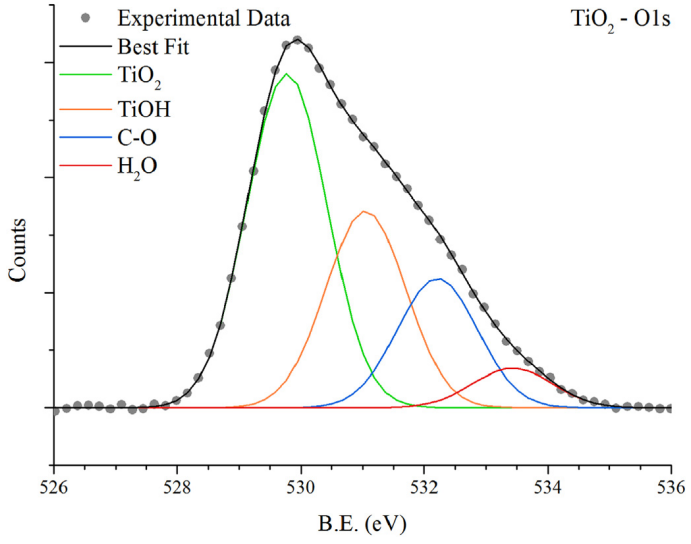

Fig. 1. XPS C1s spectrum of pristine TiO_2 surface. Gray dots represent experimental data, lines represent fitting components and calculated spectrum.

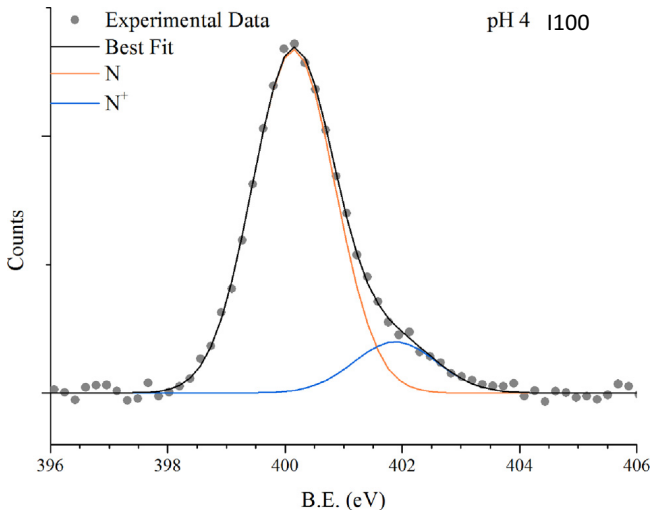

Fig. 3. XPS N1s spectrum of peptide immobilized at pH 4, I100. Gray dots represent experimental data, lines represent fitting components and calculated spectrum.

Tables S1, S2 and S3 in the Supporting Information.

The outmost surface of the titanium substrate is always oxidized and covered by a layer of hydroxyl groups. In fact $Ti2p_{3/2}$ signal of pristine surface presents a main peak at BE = 458.5 eV, the value expected for TiO_2 [18]. As expected, the O1s signal of pristine substrate surface (Fig. 1) shows a main peak (BE = 529.8 eV) related to TiO_2-like oxygen, a second signal at higher BE values related to surface hydroxyls (Ti—OH, BE = 531.0 eV), a third component due to organic oxygen, (oxygen atoms belonging to organic molecules, as the peptide; O-org, BE = 531.4 eV), and a last small peak attributed to physisorbed H_2O (BE = 533.5 eV) [11].

The ability of the TiO_2 surface to bind aminoacids has been correlated to the reaction between the basic Ti—OH groups on the surface and the carboxylic function of amino acids [19]: peptide immobilization then results in the appearance of structured C1s and O1s core-level signals, and in the presence of a strong N1s signal.

C1s spectrum of SAP chemisorbed on TiO_2 is reported in Fig. 2; for all samples, four spectral components can be individuated by following a peak-fitting procedure. More in detail, the peak with higher intensity at 285.0 eV is attributed to aliphatic C—C carbons of the amino acids

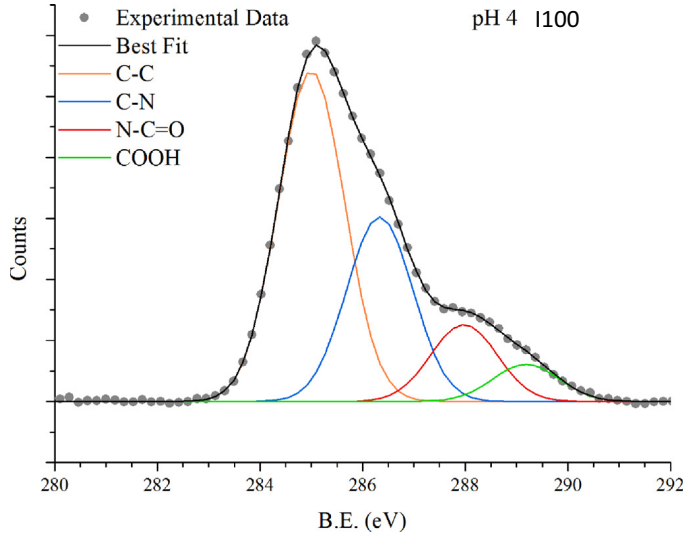

Fig. 2. XPS C1s spectrum of peptide immobilized at pH 4, I100 (considered representative for all samples). Gray dots represent experimental data, lines represent fitting components and calculated spectrum.

pending groups, the component at 286.33 eV is due to C—N carbons of peptide backbone and of lysine pending groups, the third peak at 287.98 eV is associated to carbons of the peptide backbone (N—C═O), and the last low intensity component (289.19 eV) arises from carboxyl functional groups of glutamic acids (O—C═O) [9–12].

As for O1s spectra, as expected for TiO_2 surfaces functionalized with peptides, a strong intensity increase of the organic oxygen (O-org) contribution can be detected (see Table S3).

The most significant signal for the assessment of successful biofunctionalization of a TiO_2 surface with peptides is the nitrogen core-level [9]. For all samples, N1s spectra show two peaks corresponding to unprotonated nitrogens (N, BE ~ 400 eV) and protonated (N^+, BE ~ 402 eV) nitrogens of terminal amino groups, as reported for sample pH 4 – I100 in the following Fig. 3.

Interestingly, the relative amount of protonated nitrogen (obtained as N^+ peak percent) for bioactive surfaces obtained in I10 and I100 conditions appear almost constant and of about 15% (10 mM) and 12% (100 mM) respectively. It is noteworthy that at pH 12 the signal related to protonated nitrogens was not detected, due to lysine residues. In fact lysine residues in the primary structure of the peptide are uncharged at pH 12 considering their isoelectric point at 10.53.

However, the presence of a strong N1s signal confirmed the successful biofunctionalization in all the tested conditions.

In order to select the best experimental conditions for the preparation of a functionalized surface of controlled thickness, the TiO_2 surface degree of coverage was investigated in detail by considering the Ti2p and N1s relative intensities due to SAP deposition. Since peptide immobilization results in increasing intensity of the nitrogen signal and in decreasing intensity of the Ti signal, the thickness of the organic overlayer adsorbed on substrate can be calculated according to the Eq. (1) (see Section 2.2.1). The obtained results are summarized in Fig. 4a, as described hereafter, and numerically reported in the tables in the Supporting Information (Tables S2–S3). As shown in Fig. 4b, the semiquantitative ratio N/Ti increases by decreasing the pH, and is always higher, at the same pH, for I 100 than for I 10. Furthermore, Fig. 4b shows the correlation between adlayer thickness, pH and I experimental conditions. It is noteworthy that samples I100 are always thicker; as suggested by the semiquantitative N/Ti ratio evaluation, at lower pH a higher peptide amount is adsorbed on the TiO_2 surface. The capability of the TiO_2 surface to bind amino acids, by reaction between the basic Ti-OH groups on the TiO_2 surface and the amino acid carboxylic function increases at low pH [17,20]; therefore, it is not surprising that a similar trend is found for SAP immobilization.

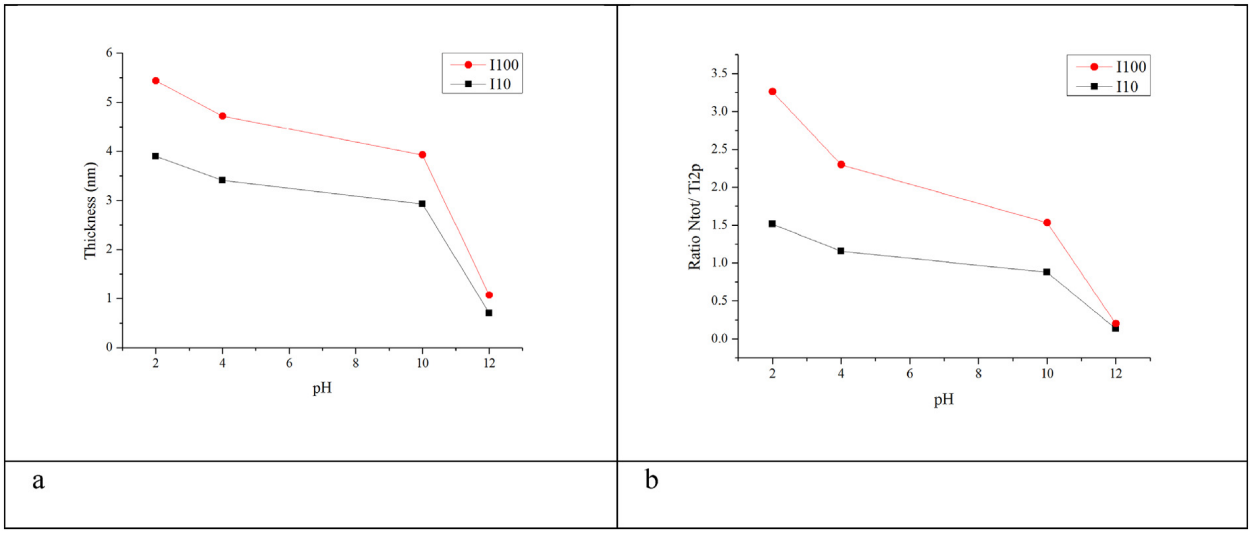

Fig. 4. a) Calculated thickness of the organic overlayer reported as a function of pH conditions solution for I10 (black) and I100 (red) concentration; b). N_{tot}/Ti2p atomic ratios. (For interpretation of the references to colour in this figure legend, the reader is referred to the web version of this article.)

3.2. Near Edge x-ray Absorption Fine Structure studies

3.2.1. Molecular structure

With the aim to further investigate the molecular structure of SAP interacting with the substrate, Near Edge X-Ray Absorption Fine Structure (NEXAFS) spectroscopy measurements have been performed at both C and N k-edges on samples obtained from peptide solutions prepared at different I and pH values. In Fig. 5, C k-edge spectra recorded at Magic angle incidence (54.7°) for TiO_2/SAPs prepared at a I10 (a) and I100 (b) are reported; spectra corresponding to samples at different pH values are superimposed in the two figures, with lines of different colour.

In the carbon spectra several structures appear in both π* and σ* resonances region. The sharp feature at about 290 eV is assigned to a C1s → π* transition of C═O molecular orbital, the shoulder around 289.5 eV to a σ* resonance by the C−H groups, additional features at ≈296 and ≈303 eV can be associated to 1s → σ* transitions by the C−C and C═O molecular groups in agreement with the molecular structure. The SAP's stability is preserved regardless of the variation of pH conditions. The feature at about 285 eV is attributed to graphite impurities in the beam line optics [21]; this feature, often observed in C k-edge spectra [10,12], is here unusually intense due to the very low thickness of SAP layers (monolayer or sub-monolayer regime). This finding is in excellent agreement with XPS-based thickness evaluation (Fig. 4a).

N K-edge spectra are in good agreement with the observed SR-XPS N1s signals on all samples. Fig. 6 shows the N k-edge NEXAFS spectra of the peptides at prepared at I10 (a) and I100 (b), recorded at Magic angle incidence (54.7°) at different pH values. The sharp peak at 403.7 eV is assigned to N1s → π* transitions of the peptide bonds and the broad bands at 408 and 415 eV to σ* resonances, as expected from the oligopeptide molecular structure [3,4,10].

3.2.2. Molecular organization

At this stage, we can further deepen the investigation, by checking orientation of biomolecules on the titania surface, by following the procedure already described in refs [10–12].

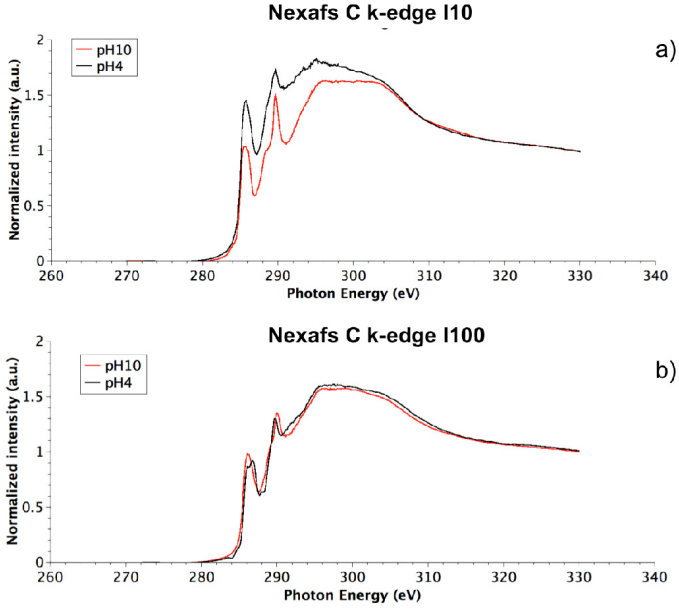

Fig. 5. C k-edge NEXAFS spectra of the SAP prepared at I10 (a) and I100 (b) and at different pH values, recorded at Magic angle incidence (54.7), as to avoid dichroic effects on features intensity.

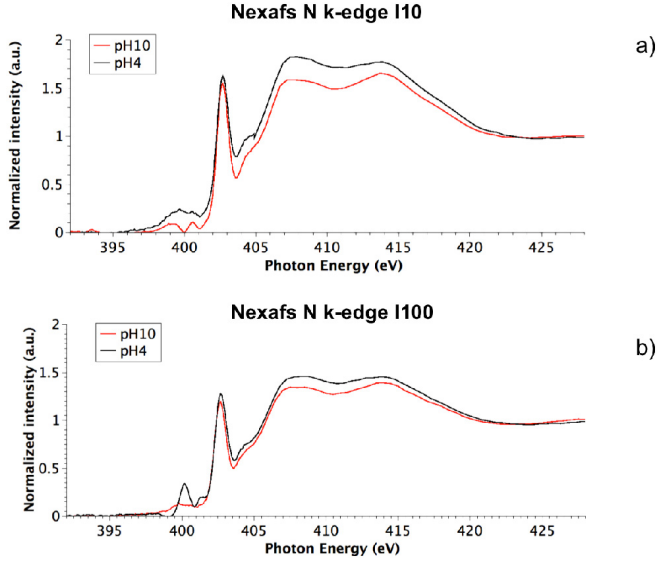

Fig. 6. N k-edge NEXAFS spectra of the peptide prepared at I10 (a) and I100 (b) and at different pH values, recorded at Magic angle incidence (54.7), as to avoid dichroic effects on features intensity.

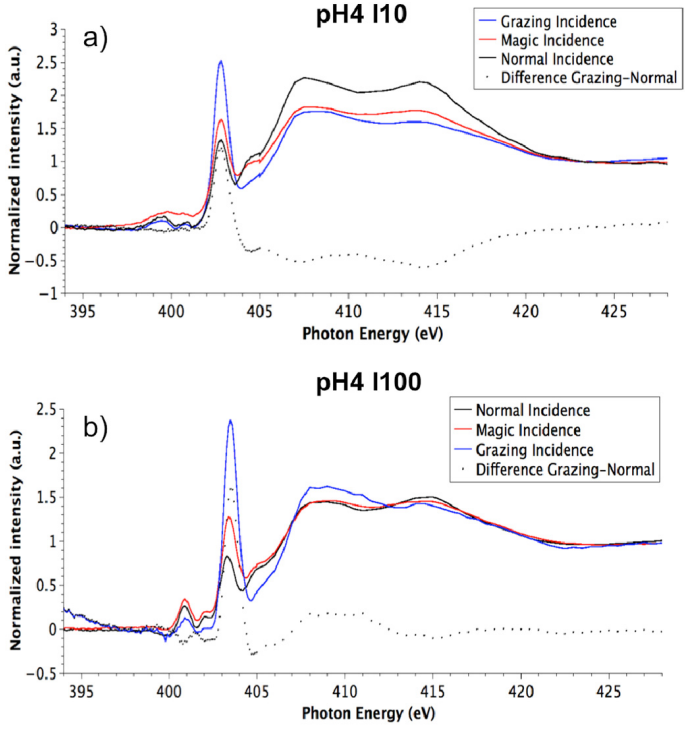

Fig. 7. N K-edge spectra collected by varying the photon beam incidence angle on the sample surface from 20 (grazing) to 90 (normal) degrees a) SAP pH 4 I10, b) SAP pH 4 I100.

Table 1
Calculated tilt angles of the peptide bond and the angles between the axis of the main chain and the sample surface, correlated with pH and Ionic Strength.

θ = (120 − α) (°)		
pH	10 mM	100 mM
2	83	82
4	77	85
10	82	80

The NEXAFS resonances intensity depends on the orientation of the transition dipole moment (μ) of the probed molecules relative to the polarization vector (p) of the incoming radiation. If the directions of the electric field of the incoming radiation (E) and μ are parallel to each other, the intensity is at the maximum. On the other hand, the excitation does not occur when the vectors E and μ are orthogonal between each other [21].

Specifically, we focus our attention on TiO_2/SAPs prepared at pH 4, to compare the molecular organization at different Ionic Strength (samples I10 and I100) at the best pH condition based on the previously calculated thickness values of the organic overlayer shown in Fig. 4.

In the following Fig. 7, N k-edge spectra collected by varying the photon beam incidence angle on the sample surface from 20 (grazing) to 90 (normal) degrees are reported for TiO_2/SAPs prepared at pH 4 for I10 (a) and I100 (b).

The polarization dependence of the π* resonance (≈403 eV) is evident. The ratio between the π* peak intensities at normal (90°) and grazing (20°) incidence, determined by peak fitting of the experimental data, can be used to calculate the average tilt angle between the π* vector orbital of the peptide bond and the normal to the surface (77° for I10 and 84.7° and for I100), using the equation reported by Stohr for three fold or higher symmetry substrates, assuming polarization factor P = 0.95. The following Table 1 shows the angles between the axis of the main chain and the sample surface calculated considering θ = (120 − α) (°) [22]. The tilt angles were calculated for pH values in the range 2–10; the spectra of samples prepared at pH = 12 are too noisy, due to low overlayer thickness, to allow a reliable calculation of the tilt angle.

It is noteworthy that the incertitude in the determination of the tilt angle by NEXAFS is 15% of the estimated value; therefore, the molecular organization of the peptide is equivalent for the two samples prepared at different I, as well as for the samples prepared at different pH. On the other hand, film thickness evaluation (Fig. 4, Section 3.1) shows that the overlayer is thicker at low pH and considerably thinner at high pH values. By matching the complementary information obtained by XPS and AD-NEXAFS techniques, we can deduce that a substantially lower amount of peptide is immobilized at high pH values than in acidic condition. This observation suggests that acidic conditions are the best-suited to graft an ordered and homogeneous film of SAP on the TiO_2 surface, as required for the envisaged applications.

4. Conclusion

SAP immobilization on the TiO_2 surface was investigated as a function of pH and Ionic Strength of the mother solution with the aim of determining the best experimental conditions for peptide adhesion. The amount of immobilized peptide and the resulting thickness of the organic overlayer decrease with increasing the pH of the mother solution; the highest values are measured in acidic environment (pH 2), a plateau is observed in the pH range 4–10 and a steep decrease at pH 12. The percentage of protonated nitrogens remains approximately constant in the pH range 2–10, while at pH 12 the corresponding signal disappears; protonated nitrogens are located in the lysine side chains and play a fundamental role in the self-assembling process.

At all the investigated pH values, increase in the Ionic Strength of the peptide solution results in an increase of the peptide overlayer thickness.

Preparation of an order and homogeneous SAP layer is mandatory in order to enhance biocompatibility and osteoblasts adhesion; the here reported result show that the SAP molecular orientation can be considered constant in a rather wide pH range, while the SAP immobilization on the TiO_2 surface is enhanced in acid pH conditions.

Acknowledgments

The Grant of Excellence Departments, MIUR (ARTICOLO 1, COMMI 314-337 LEGGE 232/2016), is gratefully acknowledged.

Appendix A. Supplementary data

Supplementary data to this article can be found online at https://doi.org/10.1016/j.msec.2018.05.006.

References

[1] R. Shalak, C.F. Fox, Preface, in: A.R. Liss (Ed.), Tissue Engineering, 1988, pp. 22–29 New York.
[2] L. Bakacova, E. Filova, M. Parizek, T. Ruml, V. Svorcik, Modulation of cell adhesion, proliferation and differentiation on materials designed for body implants, Biotechnol. Adv. 29 (2011) 739–767, http://dx.doi.org/10.1016/j.biotechadv.2011.06.004.
[3] A. Palmquist, O.M. Omar, M. Esposito, J. Lausmaa, P. Thomsen, Titanium oral implants: surface characteristics, interface biology and clinical outcome, J. R. Soc. Interface 7 (Suppl. 5) (Oct 6 2010) S515–S527.
[4] S. Nayak, T. Dey, D. Naskar, S.C. Kundu, The promotion of osseointegration of titanium surfaces by coating with silk protein sericin, Biomaterials 34 (2013) 2855–2864.
[5] S. Zhang, T.C. Holmes, C. Lockshin, A. Rich, Spontaneous assembly of a self-complementary oligopeptide to form a stable macroscopic membrane, Proc. Natl. Acad. Sci. 90 (1993) 3334 (USA).
[6] P. Moscarelli, F. Boraldi, B. Bochicchio, A. Pepe, A.M. Salvi, D. Quaglino, Structural characterization and biological properties of the amyloidogenic elastin peptide $(VGGVG)_3$, Matrix Biol. 36 (2014) 15–27, http://dx.doi.org/10.1016/j.matbio.2014.03.004.

[7] M. Dettin, A. Zamuner, G. Iucci, G.M.L. Messina, C. Battocchio, G. Picariello, G. Gallina, G. Marletta, I. Castagliuolo, P. Brun, Driving h-osteoblast adhesion and proliferation on titania: peptide hydrogels decorated with growth factors and adhesive conjugate, J. Pept. Sci. 20 (2014) 585–594, http://dx.doi.org/10.1002/psc.2652.
[8] M. Ozeki, S. Kuroda, K. Kon, S. Kasugai, Differentiation of bone marrow stromal cells into osteoblasts in a self-assembling peptide hydrogel: in vitro and in vivo studies, J. Biomater. Appl. 25 (2011) 663–684, http://dx.doi.org/10.1177/0885328209356328.
[9] R. Danesin, P. Brun, M. Roso, F. Delaunay, V. Samouillan, K. Brunelli, G. Iucci, F. Ghezzo, M. Modesti, I. Castagliuolo, M. Dettin, Self-assembling peptide enriched electrospun scaffolds promote the h-osteoblast adhesion and modulate differentiation-associated gene-expression, Bone 51 (2012) 851–859, http://dx.doi.org/10.1016/j.bone.2012.08.119.
[10] G. Polzonetti, C. Battocchio, G. Iucci, M. Dettin, R. Gambaretto, C. Di Bello, V. Carravetta, Thin films of a self-assembling peptide on TiO_2 and Au studied by NEXAFS, XPS and IR spectroscopies, Mater. Sci. Eng. C 26 (2006) 929–934, http://dx.doi.org/10.1016/j.msec.2005.09.062.
[11] G. Iucci, M. Dettin, C. Battocchio, R. Gambaretto, C. Di Bello, G. Polzonetti, Novel immobilizations of an adhesion peptide on the TiO_2 surface: an XPS investigation, Mater. Sci. Eng. C 27 (2007) 1201R–1206, http://dx.doi.org/10.1016/j.msec.2006.09.038.
[12] C. Battocchio, G. Iucci, M. Dettin, V. Carravetta, S. Monti, G. Polzonetti, Self-assembling behaviour of self-complementary oligopeptides on biocompatible substrates, Mater. Sci. Eng. C 169 (2010) 36–42, http://dx.doi.org/10.1016/j.mseb.2009.12.051.
[13] M.P. Seah, W.A. Dench, Quantitative electron spectroscopy of surfaces: standard data base for electron inelastic mean free path in solids, Surf. Interface Anal. 1 (1979) 2–11, http://dx.doi.org/10.1002/sia.740010103.
[14] C.R. Brundle, A.D. Baker, Electron Spectroscopy: Theory, Techniques and Applications, Academic Press, New York, 1979, p. 2.
[15] H. Fischer, I. Polikarpov, A.F. Craievich, Average protein density is a molecular-weight-dependent function, Protein Sci. 13 (10) (2004) 2825–2828, http://dx.doi.org/10.1110/ps.04688204.
[16] D. Costa, L. Savio, C.-M. Pradier, Adsorption of amino acids and peptides on metal and oxide surfaces in water environment: a synthetic and prospective review, J. Phys. Chem. B 120 (2016) 7039–7052, http://dx.doi.org/10.1021/acs.jpcb.6b05954.
[17] S. Monti, V. Carravetta, C. Battocchio, et al., Peptide/TiO_2 surface interaction: a theoretical and experimental study on the structure of adsorbed ALA-GLU and ALA-LYS, Langmuir 24 (7) (2008) 3205–3214.
[18] J.F. Moulder, W.F. Stickle, P.E. Sobol, K.D. Bomben, Handbook of X-ray Photoelectron Spectroscopy. Physical Electronics Inc. (1979).
[19] M. Schmidt, X-ray photoelectron spectroscopy studies on adsorption of amino acids from aqueous solutions onto oxidised titanium surfaces, Arch. Orthop.Trauma Surg. 121 (7) (2001) 403–410, http://dx.doi.org/10.1007/s004020100262.
[20] M. Schmidt, S.G. Steinemann, XPS studies of amino acids adsorbed on titanium dioxide surfaces, Fresenius J. Anal. Chem. 341 (1991) 412–415.
[21] J. Stohr, Gomer (Ed.), NEXAFS Spectroscopy Springer Series in Surface Sciences, Springer Verlag, 1991.
[22] G. Iucci, C. Battocchio, M. Dettin, R. Gambaretto, G. Polzonetti, A NEXAFS and XPS study of the adsorption of self-assembling peptides on TiO_2: the influence of the side chains, Surf. Interface Anal. 40 (2008) 210–214.

Chapter 5

Biocompatible Materials Based on Self-Assembling Peptides on Ti25Nb10Zr Alloy: Molecular Structure and Organization Investigated by Synchrotron Radiation Induced Techniques

V. Secchi [a], S. Franchi [a], M. Santi [a], A. Vladescu [b], M. Braic [b], T. Skála [c], J. Nováková [c], M. Dettin [d], A. Zamuner [d], G. Iucci [a], C. Battocchio [a]

[a] Department of Science, Roma Tre University of Rome, Via della Vasca Navale 79, 00146 Rome, Italy;

[b] National Institute for Optoelectronics, 409 Atomistilor St., 077125 Magurele, Romania;

[c] Department of Surface and Plasma Science, Faculty of Mathematics and Physics, Charles University, V Holešovicˇkách 2, 18000 Prague, Czech Republic;

[d] Department of Industrial Engineering, University of Padua, Via Marzolo, 9, Padua 35131, Italy;

Nanomaterials 2018, 8, 148;

DOI: 10.3390/nano8030148

5. Biocompatible Materials Based on Self-Assembling Peptides on Ti25Nb10Zr Alloy: Molecular Structure and Organization Investigated by Synchrotron Radiation Induced Techniques

Alloying improves the mechanical properties of titanium for use in high load-bearing applications, total hip, and total knee replacements. However, some concerns related to the toxicity of various alloying elements do exist. On this basis, a lot of experiments have been carried out to develop a novel Ti based alloy consisting only of biocompatible elements. The here reported Ti-Zr-Nb system was selected for the following reasons: all of the constituent elements are considered to be highly biocompatible and show high affinity to oxygen, leading to the formation of stable oxides which improve the corrosion resistance. Furthermore a possible strategy to promote osseo-integration and enhance the biological acceptance of the implants is the biofunctionalization of the Ti25Nb10Zr surface with self-assembling peptides (SAPs) are extremely promising candidates as seen in chapter 4, since thanks to their on-purpose designed sequence they are able to self-assemble in a beta-sheet secondary structure. The aim of this work was to applied advanced Synchrotron Radiation (SR) induced techniques to the study of the chemisorption of the Self Assembling Peptide EAbuK16 that is able to spontaneously aggregate in anti-parallel ß-sheet conformation, onto annealed Ti25Nb10Zr alloy surfaces at five different pH values, selected on purpose to investigate the best conditions for peptide immobilization.

nanomaterials

MDPI

Article

Biocompatible Materials Based on Self-Assembling Peptides on Ti25Nb10Zr Alloy: Molecular Structure and Organization Investigated by Synchrotron Radiation Induced Techniques

Valeria Secchi [1], Stefano Franchi [1,*,†], Marta Santi [1], Alina Vladescu [2], Mariana Braic [2], Tomáš Skála [3], Jaroslava Nováková [3], Monica Dettin [4], Annj Zamuner [4], Giovanna Iucci [1] and Chiara Battocchio [1,*]

1 Department of Science, Roma Tre University of Rome, Via della Vasca Navale 79, 00146 Rome, Italy; valeria.secchi@uniroma3.it (V.S.); santimarta3@gmail.com (M.S.); giovanna.iucci@uniroma3.it (G.I.)
2 National Institute for Optoelectronics, 409 Atomistilor St., 077125 Magurele, Romania; alinava@inoe.ro (A.V.); mariana.braic@inoe.ro (M.B.)
3 Department of Surface and Plasma Science, Faculty of Mathematics and Physics, Charles University, V Holešovičkách 2, 18000 Prague, Czech Republic; tomas.skala@elettra.eu (T.S.); jaroslava.lavkova@gmail.com (J.N.)
4 Department of Industrial Engineering, University of Padua, Via Marzolo, 9, Padua 35131, Italy; monica.dettin@unipd.it (M.D.); annj.zamuner@studenti.unipd.it (A.Z.)
* Correspondence: stefano.franchi@elettra.eu (S.F.); chiara.battocchio@uniroma3.it (C.B.); Tel.: +39-040-3758059 (S.F.); +39-06-5733-3400 (C.B.)
† Present Address: Elettra-Sincrotrone Trieste S.C.p.A. di interesse nazionale, Strada Statale 14-km 163,5 in AREA Science Park, 34149 Basovizza, Trieste, Italy.

Received: 31 January 2018; Accepted: 5 March 2018; Published: 7 March 2018

Abstract: In this work, we applied advanced Synchrotron Radiation (SR) induced techniques to the study of the chemisorption of the Self Assembling Peptide EAbuK16, i.e., H-Abu-Glu-Abu-Glu-Abu-Lys-Abu-Lys-Abu-Glu-Abu-Glu-Abu-Lys-Abu-Lys-NH_2 that is able to spontaneously aggregate in anti-parallel β-sheet conformation, onto annealed Ti25Nb10Zr alloy surfaces. This synthetic amphiphilic oligopeptide is a good candidate to mimic extracellular matrix for bone prosthesis, since its β-sheets stack onto each other in a multilayer oriented nanostructure with internal pores of 5–200 nm size. To prepare the biomimetic material, Ti25Nb10Zr discs were treated with aqueous solutions of EAbuK16 at different pH values. Here we present the results achieved by performing SR-induced X-ray Photoelectron Spectroscopy (SR-XPS), angle-dependent Near Edge X-ray Absorption Fine Structure (NEXAFS) spectroscopy, FESEM and AFM imaging on Ti25Nb10Zr discs after incubation with self-assembling peptide solution at five different pH values, selected deliberately to investigate the best conditions for peptide immobilization.

Keywords: synchrotron radiation induced spectroscopies; XPS; NEXAFS; nanostructures; titanium alloy; self-assembling peptides; bioactive materials

1. Introduction

The increased interest in titanium (Ti) and its alloys for dental implants and prosthesis application derives from their exceptional mechanical properties, corrosion resistance and biocompatibility [1,2]. A gentle surgical technique combined with sufficient healing time has long been considered the key to osseo-integration, and excellent long-term clinical outcome for dental implant thus validates the results of pre-clinical experimental studies. Alloying improves the mechanical properties of titanium

for use in high load-bearing applications, total hip, and total knee replacements. However, some concerns related to the toxicity of various alloying elements do exist [3]. In particular, Ti6Al4V alloy is commonly used in clinical practice as biocompatible material for prosthetics applications and dental implants [4–9]. In the last years, the in vitro and in vivo tests performed on Ti6Al4V alloy showed that this alloy has a toxic effect resulting from released V and Al and that its elastic modulus is very distant from the bone value [10–16], restricting its use in biomaterial applications. On this basis, a lot of experiments have been carried out to develop a novel Ti based alloy consisting only of biocompatible elements, which could replace the Ti6Al4V alloy in clinical practice [9,17–19]. For example, Ti6Al7Nb (ASTM F1295), Ti13Nb13Zr (ASTM F1713), and Ti12Mo6Zr (ASTM F1813) were proposed as candidates for manufacturing surgical implants. It is worth mentioning that there are a lot of other proposed alloys in the literature, such as Ti-Nb-Zr-Ta [20–24], Ti-Mo-Zr-Fe [25,26], Ti-Al-Zr [27], Ti-Al-Fe [18], Ti-Nb-Fe [28,29], Ti-Nb-Zr-Sn [30] and Ti-Nb [31] systems, but no standards have been published.

The here reported Ti-Zr-Nb system was selected for the following reasons: all of the constituent elements are considered to be highly biocompatible [32–34] and show high affinity to oxygen, leading to the formation of stable oxides which improve the corrosion resistance [35–39]; moreover, Zr is added in the alloy due to its capacity to stabilize the β phase. In fact, Abdel-Hady et al. showed that a Zr content ranging from 6 to 30 at % stabilized the β phase in alloys [40]. In the literature, there are few papers dealing with the effect of Zr content on the mechanical, tribological, and anticorrosive properties of Ti-Zr-Nb systems used for biomedical applications. In all published literature, the Zr content is up to 10 at % [41–46] or of about 30 at % [43]. Nb addition is also required because it maintains the β phase formed during the annealing. Furthermore a possible strategy to promote osseo-integration and enhance the biological acceptance of the implants is the biofunctionalization of the Ti25Nb10Zr surface with bioactive molecules that can be grafted on the surface in order to establish a molecular dialogue with host cells [47]. Among other bioactive molecules, self-assembling peptides (SAPs) are extremely promising candidates, since thanks to their on-purpose designed sequence they are able to self-assemble in a beta-sheet secondary structure [48,49]. They can then aggregate in the presence of saline creating hydrogels that can be used either as drug delivery vehicles, in the case of factors to release with a precise kinetic, or can be decorated with adhesive sequences or proteins, appropriately conjugated with a self-assembling sequence, allowing the functionalization of the scaffold with adhesive signals in a 3D structure by simple co-aggregation. The chemically stable SAP adhesion to the substrate is usually obtained by covalently and selectively functionalizing the alloy surface of the ion complementary peptide [50,51].

In this work, we present the characterization, carried out by synchrotron radiation-induced X-ray Photoemission Spectroscopy (SR-XPS), angle-dependent Near Edge X-rays Absorption Fine Structure (NEXAFS) spectroscopy, Field Emission Scanning Electron Microscopy (FE-SEM) and Atomic Force Microscopy (AFM) investigations of Ti25Nb10Zr alloy surfaces functionalized by the SAP EAbuK16 (Abu stands for α-aminobutyric acid), i.e., H-Abu-Glu-Abu-Glu-Abu-Lys-Abu-Lys-Abu-Glu-Abu-Glu-Abu-Lys-Abu-Lys-NH_2. The proposed SAP is able to self-assemble in aqueous solution in the presence of monovalent cations. To prepare the material, Ti25Nb10Zr discs were exposed to self-assembling peptide solutions at pH values ranging from 2 to 12, in order to understand the best conditions for peptide immobilization.

2. Materials and Methods

2.1. Samples Preparation

2.1.1. Ti25Nb10Zr Alloy Preparation and Preliminary Characterization

Ti25Nb10Zr (in wt %) was manufactured by Romanian Company (R&D Consulting and Services, Bucharest, Romania). Ti25Nb10Zr alloy was casted by a cold crucible levitation melting technique (CCLM), using a FIVES CELES—CELLES MP 25 furnace with nominal power 25 kW (Fives Celes, Lautenbach, France). The alloy was produced by mixing ultra-pure raw metals, subsequently annealed

at 900 °C for 5 h in an oven (Caloris-CD 1121) (Caloris, Bucharest, Romania) and cooled in air. For this study, the alloy was cut as discs by a turning machine and mid-polished using 3 μm diamond emery paste.

The elemental composition and distribution of each constituent element of the alloy was checked by means of energy-dispersive X-ray spectroscopy (EDS), using the X-ray detector (EDS-Quantax70, Bruker, Billerica, MA, USA) attached to a scanning electron microscope (SEM, Hitachi TM3030PLUS) (Hitachi, Tokyo, Japan). The compositional analysis was performed automatically by the Quantax 70 microanalysis software (Bruker). The surface morphology of the Ti25Nb10Zr alloy substrates was investigated by atomic force microscopy (AFM) and scanning electron microscopy (SEM). AFM measurements were performed in tapping mode on 30 × 30 μm^2 area using an INNOVA microscope (Veeco, Plainview, NY, USA). The crystallographic structure was analyzed by X-ray diffraction (XRD) (Rigaku, Tokyo, Japan) using a diffractometer SmartLab Rigaku in the 2θ range 20–100°. The step Δ2θ was 0.02, and the minimum speed was 0.0002 deg/min. The CuKα radiation was used with a wavelength of λ = 1.5411 Å at 45 kV high voltage and 200 mA of the X-ray tube.

Since the alloy is prepared with the aim to be used as material for orthopaedic implants, special attention was devoted to the evaluation of the corrosion resistance in two solutions mimicking the physiological conditions: simulated body solution (SBF, composition: 8.035 g/L NaCl, 0.335 g/L $NaHCO_3$, 0.225 g/L KCl, 0.231 g/L $K_2HPO_4 \cdot 3H_2O$, 0.311 g/L $MgCl_2 \cdot 6H_2O$, 0.292 g/L $CaCl_2$, 0.072 g/L Na_2SO_4, 6.228 g/L Tris-$(HOCH_2)_3CNH_2$ [52]) and Hank solution (composition: 8 g/L NaCl, 0.4 g/L KCl, 0.1 g/L $MgCl_2 \cdot 6H_2O$, 0.14 g/L $CaCl_2$, 1 g/L glucose, 0.35 g/L $NaHCO_3$, 0.06 g/L $NaH_2PO_4 \cdot 6H_2O$, 0.06 g/L KH_2PO_4, 0.06 g/L $MgSO_4$ [53]). The corrosion resistance was evaluated by potentiodynamic polarization tests at 37 ± 0.4 °C using a VersaSTAT 3 Potentiostat/Galvanostat (Princeton Applied Research-AMETEK, Oak Ridge, TN, USA), following the steps:

Monitoring the open circuit potential (OCP) for 15 h after the immersion in electrolyte.

Plotting potentiodynamic curves −2 V vs. OCP to 2 V vs. SCE.

A conventional three-electrode cell was used, with a saturated calomel electrode (SCE) as reference, a platinum one as counter electrode, and the sample (1 cm^2) as working electrode. For the tests, the scanning rate was of 1 mV/s, value recommended also by ASTM G 59–97. During the tests, the solution was agitated by magnetic stirrer at 150 rpm for elimination of the gas bubbles formed during the test.

On the basis of potentiodynamic curves, both the corrosion potential ($E_{i=0}$) and corrosion current density (i_{corr}) were estimated. The polarization resistance (R_p) was calculated using the Stern–Geary Equation (1) [54]:

$$R_p = \frac{1}{2.3 \cdot i_{corr}} \cdot \frac{b_a \cdot b_c}{(b_a + b_c)} \quad (1)$$

where i_{corr} is corrosion current density, b_a is anodic slope and b_c is cathodic slope of the alloy.

The corrosion rates (*CR*) were calculated, on the basis of the values of the electrochemical parameters determined from the polarization curve, using Equation (2) according to the ISO G102-89 standard, reapproved in 1999:

$$CR = \frac{K \cdot i_{corr} \cdot EW}{\rho} \quad (2)$$

where K is a constant for units conversion, i_{corr}, the corrosion current density of the alloy (μA/cm^2 or A/cm^2), *EW* alloy equivalent weight (gram/equivalent), ρ alloy density (gram/cm^3).

2.1.2. Ti25Nb10Zr Alloy Surfaces Functionalization

SAP EAbuK16 was synthesized on solid phase as reported in [49].

Substrates were incubated for 18 h in aqueous solution at different pHs containing 1 mg/mL of EAbuK16. The SAP was dissolved in 10 mM NaCl (Carlo Erba, Cornaredo, Italy) aqueous solutions having different pH values: 0.1 mM HCl (J. T. Baker, Phillisburg, NJ, USA) (pH 4), 0.01 M HCl (pH 2), 0.1 mM NaOH (Carlo Erba) (pH 10), 0.01 M NaOH (pH 12). The pH 7 solution was prepared in two

different ways: (a) buffered by Hank's solution (146.15 mg NaCl; 50 mg KCl (Carlo Erba); 287 mg Na_2HPO_4 (Carlo Erba); 50 mg KH_2PO_4 (Carlo Erba) in 250 mL distilled water); (b) 10 mM NaCl in distilled water.

The five solutions were then used to cover the alloy surfaces with a layer of SAP. More in detail, thin and thick self-assembling peptide layers namely monolayers, (MLs), and multilayers (MULs), were supported onto Ti25Nb10Zr surfaces as follows:

- MLs: Ti25Nb10Zr discs were sonicated in acetone for 5 min, dried, incubated in the peptide solution for 18 h, washed three times with NaCl 0.10 M at pH 7 and finally three times with distilled water. In these samples the set pH 7 solution was buffered with Hank's solution to mimic the extracellular physiological environment. Unfortunately, Hank's solution altered the ionic strength and interfered with peptide deposition. For this reason, the pH 7 sample was prepared again, avoiding the addition of sodium phosphate and other salts, except NaCl 10 mM, and maintaining the 10 mM NaCl washing treatment.
- MULs: Ti25Nb10Zr discs were sonicated in acetone for 5 min and dried. Peptide films were cast by covering the alloy surface with 2–3 drops of 1 mg/mL solutions of EAbuK16 oligopeptide prepared at different pHs, then dried in a low vacuum glass line.

2.2. Spectroscopic Techniques

2.2.1. X-ray Photoelectron Spectroscopy

High Resolution X-ray Photoelectron Spectroscopy (XPS) measurements on pristine alloy and multilayer samples were performed at the Materials Science Beamline (MSB) at the Elettra synchrotron radiation source (Trieste, Italy). MSB, placed at the left end of bending magnet 6.1, is equipped with a plane grating monochromator that provides light in the energy range of 21–1000 eV. The UHV endstation, with a base pressure of 1×10^{-8} Pa is equipped with a Specs Phoibos 150 hemispherical electron analyzer. Photoelectrons emitted by C1s, N1s, O1s, and Ti2p were detected at normal emission geometry using photon energy of 630 eV, estimated Energy Resolution = 0.6 eV. Binding energies were reported after correction for charging using the aliphatic C1s as a reference (B.E. 285.0 eV). Core-level spectra were fitted with a Shirley background and Gaussian peak functions.

Monolayer samples were investigated at the PM4-LowDosePES beamline at Helmholtz-Zentrum Berlin (BessyII Synchrotron Radiation facility), allowing for a lower flux on the sample, mandatory to avoid damaging the extremely thin layers of peptides. This soft X-ray bending magnet beamline is equipped with a Plane Grating Monochromator operating in collimated light (collimated PGM). It has two permanent end-stations, the reflectometer and the SURICAT (photoemission and X-ray absorption spectroscopy), which are in alternative operation. The LowDose PES end-station is equipped with an SES100 hemispherical analyzer [55]. Energy Resolution was estimated as 0.2 eV.

Conventional XPS studies were performed with an instrument designed by us, consisting of preparation and analysis chambers separated by a gate valve. The analysis chamber is equipped with a six-degree-of freedom manipulator and a 150-mm-mean radius hemispherical electron analyzer with a five-lens output system combined with a 16-channel detector. Ti2p, Nb3d, Zr3d, C1s, O1s, and N1s core level signals were recorded on the investigated samples unmonochromatized MgKα radiation; at least two specimens were analyzed for each sample type. Experimental spectra were analyzed by curve fitting using Gaussian curves as fitting functions; the analyzed spectra were energy referenced to the C1s signal of aliphatic–aromatic C–C carbons located at a binding energy B.E. = 285.0 eV [56,57]. Atomic ratios were calculated from peak areas using Scofield's cross as section sensitivity factors [58].

2.2.2. Near Edge X-ray Absorption Fine Structure Spectroscopy

Near Edge X-ray Absorption Fine Structure (NEXAFS) spectroscopy experiments were performed at the ELETTRA storage ring at the BEAR (bending magnet for emission absorption and reflectivity) beamline, installed at the left exit of the 8.1 bending magnet exit. The apparatus is based on a

bending magnet as a source, a beamline optics delivering photons from 5 eV up to about 1600 eV with a selectable degree of ellipticity. The UHV end station has a movable hemispherical electron analyzer and a set of photodiodes to collect angle resolved photoemission spectra, optical reflectivity, and fluorescence yield, respectively. Moreover, it is equipped with ammeters in order to measure the total electron yield from the sample for NEXAFS measurements [59]. The carbon and nitrogen K-edge spectra were collected at normal (90°), magic (54.7°), and grazing (20°) incidence angles of the linearly polarized photon beam with respect to the sample surface. The photon energy and resolution (Energy Resolution: C K-edge 0.13 eV; N K-edge 0.2 eV) were calibrated and experimentally tested at the K absorption edges of Ar, N_2, and Ne. In addition, our carbon K-edge spectra were further calibrated using the resonance at 285.50 eV assigned to the C1s π^* ring transition. The spectra were then normalized subtracting a straight line that fits the part of the spectrum below the edge and assessing to 1 the value at 320.00 eV and 425.00 eV for carbon and nitrogen, respectively [48].

2.3. Microscopy Techniques

2.3.1. Field Emission Scanning Electron Microscopy

(FE-SEM) imaging studies on functionalized Ti25Nb10Zr surfaces were performed at the Charles University (Prague, Czech Republic) as preliminary investigation by means of a HITACHI S-4800 field emission scanning electron microscope operating at 30 keV electron beam energy.

2.3.2. Atomic Force Microscopy

AFM images were recorded on functionalized Ti25Nb10Zr surfaces using an INNOVA microscope (Veeco, Plainview, NY, USA) operating in tapping mode. Each image was acquired on 512 lines with 0.3 Hz on 30 × 30 μm^2 area. The SPMLab analysis software (Veeco) was used for data processing.

3. Results

3.1. Characterization of Pristine Ti25Nb10Zr

3.1.1. Assessment of the Elemental Composition and Homogeneity

The composition of the pristine alloy surface was probed by EDS analysis; in Table S1, presented in Supplementary material, the elemental composition determined in four different zones of the alloy surface is shown. It presents the following composition: Ti 68.8 wt %, Nb 21.9 wt %, and Zr 9.3 wt %. No significant differences were observed among the areas, indicating that each element is homogenously distributed on the whole surface. The small differences in EDS alloy composition compared to the value provided by the manufacturer are due to the uncertainty of the investigative techniques. The manufacturing company determined the chemical composition by spark emission spectroscopy. In addition, Figure S1 in the Supporting Information shows the EDS mapping images of the Ti25Nb10Zr alloy performed on the surface corresponding to zone 4 of Table S1. It is evident that each element is evenly distributed over the investigated surface, indicating that the constituent elements are homogenously mixed.

3.1.2. Crystallographic Structure

The crystallographic structure of the pristine Ti25Nb10Zr alloy was ascertained by means of XRD measurements. The XRD profile is shown in Figure 1. The reflection peaks from both α″ (orthorhombic) and β (disordered body-centered cubic) phases were detected. Phases identifications were performed by matching each peak with the JCPDS files No. 44-1284 (α″ phase) and 44-1288 (β phase)—Figure 1. Some planes of α″ and β phases were overlapped. The α″ phase is observed to be the predominant phase. Taking into account the plane of α″ phase located at 34.2°, 40.7°, and 52.2°, the grain sizes, calculated by the Scherrer formula, are about 18.7 nm, 15.9 nm, and 18.5 nm respectively, leading to an

average of 17.7 nm. In the case of the β phase, taking into account the planes located at 55.7° and 95.4°, which are not overlapped on the α″ phase, the grain sizes were calculated to be 8.4 nm and 3.9 nm, with an average of 6.1 nm.

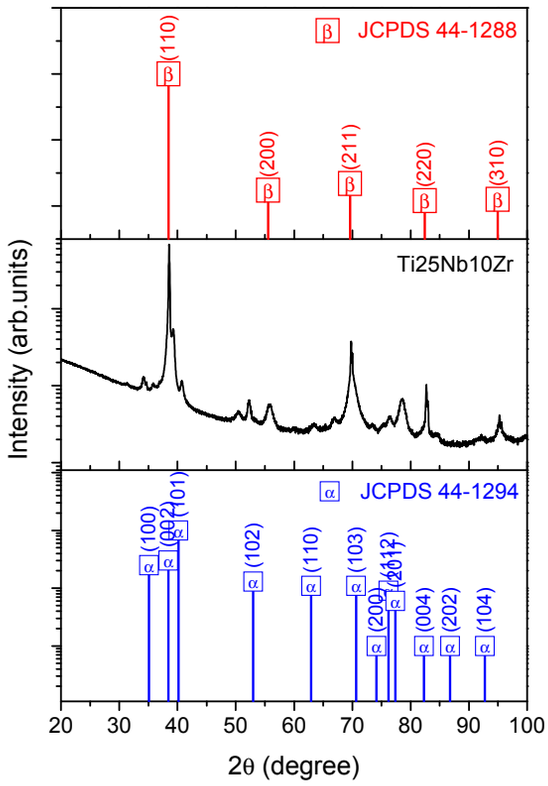

Figure 1. XRD diffraction pattern of Ti25Nb10Zr alloy and JCPDS files No. 44-1294 (α″ phase) and 44-1288 (β phase).

It is noteworthy that no diffraction peak of ω phase (hexagonal structure) was detected. This result is an advantageous one for the proposed alloy, because it is reported in the literature that ω phase causes embrittlement, leading to deterioration of mechanical properties [60–62].

3.1.3. Electrochemical Tests

Titanium has a good corrosion resistance in various corrosive environments such as seawater, organic chemicals, oxidizing or reducing acids over a wide range of concentrations and temperatures. This effect is due to oxide forming spontaneously and instantly when its surface is exposed to air and/or corrosive solutions [42]. Ishii et al. reported that the addition of a small amount (up to 3%) of alloying elements in the Ti matrix has a minor effect on the corrosion resistance of Ti in normally passive environments, while under active condition a small amount of alloying elements accelerate the corrosion process, leading to a significant deterioration of the alloy [42]. Thus, when we want to produce novel Ti-based alloys, the effect on its anticorrosive properties of the addition of a new alloying element in the basic matrix is the most important issue in determining whether the Ti passivity is lost and the surface has become fully active.

In the field of the design and production of novel materials for biomedical applications, the high corrosion resistance in physiological solutions is one the most important requirements, because it improves biocompatibility. Thus, for the present study, the Ti25Nb10Zr alloy was tested in terms of its corrosion resistance in two solutions: SBF and Hank at 37 ± 0.4 °C.

The evolution of the open circuit potential (E_{OCP}) during 15 h of immersion in SBF and Hank solutions at 37 °C is presented in Figure 2a. It is well known that a positive value of E_{OCP} indicates that the surface is coved with a protective oxide. In our study, one may see that the alloy immersed in

SBF exhibited a more negative value of E_{OCP} than that of alloy in Hank solution, but it was stabilized after 4 h of immersion. The evolution of E_{OCP} of Ti25Nb10Zr alloy immersed in Hank solution showed many fluctuations, indicating that the oxide is formed and destroyed due to the dissolution and re-passivation processes. This behavior is usually observed for metallic materials immersed in aggressive solutions, due to the presence of aggressive chloride or sulfate ions. Ti25Nb10Zr alloy tested in Hank solution showed some sudden falls of E_{OCP}, which can be attributed to the metastable pitting corrosion, apparently due to the pit anodic growth. After these falls, the E_{OCP} increased, indicating that the surface is re-passivated, by a cathodic oxygen-reduction reaction. This effect was also observed and reported in the literature by Isaacs et al. [63]. So, taking into account the E_{OCP} values, we can summarize that the Ti25Nb10Zr alloy is less affected by SBF attack.

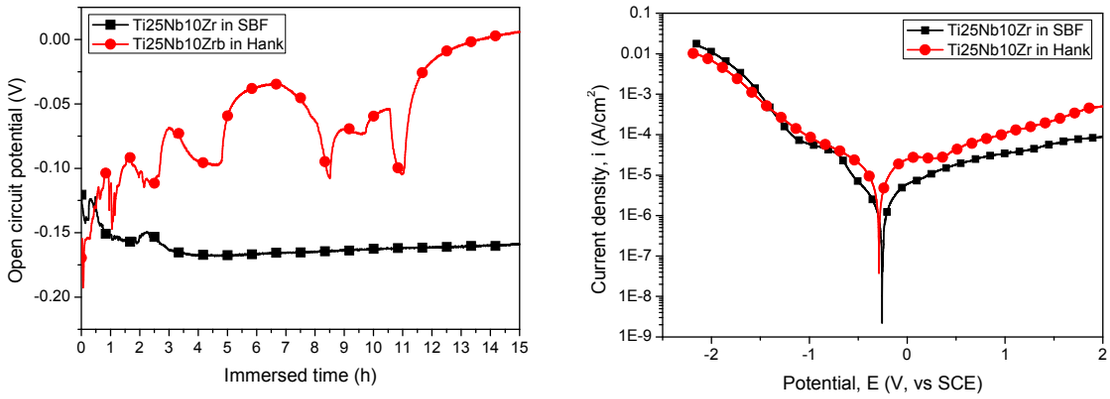

Figure 2. (**a**) Open circuit potential curves of Ti25Nb10Zr alloy in simulated body fluid (SBF) and Hank solutions (symbols are used only for identifying the curves in grey scale printing); (**b**) potentiodynamic polarization curves of Ti25Nb10Zr alloy in SBF and Hank solutions.

The potentiodynamic curves of the Ti25Nb10Zr alloy tested in SBF and Hank solutions at 37 °C are presented in Figure 2b. Based on these curves, the electrochemical parameters were determined, as summarized in Table 1. It is commonly accepted that a surface with a more electropositive corrosion potential, low corrosion current density, and high polarization resistance shows high corrosion behavior. Based on this statement, one may note that Ti25Nb10Zr alloy is more resistant to SBF corrosive attack. This result is also in good agreement with the corrosion rate results. A low corrosion rate was found for the alloy tested in SBF, indicating again that the alloy exhibited good resistance to SBF attack.

Table 1. The electrochemical parameters of Ti25Nb10Zr alloy after tests in simulated body fluid (SBF) and Hank solutions (E_{OCP}—open circuit potential; R_p—polarization resistance; E_{corr}—corrosion potential at $i = 0$; i_{corr}—corrosion current density; *CR*—corrosion rate). The E_{OCP} values were the last measured values in Figure 2a.

Electrolyte	E_{OC} (mV)	E_{corr} (mV)	i_{corr} (μA/cm^2)	R_p (Ω)	*CR* (mm/year)
SBF	−159	−253	1.15	45,011	0.011
Hank	6	−288	14.33	10,676	0.134

In the literature, it is reported that the corrosion rate is an inversely proportional relationship with pH, the corrosion rate decreasing when the pH increases [64]. In our study, the pH of solutions before corrosion tests was 7.4 for both solutions. After the corrosion tests, the pH values were 7.8 and 8.4 for SBF and Hank, respectively, indicating that the alloy is affected more or less by both solutions. In vivo, there is the possibility that the pH exceeds 7.8 in the vicinity of the implant, leading to an alkaline poisoning effect; all the physiological reactions will therefore be unbalanced and a more intense corrosion process will take place with a fast hydrogen evolution process [65]. On this basis,

it can be expected that the alloy does not affect the tissue in the vicinity of implant in vivo because is more resistant in SBF. It is important to mention that the Ti25Nb10Zr alloy demonstrated good viability and proliferation after five days of culture with MG63 cells, having values approximately 10% higher than pure Ti [64].

Figure 3 shows SEM micrographs of the Ti25Nb10Zr alloy before and after corrosion tests at different magnifications. The corrosion tests showed a visible indication of deterioration of alloy in both solutions. No cracks, pores or macro-segregations can be observed on the alloy surface before corrosion (Figure 3a). Some defects can be observed on the alloy surface, probably generated during the polishing process. In both corrosive solutions, the Ti25Nb10Zr alloy suffers a localized corrosion; a relatively uniform attack over the exposed surface of the alloy was found. After corrosion, on the alloy surfaces, pits and cracks can be seen which are the main damage to the surface. Under the Hank testing solution, the alloy corroded more severely compared with alloy tested in SBF solution. Many pits are observed on the alloy tested in Hank solution compared with the SBF one. The localized corrosion increased the current density. According to SEM images, the surface tested in Hank solution is more affected, leading to an increase of current density. This finding is in good agreement with the above potentiodynamic curves. Some grey deposits are found on the alloy surfaces tested in both solutions, which can be related to corrosion products.

The SEM analysis is in good accordance with the open circuit potential measurements and polarization tests.

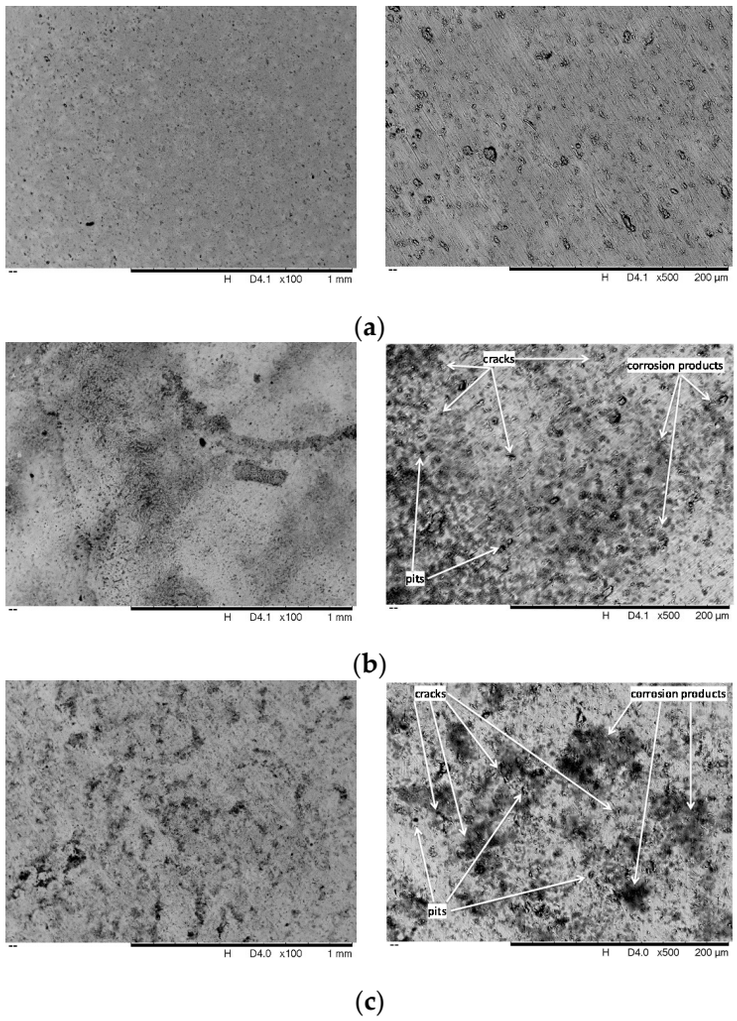

Figure 3. Scanning Electron Microscopy (SEM) images of the alloy surface before and after electrochemical tests. (**a**) Before corrosion; (**b**) after corrosion in SBF; (**c**) after corrosion in Hank.

3.1.4. Surface Composition

Pristine alloy discs were investigated by both Mg K-α source and SR-induced X-ray Photoelectron Spectroscopy (XPS) and with the aim to ascertain the chemical composition at the substrate surface; core level spectra of metal components, i.e., Ti, Nb, and Zr. Ti2p, Nb3d, and Zr3d signals were acquired, confirming the presence of the expected species TiO_2 (B.E. = 458.35 eV), Nb_2O_5 (B.E. = 206.98 eV) and ZrO_2 (B.E. = 182.10 eV) [56]. The observed atomic ratios Ti 75.4%, Zr 9.4%, Nb 15.2% do not exactly correspond to the expected stoichiometry due to the XPS sensitivity to the sample surface. In fact, since XPS is a surface-sensitive technique, the stoichiometry revealed refers to the outermost layers of the sample surface. Disparity with respect to the expected value could be due to phenomena of interdiffusion towards the outward layers.

Since pristine alloy XPS spectra were used as reference for the data analysis of the functionalized samples, O1s, C1s, and N1s core level signal, that are the most indicative for evaluating peptide grafting efficiency at different pH conditions, were also acquired. The O1s signal, reported in Figure 4a, shows a complex structure and, by following a peak-fitting procedure, at least three spectral components can be identified. The first peak at about 530 eV B.E. is attributed to the different metal oxides TiO_2, Nb_2O_5, and ZrO_2, which we were not able to discriminate, and therefore appear all grouped. At higher BE values a feature due to organic oxygen, arising by contaminating organic matter on the clean alloy surfaces (O–org, B.E. ~532 eV) can be singled out; a last component of lower intensity arising by physisorbed water is observed at about 533 eV B.E., as expected from literature for similar samples [65,66]. C1s spectrum is reported in Figure 4b. The curve fitting shows the presence of surface-contaminating carbons, leading to at least four contributions identified as aliphatic (C–C, B.E. = 285,0 eV), single-bonded to oxygen (C–O, B.E. = 286.23 eV), carbonyl-like (C=O, B.E. = 287.63 eV), and carboxyl-like (COOH, B.E. = 288.94 eV) carbons respectively. As expected, the N1s signal is not detected on the surface of "clean" samples.

On the other hand, a complete collection of B.E., Full Width Half Maximum (FWHM), Atomic Ratio values and Feature Assignments for the clean sample is reported in Table S2 in the Supporting Information.

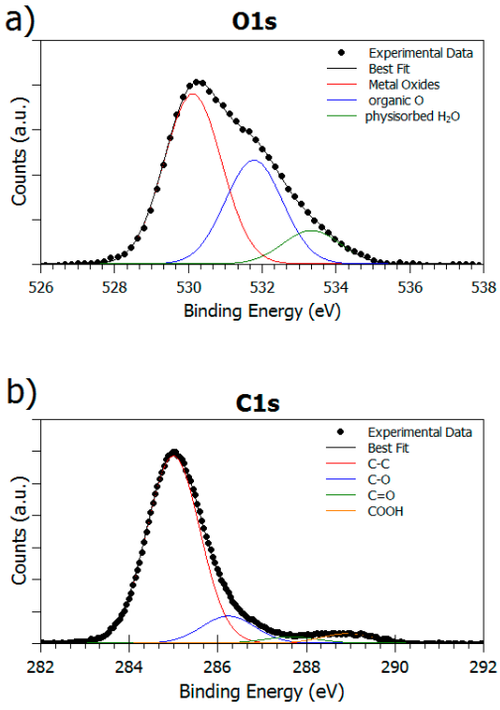

Figure 4. (**a**) XPS O1s and (**b**) XPS C1s spectra of the pristine sample surface.

3.2. Characterization of Ti25Nb10Zr Surfaces Functionalized with EAbuK16

3.2.1. Analysis of SAP Multilayer (MUL) Adsorbed at Different pH Values

Samples prepared as MULs from EAbuK16 solutions at pH 2, 4, 7, 10, and 12 were analyzed with both Mg K-α source and SR-induced radiation with the aim to probe molecular stability and anchoring efficiency at different pH values. As shown in Figure 5a for the sample prepared at pH 2 (taken as example), all samples show complex C1s signals (Figure 5a, top spectrum) which were analyzed by the curve-fitting procedure. The main component at lower B.E. values is attributed to aliphatic carbon atoms (C–C, B.E. = 285 eV) and was always used as calibration signal; the peak at about 286.3 eV BE is due to carbons bonded to nitrogens (as expected for aminoacids alpha-carbons, and lysine lateral groups) and/or oxygens; the third component is indicative of peptidic carbons N–C=O (amide-like, B.E. ~ 288.3 eV). The last feature, that can be observed as a small shoulder at higher BE values, is due to glutamic acid carboxyl groups (COOH, B.E. ~ 289 eV) [50,57]. C atoms due to contaminants are also observed in samples functionalized with peptides, giving rise to a signal that is superimposed to the peptide-one, but their amount is comparable in all investigated samples, since they were all treated by following the same procedure.

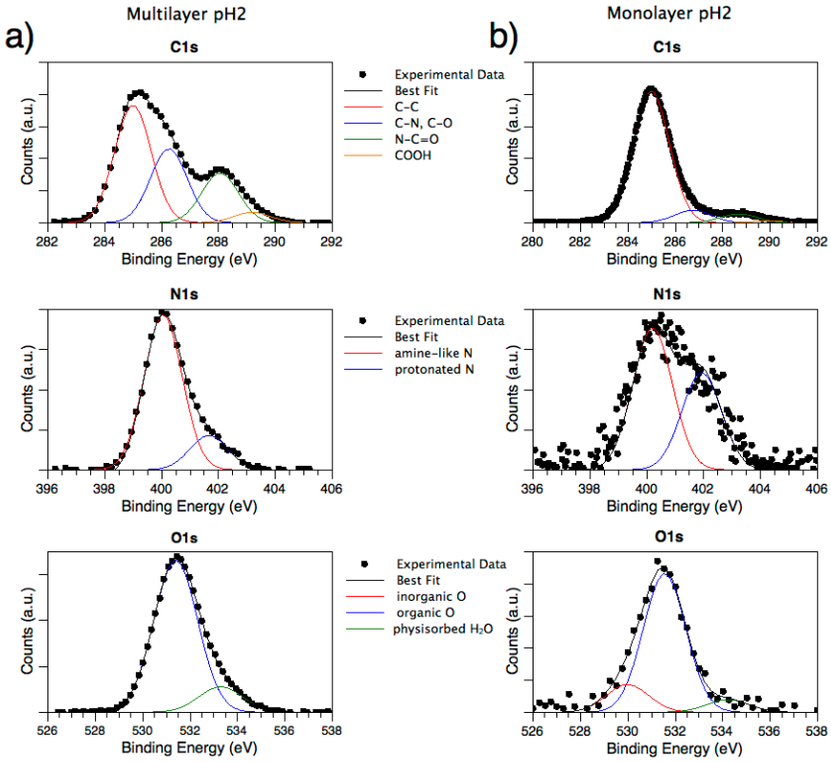

Figure 5. (**a**) X-ray Photoemission Spectroscopy (XPS) C1s, N1s, O1s MUL sample pH 2; (**b**) XPS C1s, N1s, O1s ML sample pH 2.

A complete collection of B.E. and FWHM values is reported in Tables S3 and S4 of Supporting Information. Quantitative estimations of different functional groups are reported in the following Table 2.

By exposing metal substrates to peptide solution, the signals related to nitrogen appear. More in detail, we can discriminate between protonated (B.E. ~ 402 eV) and non-protonated nitrogens (B.E. ~ 400 eV), as expected for peptides layers on metal surfaces, as shown in Figure 5a (spectrum in the middle) [50,57] O1s signals (Figure 5a, bottom) were also collected and compared with the ones observed for the clean substrate. Different from pristine alloy spectra, where all three oxygen species were detected, for MUL samples the signal related to metal oxides is absent, except in pH 7 and pH 12

samples. This indicates that in these two samples the peptide layer is thinner than in others, and since photoelectrons coming from metals are also detected, it is possible to estimate the peptide overlayer thickness by calculating the $Ti2p_{3/2}$ signal's intensity attenuation in samples with peptide, with respect to the signal intensity in a clean sample, according to equation 3.13 in [58].

Table 2. Atomic ratios of the species present on the multilayer (MUL) Self Assembling Peptide (SAP) surface. N^+: protonated nitrogen; $Me–O_x$: oxygen of metal oxides; O–org: organic oxygen.

MUL Sample	C–N/C–C Ratio	N–C=O/C–C Ratio	COOH/C–C Ratio	N_{tot}/C_{tot} Ratio	N/C_{-SAP} Ratio	N^+/N_{tot} (%) Ratio	O–org/Me–O_x Ratio	C_{-SAP}/Ti Ratio	SAP Thickness (nm)
pH 2	0.63	0.42	0.09	0.18	0.90	18.11	—	—	—
pH 4	0.57	0.37	0.05	0.14	0.77	15.57	—	—	—
pH 7	0.37	0.13	0.17	0.02	0.28	0.00	1.29	4.07	1.54
pH 10	0.56	0.37	0.06	0.16	0.87	10.99	—	—	—
pH 12	0.48	0.27	0.10	0.11	0.76	11.33	1.75	8.17	4.31

Calculated MUL thicknesses for pH 7 and pH 12 are reported in the last column of Table 2.

As for the semiquantitative analysis, C–N/C–C and N–C=O/C–N ratios are more or less constant in all samples, except for sample pH 7, where they are the lowest, as observed in Table 2. This could be due to peptide degradation or non-uniform deposition, as seen in microscopy images, since it has also a greater component related to oxidized carbons (COOH).

3.2.2. Analysis of SAP Monolayer (ML) Adsorbed at Different pH Values

As already observed for MULs, MLs samples (investigated by SR-induced XPS) show complex C1s signals due to the presence of different functional groups, as depicted in Figure 5b for the pH 2 sample. Similar to MULs, B.E. values were calibrated according to C–C aliphatic carbon (285.0 eV); all contributions show the expected value: main peak C–C 285.0 eV B.E., C–N ~ 286.3 eV BE, N–C=O (amide-like) ~ 288.3 eV BE and COOH ~ 289 eV BE. Atomic ratios, reported in Table 3, show a very high amount of aliphatic carbons with respect to MULs, probably due to the higher relative amount of contaminants with respect to the amount of immobilized peptide. However, the relative amounts of C1s spectral components are not influenced by the preparation pH, confirming that the molecular structure of the oligopeptides is always preserved in the anchoring process.

Table 3. Atomic ratios of the species present on ML. N^+: protonated nitrogen; $Me–O_x$: oxygen of metal oxides; O–org: organic oxygen.

ML Sample	C–N/C–C Ratio	N–C=O/C–C Ratio	COOH/C–C Ratio	N_{tot}/C_{tot} Ratio	N/C_{-SAP} Ratio	N^+/N_{tot} (%) Ratio	O–org/Me–O_x Ratio	C_{-SAP}/Ti Ratio	SAP Thickness (nm)
pH 2	0.44	0.25	0.10	0.11	0.77	13.47	24.76	2.91	1.22
pH 4	0.42	0.21	0.12	0.06	0.23	9.20	1.83	13.41	3.10
pH 7	0.34	0.12	0.10	0.04	0.58	4.13	1.04	1.76	1.28
pH 10	0.38	0.19	0.12	0.05	0.46	0.00	1.67	4.07	2.52
pH 12	0.32	0.16	0.11	0.04	0.42	0.00	0.96	2.15	1.32

As expected, all samples present a N1s signal; by applying a peak fitting procedure two main components related to protonated and unprotonated nitrogen atoms can be singled out, as already discussed for MULs. It is noteworthy that the intensity of protonated nitrogen decreases along with the increasing solution alkalinity, as expected (see Table 3). The N1s components trend is clearly observable in the following Figure 6.

Differently from MUL samples, O1s spectra show all the components observed for pristine samples, i.e., Me–O (~530 eV BE), C–O (~532 eV BE), and physisorbed water (~533 eV BE). The peptide coverage in MLs prepared at neutral and basic pH values (i.e., pH = 7, 10, 12), in fact, is not so thick as to completely screen the substrate signal, as observed in multilayers. This allows the layer thickness to be estimated from the substrate signal attenuation for ML prepared at these three pH values, as reported

in Table 3. The trend observed in film thickness is supported by the rough titanium spectra, shown in the following Figure 7.

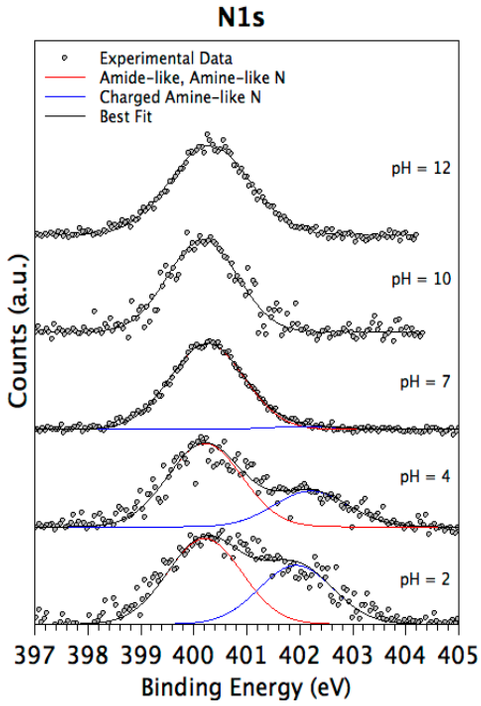

Figure 6. XPS N1s spectra collected on the four monolayer (ML) samples prepared with decreasing pH values.

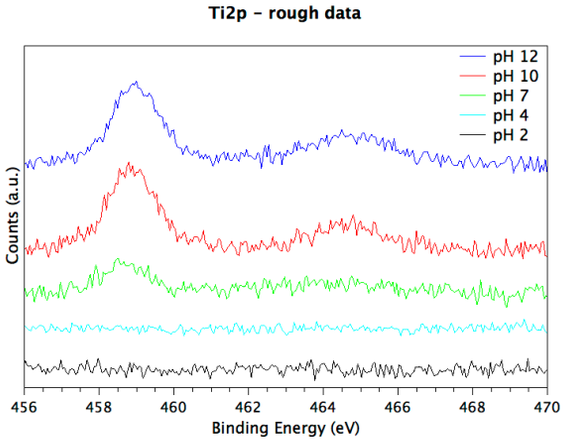

Figure 7. Rough Ti2p spectra, showing the attenuation of substrate signal with decreasing pH, indicative for a better peptide adsorption.

The observed experimental evidence (C1s components composition preserved in all samples, Ti2p signal attenuation increased with decreasing pH, film thicknesses increased at low pHs, protonated nitrogen component appearing at lower pHs) all concurs to confirm the oligopeptide stability upon anchoring at the titanium alloy surface, and to point out a better surface functionalization performance at low pH values, in good agreement with previous studies carried out on titania surfaces [50,51]. This effect could be related to the net charge of the EAbuK peptide; due to amidation of the carboxyl terminal, the investigated sample has a basic function more than an acidic one and a resulting net charge of +1, increasing peptide solubility at low pH.

3.2.3. Near Edge X-ray Absorption Fine Structure Spectroscopy

NEXAFS (Near Edge X-ray Absorption Fine Structure) is an X-ray absorption technique that, when performed in Angular Dependent mode (i.e., by measuring the X-rays absorption as a function of the incidence angle of the impinging photons with respect to the sample surface), can be usefully applied to evidence whether the peptide molecules are oriented with respect to the surface [51,67]. Data were collected at the C and N K-edges for both MULs and MLs. When the peptide is oriented and organized with respect to the surface a difference in radiation absorption is expected when the angle of the impinging radiation is changed from grazing to normal. The magic incidence is the peculiar angle at which the signal looks as if the peptide was not organized.

The carbon spectrum of MUL prepared at pH 2 is reported in the following Figure 8a; in C K-edge spectrum several structures can be observed in both π* and σ* resonances region. The sharp feature at about 288.7 eV is assigned to a C1s → π* transition of C=O molecular orbital, the shoulder around 288 eV to a σ* resonance by the C–H groups, additional features at ≈293 and ≈303 eV can be associated to 1 s → σ* transitions by the C–C and respectively C=O molecular groups.

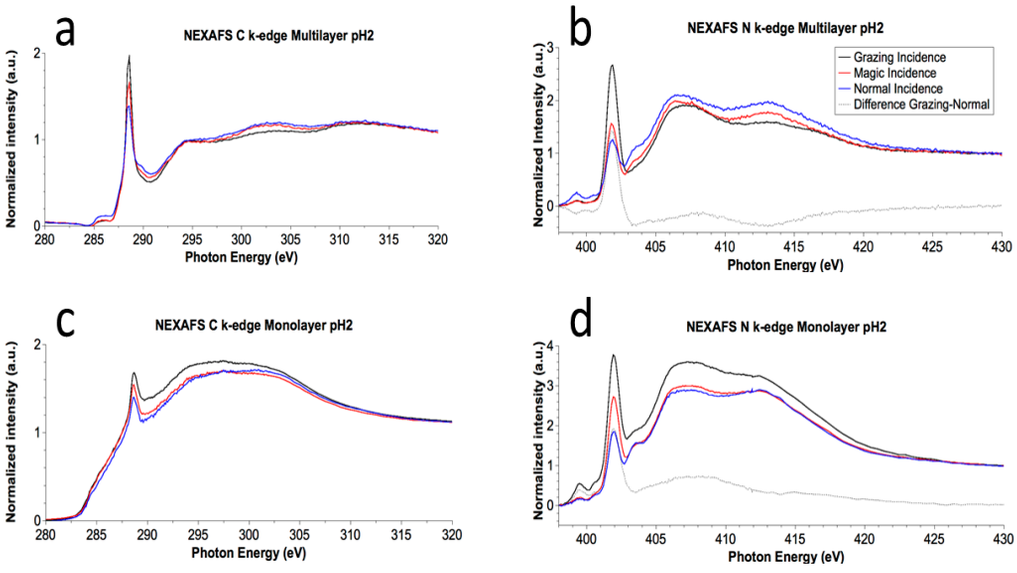

Figure 8. (**a**) C K-edge Near Edge X-ray Absorption Fine Structure (NEXAFS) spectrum of EAbuK multilayer deposited at pH = 2; (**b**) N K-edge NEXAFS spectrum of EAbuK at pH = 2; (**c**) C K-edge NEXAFS spectrum of EAbuK monolayer deposited at pH = 2; (**d**) N K-edge NEXAFS spectrum of EAbuK monolayer at pH = 2.

N K-edge spectra (Figure 8b, MUL pH 2, as an example) show the π* (402 eV) and σ* features (406 eV and ~413 eV) associated with the electronic transitions from N1s to the related antibonding molecular orbitals, as expected from the molecular structure and amino acids sequence [50,51].

The single transition π → π* and the two σ → σ* are represented by the sharp strong peak at 402 eV and 406eV and 412 eV respectively. It is noteworthy how the intensity of transitions π → π* increases from normal to grazing incidence while the intensity of σ → σ* transitions decreases.

ML spectra are completely analogous, as shown in Figure 8c,d for the ML prepared at pH = 2.

The angular dependence analysis evidences changes in the relative intensity for the π* and σ* at different angle resonances in all samples, both MUL and ML, a phenomenon that can be associated with molecular orientation with respect to the surface.

The dichroic behavior of the π* band associated with the peptide bond allowed the tilt angle to be calculated between the π* vector orbital of the peptide bond and normal to the surface, by using the equation reported by Stöhr [67] for threefold or higher symmetry substrates, with a polarization factor $p = 0.95$, and the intensity ratio $I_{20^\circ}/I_{90^\circ}$ determined for the selected resonance by peak fitting

of the experimental data. For the samples prepared at pH 2, the calculated value for the angle gives rise to a value of the tilt angle between the peptide bond axis (the axis of the main chain) and the substrate surface of nearly 80° (ML θ = 80.2°; MUL θ = 78.2°) for a β-sheet conformation of the peptide backbone. Considering that the incertitude on the tilt angle evaluation is 15% of the calculated value, the two systems have approximately the same molecular orientation.

3.3. Microscopy Analysis

3.3.1. FESEM Analysis

FESEM analysis was performed on MULs in order to investigate whether the peptide aggregates give rise to any peculiar structure. The result is that the peptide covers evenly the surface without assembling in any microscopic or nanoscopic structure detectable with this technique. For all here reported images the yellow bar is 200 μm, except for Figure 9D where the bar is 5 μm. The pristine surface (Figure 9A) appears quite smooth and regular, and peptide immobilization at pH 2, 10 and 12 does not change the appearance (Figure 9B,F,G, respectively). At pH 7 (Figure 9E) the peptide multilayer does not evenly cover the surface, most likely making the layer appear thin at XPS analysis. This result is likely due to the presence of phosphate in solution, in fact the sample prepared without Hank solution is analogous to the other ones. The pH 4 sample (Figure 9C) shows the thickest layer: in fact the peptide surface is extensively cracked because of its thickness. The yellow square identifies the region magnified in Figure 9D, where it is evident how the peptide makes a really thick layer that detaches from the substrate.

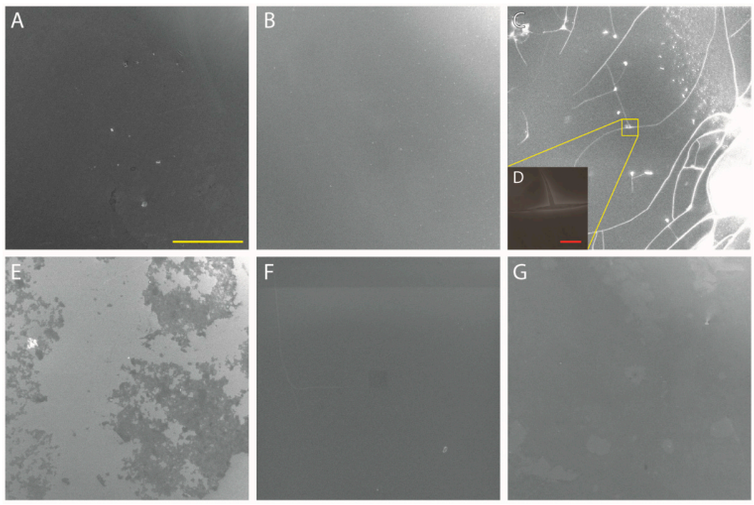

Figure 9. Field Emission Scanning Electron Microscopy (FESEM) images of MUL samples. (**A**): Pristine surface; (**B**): pH 2; (**C**): pH 4; (**D**): magnification of pH 4 region of interest; (**E**): pH 7; (**F**): pH 10; (**G**): pH 12. Yellow bar = 200 μm; Red bar (only D) = 5 μm.

3.3.2. AFM Measurements

Figure 10 shows AFM images acquired on all samples and on pristine surface. RMS values reported in Table 4 refer to the 900 μm^2 areas illustrated in Figure 10. It is evident how MUL samples show a more uniform surface with respect to the ML ones, especially at acidic pHs. According to the thickness evaluation reported in Tables 3 and 4, a thicker layer hides surface irregularity thus establishing an even surface. The pristine surface AFM image is shown in Supplementary Material Figure S2.

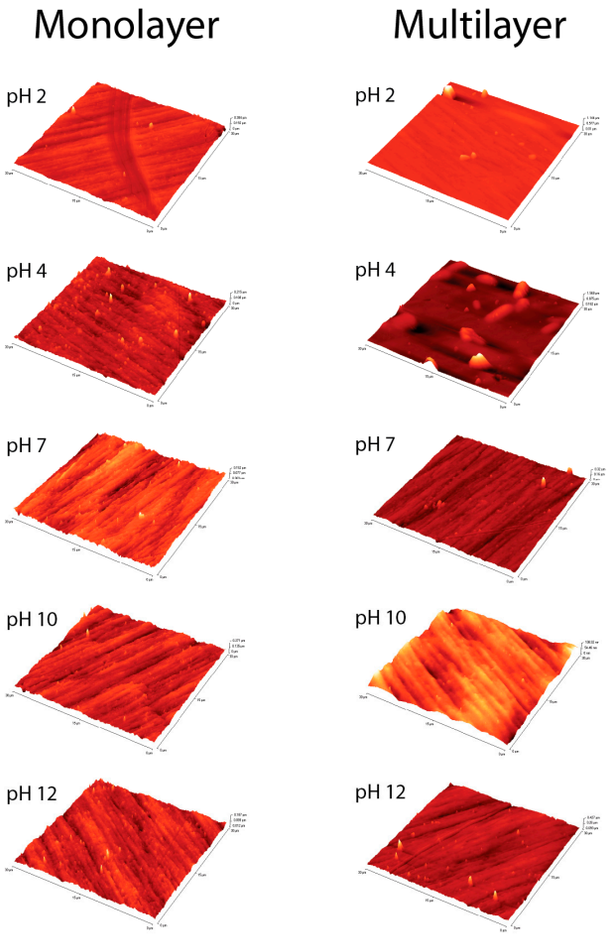

Figure 10. Atomic Force Microscopy (AFM) images of ML and MUL samples. It is evident how surfaces are more uniform at acidic pH. Pristine surface is shown in Supplementary Material Figure S2.

Table 4. Root mean square (RMS) roughness values for multilayer samples (MUL) and monolayer samples (ML).

Sample	RMS (μm)	
Clean Surface	0.0143	
	MUL RMS (μm)	ML RMS (μm)
pH 2	0.0181	0.0446
pH 4	0.0136	0.1067
pH 7	0.0155	0.0136
pH 10	0.0201	0.0141
pH 12	0.0127	0.0174

4. Conclusions

A new titanium alloy for orthopedic prostheses, containing Nb and Zr, was prepared by CCLM technique and characterized by various different techniques. Accurate characterization of the pristine alloy was carried out, revealing homogeneous mixing of the constituent elements (EDS), the presence of both α″ (orthorhombic) and β (disordered body-centered cubic) crystalline phases (XRD) and a TiO_2, Nb_2O_5, and ZrO_2 surface composition (XPS); moreover, electrochemical tests showed that Ti25Nb10Zr alloy corroded more heavily in Hank than in SBF solution, useful information for surface functionalization with peptides. We subsequently investigated the adsorption of EAbuK16, a self-assembling peptide, as a function of pH of the mother solution, both in the monolayer and multilayer. XPS analysis revealed that the amount of adsorbed peptide increases with decreasing

pH of the investigated solutions. FESEM and AFM analysis confirmed the formation of a thick and homogenous overlayer at acidic pH. This effect is probably related to the net EAbuK charge of +1, which increases peptide solubility at low pH. NEXAFS investigation yielded evidence of molecular order and orientation of the peptide overlayer with respect to the substrate surface. Formation of an ordered SAP scaffold on the alloy surface should increase osteoblast adhesion to the material surface, thus improving osseo-integration.

Supplementary Materials: The following are available online at http://www.mdpi.com/2079-4991/8/3/148/s1, Figure S1: Total EDS mapping spectrum and relative distribution of the concentration of each constituent element on the Ti25Nb10Zr alloy surface performed in a one scanned zone on the surface, Figure S2: AFM image of Clean Surface Sample, Table S1: The elemental composition of the alloy determined by EDS measurements, Table S2: Binding Energies in eV of the atomic species present on the Clean Surface Sample and the relative atomic ratios, Table S3: Binding Energies in eV of the atomic species present on the MUL sample surface, Table S4: Binding Energies in eV of the atomic species present on the ML sample surface.

Acknowledgments: The authors acknowledge the CERIC-ERIC Consortium for access to experimental facilities and financial support. Part of the present work was supported under a grant of the Romanian National Authority for Scientific Research, CNCS—UEFISCDI, project number PN-II-PT-PCCA-2014-212 (OSSEOPROMOTE). We thank HZB for the allocation of synchrotron radiation beamtime.

Author Contributions: S.F., G.I. and C.B. conceived and designed the experiments; V.S. and M.S. performed the experiments and analyzed the data; M.D. and A.Z. synthesized the self assembling peptide, A.V. and M.B. prepared the alloy and investigated their phase composition, corrosion resistance and morphology after corrosion tests, and also the AFM of alloy pristine surfaces, T.S. helped and assisted the measurements at MSB, J.N. performed FESEM imaging.

Conflicts of Interest: The authors declare no conflict of interest. The founding sponsors had no role in the design of the study; in the collection, analyses, or interpretation of data; in the writing of the manuscript, and in the decision to publish the results.

References

1. Faria, A.C.L.; Rodrigues, R.C.S.; Rosa, A.L.; Ribeiro, R.F. Experimental titanium alloys for dental applications. *J. Prosthet. Dent.* **2014**, *112*, 1448–1460. [CrossRef] [PubMed]
2. Textor, M.; Sittig, C.; Frauchiger, V.; Tosatti, S.; Brunette, D.M. Properties and biological significance of natural oxide films on titanium and its alloys. In *Titanium in Medicine*; Springer: Berlin/Heidelberg, Germany, 2001; pp. 171–230.
3. Shah, F.A.; Trobos, M.; Thomsen, P.; Palmquist, A. Commercially pure titanium (cp-Ti) versus titanium alloy (Ti6Al4V) materials as bone anchored implants—Is one truly better than the other? *Mater. Sci. Eng. C* **2016**, *62*, 960–966. [CrossRef] [PubMed]
4. Dettin, M.; Zamuner, A.; Brun, P.; Castagliuolo, I.; Iucci, G.; Battocchio, C.; Messina, M.; Marletta, G. Covalent grafting of Ti surfaces with peptide hydrogel decorated with growth factors and self-assembling adhesive sequences. *J. Pept. Sci.* **2014**, *20*, 585–594. [CrossRef] [PubMed]
5. Liu, X.; Chu, P.K.; Ding, C. Surface modification of titanium, titanium alloys, and related materials for biomedical applications. *Mater. Sci. Eng. R* **2004**, *47*, 49–121. [CrossRef]
6. Özcan, M.; Hämmerle, C. Review: Titanium as a Reconstruction and Implant Material in Dentistry: Advantages and Pitfalls. *Materials* **2012**, *5*, 1528–1545. [CrossRef]
7. Brown, S.A.; Lemons, J.E. *Medical Applications of Titanium and Its Alloys: The Material and Biological Issues*; ASTM: West Conshohocken, PA, USA, 1996.
8. Elias, C.N.; Lima, J.H.C.; Valiev, R.; Meyers, A. Biomedical applications of titanium and its alloys. *JOM* **2008**, *60*, 46–49. [CrossRef]
9. Khorasani, A.M.; Goldberg, M.; Doeven, E.H.; Littlefair, G. Titanium in biomedical applications—Properties and fabrication: A review. *J. Biomater. Tissue Eng.* **2015**, *5*, 593–619. [CrossRef]
10. Veiga, C.; Davim, J.P.; Loureiro, A.J.R. Properties and applications of titanium alloys: A brief review. *Rev. Adv. Mater. Sci.* **2012**, *32*, 133–148.
11. Geetha, M.; Singh, A.K.; Asokamani, R.; Gogia, A.K. Ti based biomaterials, the ultimate choice for orthopaedic implants—A review. *Prog. Mater. Sci.* **2009**, *54*, 397–425. [CrossRef]
12. Sidambe, A.T. Biocompatibility of Advanced Manufactured Titanium Implants—A Review. *Materials* **2014**, *7*, 8168–8188. [CrossRef] [PubMed]

13. Katzer, A.; Hockertz, S.; Buchhorn, G.H.; Loehr, J.F. In vitro toxicity and mutagenicity of CoCrMo and Ti6Al wear particles. *Toxicology* **2003**, *190*, 145–154. [CrossRef]
14. Satoh, K.; Sato, S.; Wagatsuma, K. Formation mechanism of toxic-element-free oxide layer on Ti–6Al–4V alloy in d.c. glow discharge plasma with pure oxygen gas. *Surf. Coat. Technol.* **2016**, *302*, 82–87. [CrossRef]
15. Lecocq, M.; Félix, M.S.; Linares, J.-M.; Chaves-Jacob, J.; Decherchi, P.; Dousset, E. Titanium implant impairment and surrounding muscle cell death following neuro-myoelectrostimulation: An in vivo study. *J. Biomed. Mater. Res. Part B* **2015**, *103*, 1594–1601. [CrossRef] [PubMed]
16. Hussein, M.A.; Mohammed, A.S.; Al-Aqeeli, N. Wear Characteristics of Metallic Biomaterials: A Review. *Materials* **2015**, *8*, 2749–2768. [CrossRef]
17. Mahapatro, A.J. Metals for biomedical applications and devices. *J. Biomater. Tissue Eng.* **2012**, *2*, 259–268. [CrossRef]
18. Niinomi, M.; Nakai, M.; Hieda, J. Development of new metallic alloys for biomedical applications. *Acta Biomater.* **2012**, *8*, 3888–3903. [CrossRef] [PubMed]
19. Okazaki, Y.; Rao, S.; Asao, S.; Tateishi, T.; Katsuda, S.; Furuki, Y. Effects of Ti, Al and V concentrations on cell viability. *Mater. Trans. JIM* **1998**, *39*, 1053–1062. [CrossRef]
20. Zhang, L.-C.; Attar, H.; Calin, M.; Eckert, J. Review on manufacture by selective laser melting and properties of titanium based materials for biomedical applications. *J. Mater. Technol.* **2016**, *31*, 66–76. [CrossRef]
21. Li, Y.; Yang, C.; Zhao, H.; Qu, S.; Li, X.; Li, Y. New Developments of Ti-Based Alloys for Biomedical Applications. *Materials* **2014**, *7*, 1709–1800. [CrossRef] [PubMed]
22. Hao, Y.-L.; Li, S.-J.; Yang, R. Biomedical titanium alloys and their additive manufacturing. *Rare Met.* **2016**, *35*, 661–671. [CrossRef]
23. Wang, L.; Lu, W.; Qin, J.; Zhang, F.; Zhang, D. Influence of cold deformation on martensite transformation and mechanical properties of Ti–Nb–Ta–Zr alloy. *J. Alloys Compd.* **2009**, *469*, 512–518. [CrossRef]
24. Tane, M.; Hagihara, K.; Ueda, M.; Nakano, T.; Okuda, Y. Elastic-modulus enhancement during room-temperature aging and its suppression in metastable Ti–Nb-Based alloys with low body-centered cubic phase stability. *Acta Mater.* **2016**, *102*, 373–384. [CrossRef]
25. Stenlund, P.; Omar, O.; Brohede, U.; Norgren, S.; Norlindh, B.; Johansson, A.; Lausmaa, J.; Thomsen, P.; Palmquist, A. Bone response to a novel Ti–Ta–Nb–Zr alloy. *Acta Biomater.* **2015**, *20*, 165–175. [CrossRef] [PubMed]
26. Okazaki, Y. A New Ti–15Zr–4Nb–4Ta alloy for medical applications. *Curr. Opin. Solid State Mater. Sci.* **2001**, *5*, 45–53. [CrossRef]
27. Okazaki, Y.; Gotoh, E. Comparison of fatigue strengths of biocompatible Ti-15Zr-4Nb-4Ta alloy and other titanium materials. *Mater. Sci. Eng. C* **2011**, *31*, 325–333. [CrossRef]
28. Banerjee, R.; Nag, S.; Stechschulte, J.; Fraser, H.L. Strengthening mechanisms in Ti–Nb–Zr–Ta and Ti–Mo–Zr–Fe orthopaedic alloys. *Biomaterials* **2004**, *25*, 3413–3419. [CrossRef] [PubMed]
29. Nag, S.; Banerjee, R.; Fraser, H.L. Microstructural evolution and strengthening mechanisms in Ti–Nb–Zr–Ta, Ti–Mo–Zr–Fe and Ti–15Mo biocompatible alloys. *Mater. Sci. Eng. C* **2005**, *25*, 357–362. [CrossRef]
30. Liu, Y.Z.; Zu, X.T.; Qiu, S.Y.; Wang, L.; Ma, W.G.; Wei, C.F. Surface characterization and corrosion resistance of Ti–Al–Zr alloy by niobium ion implantation. *Nucl. Instrum. Methods Phys. Res. Sect. B* **2006**, *244*, 397–402. [CrossRef]
31. Chaves, J.M.; Florêncio, O.; Silva, P.S.; Marques, P.W.B.; Afonso, C.R.M. Influence of phase transformations on dynamical elastic modulus and anelasticity of beta Ti–Nb–Fe alloys for biomedical applications. *J. Mech. Behav. Biomed. Mater.* **2015**, *46*, 184–196. [CrossRef] [PubMed]
32. Miyazaki, S.; Kim, H.Y.; Hosoda, H. Development and characterization of Ni-free Ti-base shape memory and superelastic alloys. *Mater. Sci. Eng. A* **2006**, *438–440*, 18–24. [CrossRef]
33. Bai, Y.; Hao, Y.L.; Li, S.J.; Hao, Y.Q.; Yang, R.; Prima, F. Corrosion behavior of biomedical Ti–24Nb–4Zr–8Sn alloy in different simulated body solutions. *Mater. Sci. Eng. C* **2013**, *33*, 2159–2167. [CrossRef] [PubMed]
34. Fojt, J.; Joska, L.; Málek, J. Corrosion behaviour of porous Ti–39Nb alloy for biomedical applications. *Corros. Sci.* **2013**, *71*, 78–83. [CrossRef]
35. Okazaki, Y.; Rao, S.; Asao, S.; Tateishi, T. Effects of metallic concentrations other than Ti, Al and V on cell viability. *Mater. Trans. JIM* **1998**, *39*, 1070–1079. [CrossRef]
36. Li, Y.; Wong, C.; Xiong, J.; Hodgson, P.; Wen, C. Cytotoxicity of titanium and titanium alloying elements. *J. Dent. Res.* **2010**, *89*, 493–497. [CrossRef] [PubMed]

37. Matsuno, H.; Yokoyama, A.; Watari, F.; Uo, M.; Kawasaki, T. Biocompatibility and osteogenesis of refractory metal implants, titanium, hafnium, niobium, tantalum and rhenium. *Biomaterials* **2001**, *22*, 1253–1262. [CrossRef]
38. Hickman, J.W.; Gulbransen, E.A. Oxide films formed on titanium, zirconium, and their alloys with nickel, copper, and cobalt. *Anal. Chem.* **1948**, *20*, 158–165. [CrossRef]
39. Yilmazbayhan, A.; Motta, A.T.; Comstock, R.J.; Sabol, G.P.; Laid, B.; Cai, Z. Structure of zirconium alloy oxides formed in pure water studied with synchrotron radiation and optical microscopy: Relation to corrosion rate. *J. Nucl. Mater.* **2004**, *324*, 6–22. [CrossRef]
40. Motta, A.T.; Gomes da Silva, M.J.; Yilmazbayhan, A.; Comstock, R.J.; Cai, Z.; Lai, B. Microstructural characterization of oxides formed on model Zr alloys using synchrotron radiation. *J. ASTM Int.* **2008**, *5*, 1–20. [CrossRef]
41. Wang, B.L.; Zheng, Y.F.; Zhao, L.C. Electrochemical corrosion behavior of biomedical Ti–22Nb and Ti–22Nb–6Zr alloys in saline medium. *Mater. Corros.* **2009**, *60*, 788–794. [CrossRef]
42. Ishii, M.; Kaneko, M.; Oda, T. *Titanium and Its Alloys as Key Materials for Corrosion Protection Engineering*; Shin-Nittetsu Giho: Tokyo, Japan, 2002; pp. 49–56.
43. Abdel-Hady, M.; Fuwa, H.; Hinoshita, K.; Kimura, H.; Shinzato, Y.; Morinaga, M. Phase stability change with Zr content in β-type Ti–Nb alloys. *Scr. Mater.* **2007**, *57*, 1000–1003. [CrossRef]
44. Kim, J.I.; Kim, H.Y.; Inamura, T.; Hosoda, H.; Miyazaki, S. Shape memory characteristics of Ti–22Nb–(2–8)Zr(at %) biomedical alloys. *Mater. Sci. Eng. A* **2005**, *403*, 334–339. [CrossRef]
45. Wang, B.L.; Li, L.; Zheng, Y.F. In vitro cytotoxicity and hemocompatibility studies of Ti-Nb, Ti-Nb-Zr and Ti-Nb-Hf biomedical shape memory alloys. *Biomed. Mater.* **2010**, *5*, 44102. [CrossRef] [PubMed]
46. Kim, J.I.; Kim, H.Y.; Inamura, T.; Hosoda, H.; Miyazaki, S. Effect of annealing temperature on microstructure and shape memory characteristics of Ti–22Nb–6Zr (at %) biomedical alloy. *Mater. Trans.* **2006**, *47*, 505–512. [CrossRef]
47. Nayak, S.; Dey, T.; Naskar, D.; Kundu, S.C. The promotion of osseointegration of titanium surfaces by coating with silk protein sericin. *Biomaterials* **2013**, *34*, 2855–2864. [CrossRef] [PubMed]
48. Franchi, S.; Battocchio, C.; Galluzzi, M.; Navisse, E.; Zamuner, A.; Dettin, M.; Iucci, G. Self-assembling peptide hydrogels immobilized on silicon surfaces. *Mater. Sci. Eng. C* **2016**, *69*, 200–207. [CrossRef] [PubMed]
49. Gambaretto, R.; Tonin, L.; Di Bello, C.; Dettin, M. Self-assembling peptides: Correlation among sequence, secondary structure in solution and film formation. *Biopolymers* **2008**, *89*, 906–915. [CrossRef] [PubMed]
50. Iucci, G.; Battocchio, C.; Dettin, M.; Gambaretto, R.; Polzonetti, G. A NEXAFS and XPS study of the adsorption of self-assembling peptides on TiO_2: The influence of the side chains. *Surf. Interface Anal.* **2008**, *40*, 210–214. [CrossRef]
51. Battocchio, C.; Iucci, G.; Dettin, M.; Carravetta, V.; Monti, S.; Polzonetti, G. Self-assembling behaviour of self-complementary oligopeptides on biocompatible substrates. *Mater. Sci. Eng. B* **2010**, *169*, 36–42. [CrossRef]
52. Kokubo, T.; Takadama, H. How useful is SBF in predicting in vivo bone bioactivity? *Biomaterials* **2006**, *27*, 2907–2915. [CrossRef] [PubMed]
53. Gilewicz, A.; Chmielewska, P.; Murzynski, D.; Dobruchowska, E.; Warcholinski, B. Corrosion resistance of CrN and CrCN/CrN coatings deposited using cathodic arc evaporation in Ringer's and Hank's solutions. *Surf. Coat. Technol.* **2016**, *299*, 7–14. [CrossRef]
54. Mansfeld, F.; Oldham, K.B. A modification of the Stern—Geary linear polarization equation. *Corros. Sci.* **1971**, *11*, 787–796. [CrossRef]
55. Erika, G.; Ruslan, O.; Florian, S.; Hikmet, S.; Alexander, F. LowDosePES: An End-Station for Low-Dose, Angular-Resolved and Time-Resolved Photoelectron Spectroscopy at BESSY II. In Proceedings of the Scientific Opportunities with Electron Spectroscopy and RIXS, HZB/BESSY II, Berlin, Germany, 16–18 October 2017.
56. Moulder, J.F.; Stickle, W.F.; Sobol, P.E.; Bomben, K.D. *Handbook of X-ray Photoelectron Spectroscopy*; Physical Electronics Inc.: Eden Prairie, MN, USA, 1996.
57. Beamson, G.; Briggs, D. *High Resolution XPS of Organic Polymers, The Scienta ESCA300 Database*; John Wiley & Sons: Chichester, UK, 1992.
58. Briggs, D.; Seah, M.P. *Practical Surface Analysis, Vol. 1, Auger and X-ray Photoelectron Spectroscopy*; John Wiley & Sons: Chichester, UK, 1994.

59. Nannarone, S.; Borgatti, F.; De Luisa, A.; Doyle, B.P.; Gazzadi, G.C.; Gigli, A.; Finetti, P.; Mahne, N.; Pasquali, L.; Pedio, M.; et al. The BEAR Beamline at Elettra. *AIP Conf. Proc.* **2004**, *705*, 450–453.
60. Kim, H.Y.; Ikehara, Y.; Kim, J.I.; Hosoda, H.; Miyazaki, S. Martensitic transformation, shape memory effect and superelasticity of Ti–Nb binary alloys. *Acta Mater.* **2006**, *54*, 2419–2429. [CrossRef]
61. Bowen, A.W. Omega phase embrittlement in aged Ti-15%Mo. *Scr. Metall.* **1971**, *5*, 709–715. [CrossRef]
62. Sass, S.L. The ω phase in a Zr-25 at % Ti alloy. *Acta Metall.* **1969**, *17*, 813–820. [CrossRef]
63. Isaacs, H.S.; Ishikawa, Y. Current and Potential Transients during Localized Corrosion of Stainless Steel. *J. Electrochem. Soc.* **1985**, *132*, 1288–1293. [CrossRef]
64. Thirumalaikumarasamy, D.; Shanmugam, K.; Balasubramanian, V. Comparison of the corrosion behaviour of AZ31B magnesium alloy under immersion test and potentiodynamic polarization test in NaCl solution. *J. Magnes. Alloys* **2014**, *2*, 36–49. [CrossRef]
65. Song, G. Control of biodegradation of biocompatable magnesium alloys. *Corros. Sci.* **2007**, *49*, 1696–1701. [CrossRef]
66. Cotrut, C.M.; Parau, A.C.; Gherghilescu, A.I.; Titorencu, I.; Pana, I.; Cojocaru, D.V.; Pruna, V.; Constantin, L.; Dan, I.; Vranceanu, D.M.; et al. Mechanical, in vitro corrosion resistance and biological compatibility of casted and annealed Ti25Nb10Zr alloy. *Metals* **2017**, *7*, 86. [CrossRef]
67. Stohr, J. *NEXAFS Spectroscopy*; Gomer, C., Ed.; Springer Series in Surface Sciences; Springer: Berlin, Germany, 1991.

Chapter 6

Biofunctionalization of TiO_2 Surfaces with Self-Assembling Layers of Oligopeptides Covalently Grafted to Chitosan

V. Secchi[a*], S. Franchi[b], D. Ciccarelli[a], M. Dettin[c], A. Zamuner[c], G. Iucci[a], C. Battocchio[a]

[a]Department of Science, Roma Tre University of Rome, Via della Vasca Navale 79, 00146 Rome, Italy;

[b]Elettra-Sincrotrone Trieste S.c.p.A., Strada statale 14, km 163.5 - 34149 Basovizza (Trieste), Italy;

[c]Department of Industrial Engineering, University of Padua, Via Marzolo, 9, Padua, 35131, Italy.

6. Biofunctionalization of TiO_2 Surfaces with Self-Assembling Layers of Oligopeptides Covalently Grafted to Chitosan

As seen in chapter 4-5 a promising approach to obtain a biocompatible and biomimetic implant based on titanium, is the functionalization of its surface with bioactive molecules like SAPs. However, recurring complications are infections related to an implant, that are among the leading reasons for failure with high economical and social associated costs. On this basis Anthony Gristina coined the term "race for the surface" to described a simplified model of implant-related infection, whereby host and bacterial cells compete for real estate on the implant's surface. According to this model, when the host cells colonize the implant surface first, the probability of attachment of bacterial cells is very low and vice versa. In line with these considerations, Gristina was acutely aware that biomaterial surfaces needed to be modified in order to prevent bacterial adhesion and colonization of implants and proliferation into the surrounding tissues and, at the same time, should promote osteointegration, offer tridimensional support for cells and promote cell adhesion. In this context a promising approach to obtain an implant based on titanium, that is at the same time bioactive, biomimetic and antibiotic, is the functionalization of its surface with (two) bioactive molecules: SAP and chitosan, a versatile hydrophilic polysaccharide derived from chitin, already known in the literature for the ability of its derivatives to firmly graft titanium alloys and show protective effects against some bacterial species either alone or in combination with other antimicrobial substances like antibiotics or antimicrobial peptides. In this work, I focus my attention to the chemical characterization, carried out by synchrotron radiation-induced X-ray Photoemission Spectroscopy (SR-XPS), angle-dependent Near Edge X-rays Absorption Fine Structure (NEXAFS) spectroscopy and IRRAS (Infrared reflection-absorption spectroscopy) of a biomaterial based on titanium coated with chitosan covalently functionalized with SAPs.

Da: **ACS Biomaterials Science & Engineering** onbehalfof@manuscriptcentral.com
Oggetto: Secchi, Valeria ab-2018-01304t Assigned to Editor 23-Oct-2018
Data: 24 ottobre 2018 00:09
A: valeria.secchi@uniroma3.it
Cc: valeria.secchi@uniroma3.it, stefano.franchi@elettra.eu, dav.ciccarelli@stud.uniroma3.it, giovanna.iucci@uniroma3.it, chiara.battocchio@uniroma3.it

AB

23-Oct-2018

RE: Manuscript Editor Assignment
Journal:ACS Biomaterials Science & Engineering
Manuscript ID: ab-2018-01304t
Title: "Biofunctionalization of TiO2 Surfaces with Self-Assembling Layers of Oligopeptides Covalently Grafted to Chitosan"
Authors: Secchi, Valeria; franchi, stefano ; ciccarelli, davide; Dettin, Monica; Zamuner, Annj; Iucci, Giovanna; Battocchio, Chiara

Dear Dr. Secchi:

Your manuscript entitled "Biofunctionalization of TiO2 Surfaces with Self-Assembling Layers of Oligopeptides Covalently Grafted to Chitosan" has been assigned to the following editor:

Dr. Chris Holland
Associate Editor
ACS Biomaterials Science & Engineering
Fax: 202-513-8254
Editor Email: holland-office@biomaterials.acs.org

Please address all future correspondence regarding this manuscript to the above editor.

Journal Publishing Agreement: ACS Biomaterials Science & Engineering offers an electronic Journal Publishing Agreement that can be completed from your Home page in ACS Paragon Plus. You will receive, in a separate email, instructions on how to access and submit your electronic Journal Publishing Agreement.

Submission of a manuscript to ACS Biomaterials Science & Engineering implies that the work reported therein has not received prior publication and is not under consideration for publication elsewhere in any medium, including electronic journals and computer databases of a public nature. This manuscript is being considered with the understanding that it is submitted on an exclusive basis. If otherwise, please advise.

Also please note that according to ACS Ethical Guidelines to Publication of Chemical Research, all authors must have reviewed and approved the submission of their manuscript. If you are a coauthor and approve its submission, no action is necessary. If you do not approve its submission to ACS Biomaterials Science & Engineering, please let us know as soon as possible. Refer to the manuscript number listed above in any correspondence, or you may simply reply to this message leaving the subject line intact. For more information on ethical responsibilities of authors, see the Ethical Guidelines to Publication of Chemical Research at http://pubs.acs.org/page/policy/ethics/index.html.

ACS Publications uses CrossCheck's iThenticate software to detect instances of similarity in submitted manuscripts. In publishing only original research, ACS is committed to deterring plagiarism, including self-plagiarism. Your manuscript may be screened for similarity to published material.

Sincerely,

Prof. David Kaplan
Editor-in-Chief
ACS Biomaterials Science & Engineering
Phone: 617-627-3251

Fax: 202-513-8021
Email: kaplan-office@biomaterials.acs.org

Biofunctionalization of TiO_2 Surfaces with Self-Assembling Layers of Oligopeptides Covalently Grafted to Chitosan

Valeria Secchi[1], Stefano Franchi[2], Davide Ciccarelli[1], Monica Dettin[3], Annj Zamuner[3], Giovanna Iucci[1], Chiara Battocchio[1]*

[1]Department of Science, Roma Tre University of Rome Via della Vasca Navale 79, 00146 Rome, Italy;

[2]Elettra-Sincrotrone Trieste S.c.p.A., Strada statale 14, km 163.5 - 34149 Basovizza (Trieste), Italy;

[3]Department of Industrial Engineering, University of Padua, Via Marzolo, 9, Padua, 35131, Italy.

*valeria.secchi@uniroma3.it

KEYWORDS. chitosan; self-assembling peptides; covalent functionalization, x-ray spectroscopies; self-assembling properties; layer-by-layer structures.

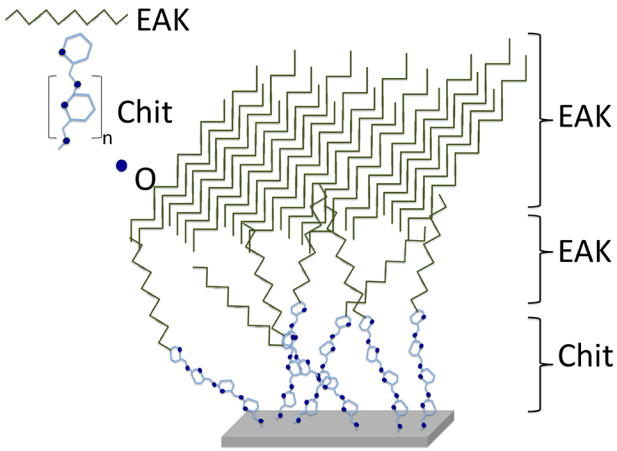

ABSTRACT

In the field of tissue engineering, a promising approach to obtain a bioactive, biomimetic and anti-biotic implant is the functionalization of a “classical” biocompatible material, as for example titanium, with appropriate biomolecules. For this purpose, we propose to prepare self-assembling films of multiple components, allowing mixing different biofunctionalities “on demand”. Self-assembling peptides (SAPs) are an appealing class of synthetic materials able to self-organize in nanostructures both in solution and as thin/thick films and adhere on titanium surface as a scaffold coating in order to mimic the extracellular matrix. Chitosan is a versatile hydrophilic polysaccharide derived from chitin, with a broad antimicrobial spectrum to which gram-negative, gram-positive bacteria and fungi are highly susceptible, already known in the literature for the ability of its derivatives to firmly graft titanium alloys and show protective effects against some bacterial species, either alone or in combination with other antimicrobial substances like antibiotics or antimicrobial peptides. In this context, we functionalized titanium surfaces with chitosan grafted to EAK16-II (a SAP) obtaining layer-by-layer structures of different degree of order, depending on the preparative stoichiometry and path. The chemical composition, molecular structure and arrangement of the obtained biofunctionalized surfaces were investigated by surface-sensitive techniques as Reflection-Absorption InfraRed Spectroscopy (RAIRS) and state-of-the-art synchrotron radiation-induced spectroscopies as X-ray Photoemission Spectroscopy (SR-XPS) and Near Edge X-rays Absorption Fine Structure (NEXAFS).

INTRODUCTION

Implanted biomaterials play a key role in current success of orthopedic, dental and trauma surgery. However, infections related to an implant are among the leading reasons for failure with high economical and social associated costs. These infections are the results of a complex interaction of various factors, including bacterial load, microorganism's and host's type, surgical procedure and technique, and type of implant and of antibacterial prophylaxis [1]. In 1987 Anthony Gristina coined the term a "race for the surface" to describe a simplified model of implant-related infection, whereby host and bacterial cells compete for real estate on the implant's surface [2,3]. According to this model, when the host cells colonize the implant surface first, the probability of attachment of bacterial cells is very low and vice versa [1]. Bacteria have successful and diversified strategies to adhere and survive on almost all natural and synthetic surfaces [4]. Surface characteristics of a biomaterial such as roughness, hydrophobicity, and electrostatic charge play only conditional roles [5], while a number of potential receptors for bacterial adhesive ligands are offered by the protein film that covers an implant immediately after its placement into the host body [6]. According to the current knowledge, probably the most critical pathogenic event in the development of implant-related infection is biofilm formation, which starts immediately after bacterial adhesion on an implant and effectively protects the microorganisms from the immune system and systemic antibiotics [1]. On the host side, the detailed process of implant osteo- and tissue-integration is also incompletely unveiled [7]. According to Gristina's model, host cells, once attached to implant surfaces, should lead to osteointegration, protecting the biomaterial against bacterial colonization [8]. However, bacteria may survive to osteointegration or to fibrous tissue encapsulation of

an implant, while peri-implant fibrous tissue may even prevent direct contact between host immunity cells and bacterial molecules, while the presence of the implant has been shown to impair innate local host response [9]. This is of utmost importance especially in patients with underlying compromised immunity and in those undergoing revision surgery in which the relative risk of infection is multiplied [10]. In line with these considerations, Gristina [8] was acutely aware that biomaterial surfaces needed to be modified in order to prevent bacterial adhesion and colonization of implants and proliferation into the surrounding tissues and, at the same time, to promote osteointegration, offer tridimensional support for cells and promote cell adhesion. Notably, surface modification remains the most frequently adopted route to reduce the incidence of biomaterial-associated infection [11]. In this context a promising approach to obtain an implant based on titanium, that is at the same time bioactive, biomimetic and anti-biotic, is the functionalization of its surface with (two) bioactive molecules: SAP and chitosan. Self-assembling peptides (SAPs) are an appealing class of synthetic materials suitable for this purpose, since they are capable to self-organize in nanostructures both in solution and as thin/thick films and adhere to the titanium surface as a scaffold coating in order to mimic the extracellular matrix [12]. The investigated SAP, EAK16-II is a self-complementary oligopeptide showing a selected sequence of the amino acids L-Alanine (A), L-Glutamic (E) acid and L-Lysine (K). The sequence (H-AEAEAKAKAEAEAKAK-NH_2), consisting of a regular alternation of positively (K) and negatively charged (E) residues separated by hydrophobic residues (A), makes EAK16-II (EAK in the following) capable of self-assembling from saline solution [13,14] generating ordered films with the peptide chains in β-sheet conformation. Chitosan is a versatile hydrophilic polysaccharide derived from chitin, with a broad antimicrobial spectrum toward gram-negative, gram-positive bacteria and fungi [15]. There is some

evidence that chitosan derivatives can be firmly anchored to titanium alloys and that they have a protective effect against some bacterial species either alone or in combination with other antimicrobial substances like antibiotics or antimicrobial peptides [16]. In this work, we present the chemical characterization, carried out by synchrotron radiation-induced X-ray Photoemission Spectroscopy (SR-XPS), angle-dependent Near Edge X-rays Absorption Fine Structure (NEXAFS) and Reflection-Absorption InfraRed Spectroscopy (RAIRS), of a biomaterial based on titanium bionfunctionalized with SAP covalently and selectively grafted to chitosan.

MATERIALS AND METHODS

Preparation of EAK-CHO

The solid phase peptide synthesis of EAK-CHO (sequence: H-Ala-Glu-Ala-Glu-Ala-Lys-Ala-Lys-Ala-Glu-Ala-Glu-Ala-Lys-Ala-Lys-7Ahp-Phe-H, where 7Ahp is 7-aminoheptanoic acid) was carried out in Fmoc Chemistry (scale 0.100 mmoles) using a Syro I synthesizer (Multisynthec, Witten, Germany). The side chain protection employed were: Glu, OtBu; Lys, Boc. The Fmoc removal was performed by two treatments with 40% and 20% piperidine/DMF for 3 min and 12 min respectively. The coupling reaction was carried out using 5-fold excess of Fmoc protected amino acid and HOBt/HBTU/DIPEA (5 equivalents of HOBt/HBTU and 10 equivalents of DPEA; 45 min) in DMF. The first four amino acids were condensated through single couplings, whilst all the remaining couplings were carried out in double. At the end of the synthesis, the Fmoc was removed and the resin was washed 3 times with DCM and dried under vacuum for 2hrs. The side chain protections were removed with 30 minutes TFA treatment. After DCM washes, the resin was dried under vacuum for 1 hr. The peptide

cleavage from the solid support was performed by addition of acetic acid: H_2O: DCM: methanol (10:5:64:21) mixture for 1 hr. The filtered solution and the following resin washings were collected and evaporated. After the addition of water the solution was freeze-dried. The crude peptide was purified in the following conditions: column, Nova Pak C18 (6μm, 60Å, 7.8×300 mm, Waters); eluent A, 0.05% TFA in MilliQ water; eluent B, 0.05% TFA in CH_3CN; gradient, from 10%B to 23%B in 52 min; flow rate, 4 mL/min; detection at 214 nm. The analytical characterization of the collected best fractions was carried out in these conditions: column, Vydac Everest C18; eluent A, 0.05% TFA in MilliQ water; eluent B, 0.05% TFA in CH_3CN; gradient, from 7%B to 27%B in 20 min; flow rate, 1 mL/min; detection at 214 nm. The target peptide retention time results 14.27 minutes. The identity of the purified product was ascertained by mass spectrometry (theoretical value=1874.18 Da, experimental value=1874.08 Da).

Covalent functionalization of chitosan with EAK-CHO

Chitosan (15 mg) was dissolved in 1.37 ml of 0.2 M acetic acid/H_2O under magnetic stirring. The solution was diluted adding 0.6 ml of ethanol. The pH was adjusted to 5.31 with 1N NaOH. The EAK-CHO peptide (15 mg; 8 μmoles) was dissolved in 1.75 ml of MilliQ water. The peptide solution was added to chitosan solution. Finally, 16.92 mg of $NaBH_3CN$ (0.27 mmoles) was dissolved. The reaction time was 24 hrs. The pH was changed to 7.0 through addition of 1N NaOH. The solution volume was doubled with ethanol. After 10 minutes stirring, the solution was cooled at 4°C to induce precipitation. The product was filtered (gooch G3) and dried under vacuum for 1 hr.

The transformation of nitrogen into nitrate for Chit and Chit-EAK samples in an elementary analysis assay [17] allowed the determination of 7.16 nmoles/mg as estimated functionalization of Chit-EAK.

Preparation of EAK

The synthesis, purification and characterization of EAK (sequence= H-Ala-Glu-Ala-Glu-Ala-Lys-Ala-Lys-Ala-Glu-Ala-Glu-Ala-Lys-Ala-Lys-NH_2 was reported elsewhere [18]

Chemicals

The solid support resin H-Phe-H NovaSyn (0.2 mmols/g) was from Novabiochem (Merck KGaA, Darmstadt, Germany). The Fmoc protected amino acids were from Novabiochem (Merck KGaA, Darmstadt, Germany). The coupling reagents 2-(1H -Benzotriazole-1-yl) -1,1,3,3-tetramethyluronium hexafluorophosphate (HBTU) and 1-Hydroxybenzotriazole (HOBt) were from Advanced Biotech (Seveso, MI, Italy). N,N-diisopropylethylamine (DIEA) and piperidine were from Biosolve (Leenderweg, Valkenswaard, Netherlands). Triethoxysilane (TES) was from Sigma-Aldrich (Steinheim, Germany). Solvents such as N,N-dimethylformamide (DMF), trifluoroacetic acid (TFA), N-methyl-2-pyrrolidone (NMP) and dichloromethane (DCM) were from Biosolve (Leenderweg, Valkenswaard, Netherlands). Chitosan 70/1000 was purchased by Heppe Medical Chitosan GmbH (Halle, Germany).

Layer-by-layer structures preparation

In order to prepare EAK and Chit-EAK samples, TiO_2/Si(111) or Au/Si(111) surfaces were incubated overnight with mother solution of the selected biomolecules (0.4 mg of EAK or respectively Chit-EAK dissolved in in 120 μL of CH_3COOH 0.2M water solution).

Samples Chit-EAK/EAK (a) and (b) were prepared by incubation of the metal substrates with mother solutions containing:

- 0.4 mg of Chit-EAK + 0.012 mg of EAK in 0.12mL of CH_3COOH 0.2M (Chit-EAK/EAK (a))

- 0.4 mg of Chit-EAK + 0.12 mg of EAK in 0.12mL of CH_3COOH 0.2M (Chit-EAK/EAK (b))

After incubation, samples were washed twice with Milli-Q water.

Synchrotron radiation (SR)-induced x-ray Photoelectron Spectroscopy (SR-XPS) measurements were performed at the materials science beamline (MSB) at the Elettra synchrotron radiation source (Trieste, Italy). MSB, placed at the left end of the bending magnet 6.1, is equipped with a plane grating monochromator that provides light in the energy range of 21–1000 eV. The UHV endstation, with a base pressure of 2×10^{-10} mbar, is equipped with a SPECS PHOIBOS 150 hemispherical electron analyzer, low-energy electron diffraction optics, a dual-anode Mg/Al X-ray source, an ion gun, and a sample manipulator with a K-type thermocouple attached to the rear side of the sample. Photoelectrons emitted by C1s, O1s and N 1s core levels were detected at normal emission geometry using photon energy of 630 eV impinging at 60°. Binding energies (BEs) are reported after correction for charging using the aliphatic C 1s as a reference (BE 285.0 eV) [19]. Core level spectra were fitted with a Shirley background and Gaussian peak functions [20,21].

Near Edge x-ray Absorption Fine Structure (NEXAFS) spectroscopy experiments were performed at the ELETTRA storage ring at the BEAR beamline (bending magnet for emission absorption and reflectivity). BEAR is installed at the left exit of the 8.1 bending magnet exit. The apparatus is based on a bending magnet as a source and beamline optics delivering photons from 5 eV up to about 1600 eV with selectable degree of ellipticity. The UHV end station has a movable hemispherical electron analyzer and a set of

photodiodes to collect angle resolved photoemission spectra, optical reflectivity and fluorescence yield. In these experiments ammeters to measure drain current from the sample for NEXAFS measurements were used. The carbon and nitrogen K-edge spectra were collected at normal (90°), grazing (20°) and magic (54.7°) incidence angles of the linearly polarized photon beam with respect to the sample surface. The photon energy and resolution were calibrated and experimentally tested at the K absorption edges of Ar, N_2 and Ne. Spectra were then normalized subtracting a straight line that fits the part of the spectrum below the edge and assessing to 1 the value at 320.00 eV and 425.00 eV for carbon and nitrogen, respectively.

Reflection-Absorption InfraRed Spectroscopy (RAIRS) measurements were performed by means of a VECTOR 22 (Bruker) FT-IR interferometer operating in the wavenumber range 400-4000 cm^{-1}, with a resolution of 1 cm^{-1}, equipped with a Specac P/N 19650 series monolayer/grazing angle accessory and with a DTGS detector. Spectra were recorded at incidence angles of 70° with respect to the normal to the sample surface.

RESULTS AND DISCUSSION

Chemical composition and biomolecules stability

Evolution of the C1s and O1s photoelectron spectra of the investigated systems deposited on TiO_2 is displayed in figure 1; the spectra of samples deposited on gold substrates substrates show an analogous trend.

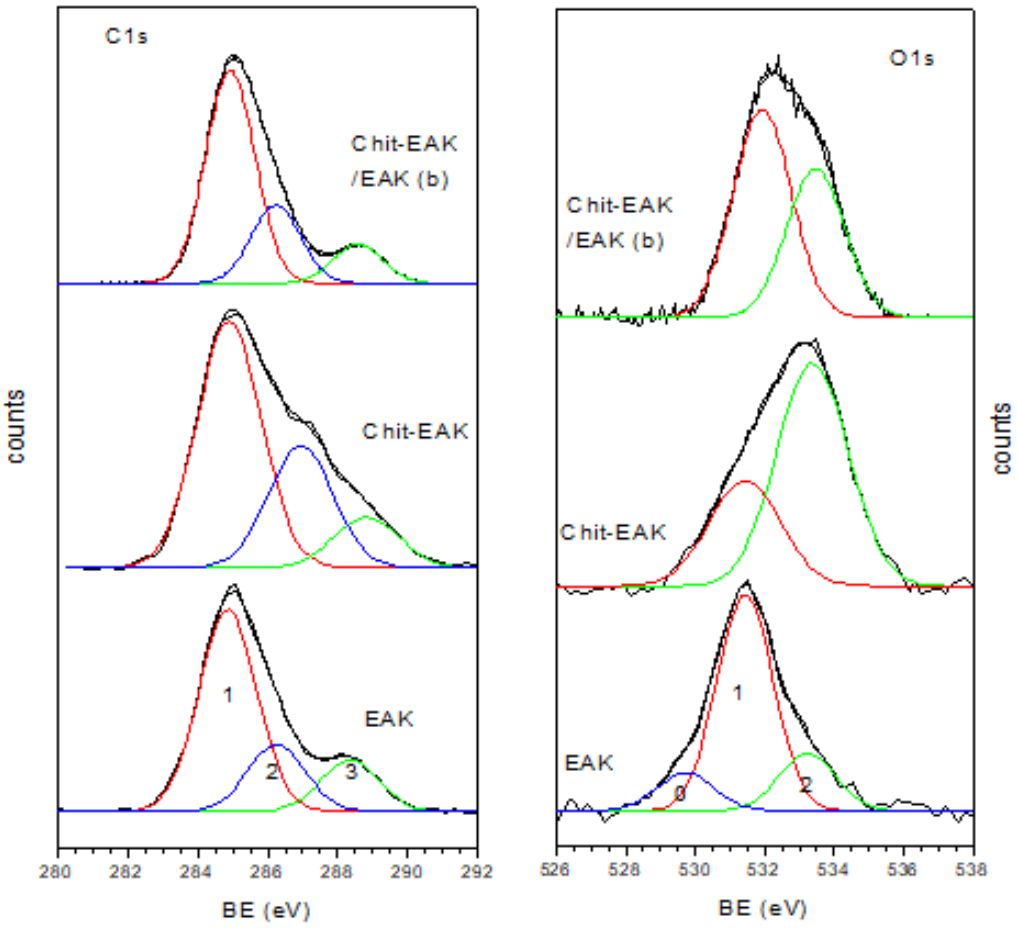

Figure 1. C1s and O1s spectra of EAK, Chit-EAK and Chit-EAK/EAK (b) deposited on titania and curve-fitting analysis of the experimental spectra.

The C1s core level spectrum of EAK results from three component peaks, due to chemically inequivalent carbon and labelled 1-3 in the figure. Peak 1 (BE=285.0 eV) is attributed to aliphatic carbons of the side chains and partially to carbon contamination; peak 2 (286.3 eV) is related to O=C-C-N carbons of the peptide backbone, with contribution from C-N carbons of the lysine pending groups; peak 3 (288.2 eV) is due to O=C-N peptide carbons and to $O=C-O^-$ carbons of the glutamate pending group [12]. In the O1s spectrum of EAK, three component peaks, labelled 0-2, in the figure are evidenced by

curve-fitting. Peak 0 (529.7 eV) is actually related to the oxygens of TiO_2 in the titania substrate, peak 1 (531.4 eV) to O=C carbons of the peptide backbone and of the carboxylate group of glutamate, peak 2 (533.2 eV) is related to physisorbed water and possibly to C-O-H groups in protonated glutamate [12, 21]. The N1s spectrum (not shown) results from a main peak at 400.0 eV, related to peptide nitrogens) with a high BE shoulder (401.5), due to protonated nitrogens of the lysine pending groups and having about 15% of the intensity of the main peak.

In the spectrum of Chit-EAK the intensity of peak 2 shows an evident increase in comparison to peak 3 and a slight shift to higher BE (286.7 eV); both effects are related to the contributions from C-O carbons of chitosan located at 286.6 eV [22]. Relevant changes are also evidenced in the O1s spectrum. Peak 0 disappears, indicating the formation of a thicker overlayer on the titania surface. A remarkable increase in intensity of peak 2 with respect to peak 1 is also evident in Figure 1 and is clearly related to contributions from O-C oxygens of chitosan [23].

In the O1s spectrum of sample Chit-EAK/EAK (b), the intensity of peak 1, dominant in the EAK spectrum, increases again with respect to the intensity of peak 2, dominant in the Chit-EAK spectrum and related to chitosan; a similar effect is observed for peaks 2 and 3 in the C1s spectrum. These data yield evidence of the formation of an EAK overlayer on the Chit-EAK surface.

Reflection-Absorption InfraRed Spectroscopy (RAIRS) measurements were carried out on Chit-EAK, Chit-EAK/EAK (a) and Chit-EAK/EAK (b) samples, as well as, for comparison, on thin films of pristine EAK and chitosan (Chit) deposited onto Au/Si(111) and TiO_2/Si(111) surfaces. Figure 2 shows results of RAIRS analysis for the samples deposited on titania; similar results are obtained when the substrate used is gold.

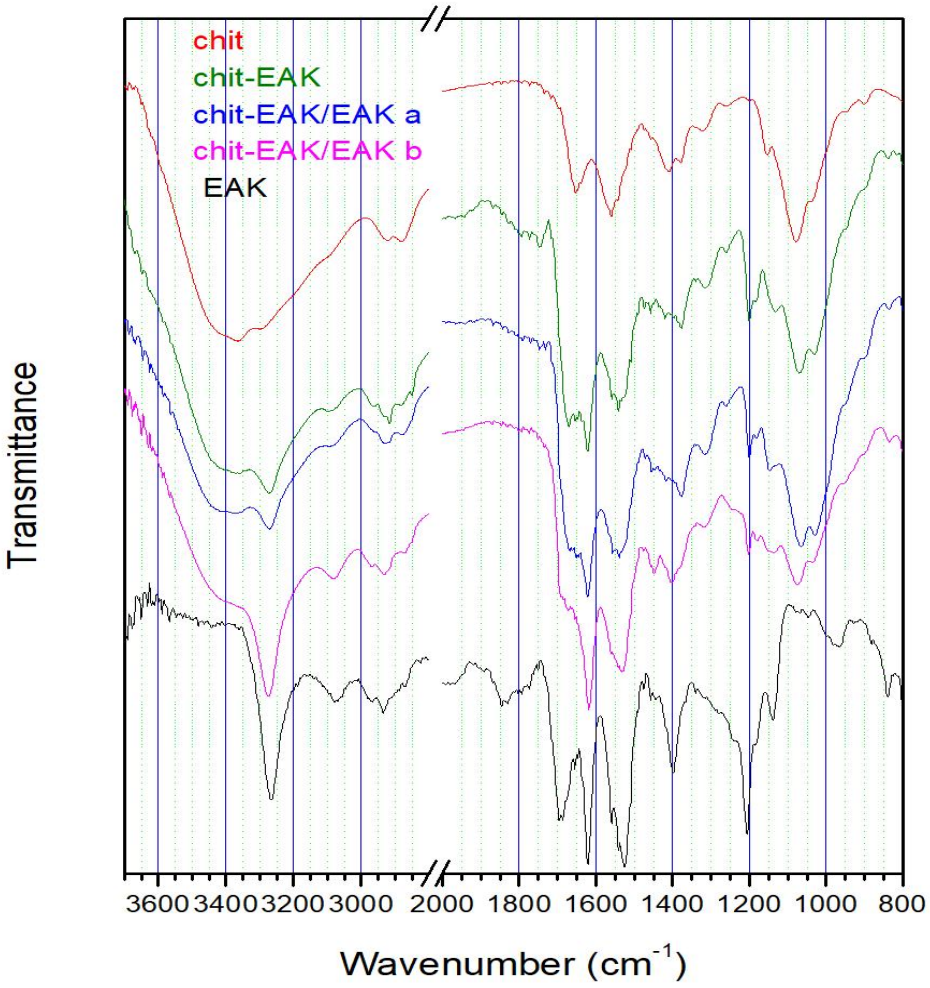

Figure 2. RAIRS spectra of chitosan (Chit), EAK, Chit-EAK, Chit-EAK/EAK (a) and Chit-EAK/EAK (b) deposited on titanium in the monolayer regime.

In the chitosan spectrum (top line) the most intense peak is the broad band located at 3550 cm^{-1} due to O-H and NH stretching vibrations, that cannot be resolved; band broadness is related to the hydrogen bonding situation of the chitosan hydroxyl and amino groups. The C-H stretching is found at 2920 cm^{-1}. Chitosan is obtained by hydrolysis of chitin, resulting in conversion of the amide moieties of chitin to amine groups; this reaction, however, is seldom complete, as shown by the peak located at 1650 cm^{-1} that can

be attributed to C=O stretching of amide groups (amide I band), due to uncomplete deacetylation. The broad band and 1560 cm^{-1} results from N-H bending vibrations of amides (amide II). Finally, the intense peak located at 1080 cm^{-1} can be attributed to C-O stretching vibrations. [24].

The RAIRS spectrum of EAK (bottom line) was reported in previous publications [12,25]. The most diagnostic region in the IR spectra of peptides is the 1700-1500 cm^{-1} range, where amide I and amide II vibrations are located. In the EAK spectrum the amide I band occurs at 1620 cm^{-1}, with a second peak (amide I') at 1680 cm^{-1}; these features are characteristic of an antiparallel β-sheet conformation of the peptide backbone [26,27]; the peak at 1540 cm^{-1} is the amide II band, related to N-H bending vibrations. At higher wavenumbers, the sharp peak at 3280 cm^{-1} is related to stretching vibrations of the N-H groups of the peptide bond. For a peptide backbone in antiparallel β-sheet conformation, N-H groups are involved in hydrogen bonding with the C=O groups of adjacent peptide chains; the sharpness of the N-H stretching vibration confirms the high stereoregularity of the EAK peptide backbones. In the central part of fig IR, the RAIRS spectra of the mixed systems are shown; from top to bottom: Chit-EAK, Chit-EAK/EAK (a) and Chit-EAK/EAK (b). The spectra of the investigated samples clearly result from the combination of the spectra of EAK and chitosan. In particular, in the 1700-1600 cm^{-1} region, the complex C=O stretching amide I band results from contributions of chitosan and EAK amide groups. However, the sharp peak at 1620 cm^{-1}, fingerprint of the antiparallel β-sheet structure, is clearly evident in the three reported spectra. In the 3600-3000 cm^{-1} region, the sharp N-H stretching peak at 3280 cm^{-1} of EAK is clearly distinguishable from the broad band due to overlapping O-H and N-H vibrations of chitosan. The spectra clearly show that EAK moieties retain their secondary structure in the mixed systems.

Moreover, a comparison of the spectra of Chit-EAK/EAK (a) and Chit-EAK/EAK (b) shows that the intensity of the peaks at 1620 at 3280 cm^{-1} increases as a function of EAK concentration in the mother solution, clearly indicating the growth of an order EAK overlayer on the chit-EAK surface.

Molecular structure and layer-by-layer organization

Near Edge X-ray Absorption Fine Structure (NEXAFS) spectroscopy is a powerful tool to gather information about local chemical and electronic structure in condensed matter, allowing to evidence bond lengths modifications ("bond length with a rule" method [28] by the study of σ* resonances position [29]. Although the precise and thoughtful attribution of all features appearing in a NEXAFS spectra of a complex molecule such as a peptide or polysaccharide (or, as in Chit-EAK samples, both) is an extremely difficult task, our previous works reporting NEXAFS investigations of amino-acids, di-peptides [30] , self assembling peptides [12] and mono or polysaccharides-based biomaterials [31], as well as literature reports on the subject [32], provide a wide database of spectral fingerprints that can be successfully used to decipher the C K-edge and N K-edge spectra discussed in this section.

As a start, we will discuss the C and N K-edge spectra collected at magic incidence angle (54.7° of incidence of the x-ray radiation on the sample surface), ensuring no dichroic contributions arising by sample spatial orientation, on the two reference EAK and Chit samples as well as on the complex Chit-EAK and Chit-EAK/EAK systems, deposited as monolayers on gold and respectively TiO_2. C K-edge spectra are reported in Figure 3A) (gold) and B) (TiO_2).

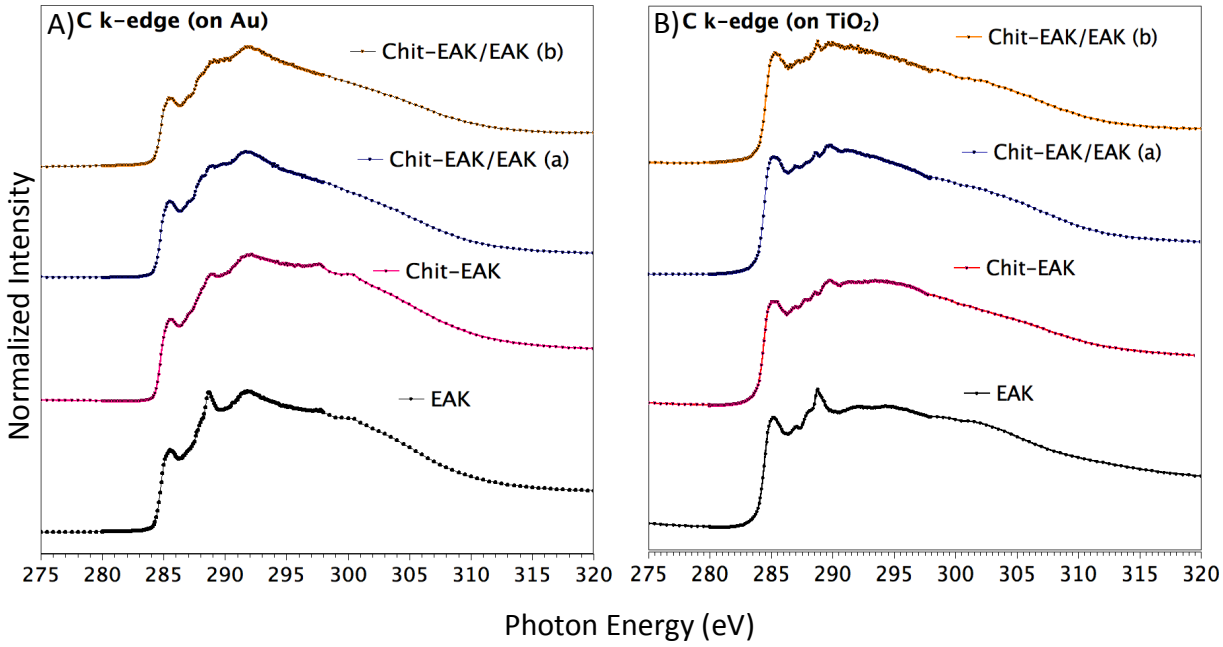

Figure 3. C K-edge spectra of Chit-EAK and Chit-EAK/EAK monolayers on A) Au/Si(111) and B) TiO_2. C K-edge NEXAFS spectra collected on EAK are also reported for comparison.

For EAK samples on gold and titania, an analogous set of features can be observed, coherently with literature [[12]]: the sharp feature at about 288.7 eV is assigned to a C1s→π* transition of C=O molecular orbital, the shoulder around 288 eV to a σ* resonance by the C-H groups and Rydberg features, additional features at about 293 and 303 eV can be associated to 1s→σ* transitions by the C-C and respectively C=O molecular groups. In Chit-EAK/Au/Si(111) sample spectrum, all the feature envisaged for the proposed molecular structures of EAK (see above) and Chitosan (292 eV C 1s→σ* C-OH transition) are observed. Chit-EAK/EAK (a) and Chit-EAK/EAK (b) systems on gold spectra appear as a sum of the reference systems (Chit-EAK + EAK) spectra, as expected

from the building-block approach [32], and confirming that the gold surface does not chemically interact with the biomolecules [33]. On the other hand, when chitosan is anchored to titania surfaces the peak assigned to C1s → σ* C-OH transitions appears red-shifted at 290 eV (instead of 292 eV, as also suggested by the literature), as evidenced by the vertical lines in Figure 4, where the 284 eV – 294 eV region of C K-edge spectra are reported for Chit-EAK anchored on gold, Chit-EAK anchored on TiO_2, and Chit-EAK/EAK (a) and (b) anchored on TiO_2.

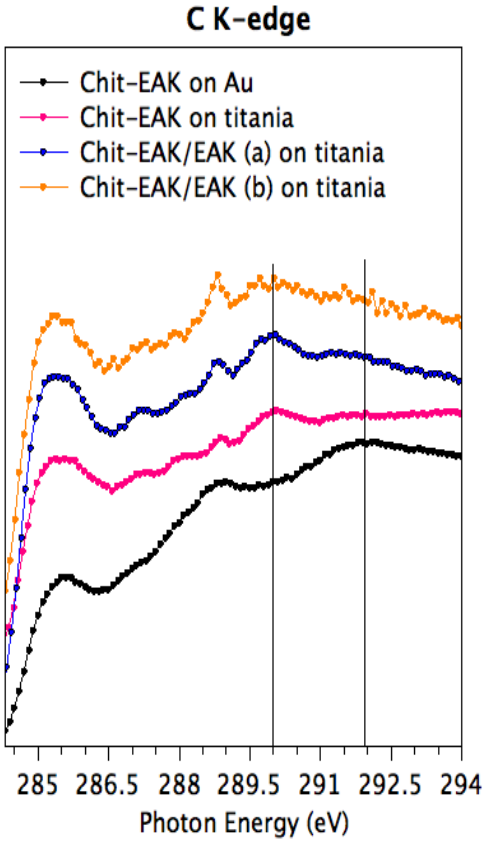

Figure 4. C K-edge spectra of Chit-EAK deposited on gold (bottom), and Chit-EAK, CHIT-EAK/EAK (a), Chit-EAK/EAK (b) anchored onto TiO_2 surfaces (284 eV – 294 eV spectral region).

Such a red-shift could be interpreted as resulting from a C-O bond length modification, as expected for an O-bridge formation between the Ti substrate and the chitosan ring. Supporting this hypothesis, a small feature at 290 eV is still observable in Chit-EAK

samples anchored to TiO_2 surfaces, while only a very small broadening can be observed in Chit-EAK/EAK (a) and (b) films deposited onto the same substrate (with an utter broadening at higher EAK amounts).

As for N K-edge spectra (reported in Figure 5A) – gold and B) – titania), all samples show a sharp peak at 402 eV assigned to N1s → π* transitions of the peptide bonds, and two broad bands at 406 and 415 eV to N1s → σ* N-H and N1s → σ* N-C resonances respectively [[12]]. It is noteworthy that in Chit-EAK and Chit-EAK/EAK (a) and (b) samples the N1s → σ* N-H feature at about 406 eV appears splitted in two large bands; this is probably due to the C-NH-C secondary amines originated by the covalent binding of EAK to Chit (as reported in detail in *Materials and Methods* section). No difference is observed, in N K-edge spectra, between the series of Chit-EAK and Chit-EAK/EAK samples anchored to different substrates (either gold or titania), confirming the hypothesized biomolecule-substrate interaction mechanism involving the C-OH moieties of chitosan. It is noteworthy that increasing the EAK amount N K-edge spectra became similar to the pristine EAK spectrum, as also observed in RAIRS spectra.

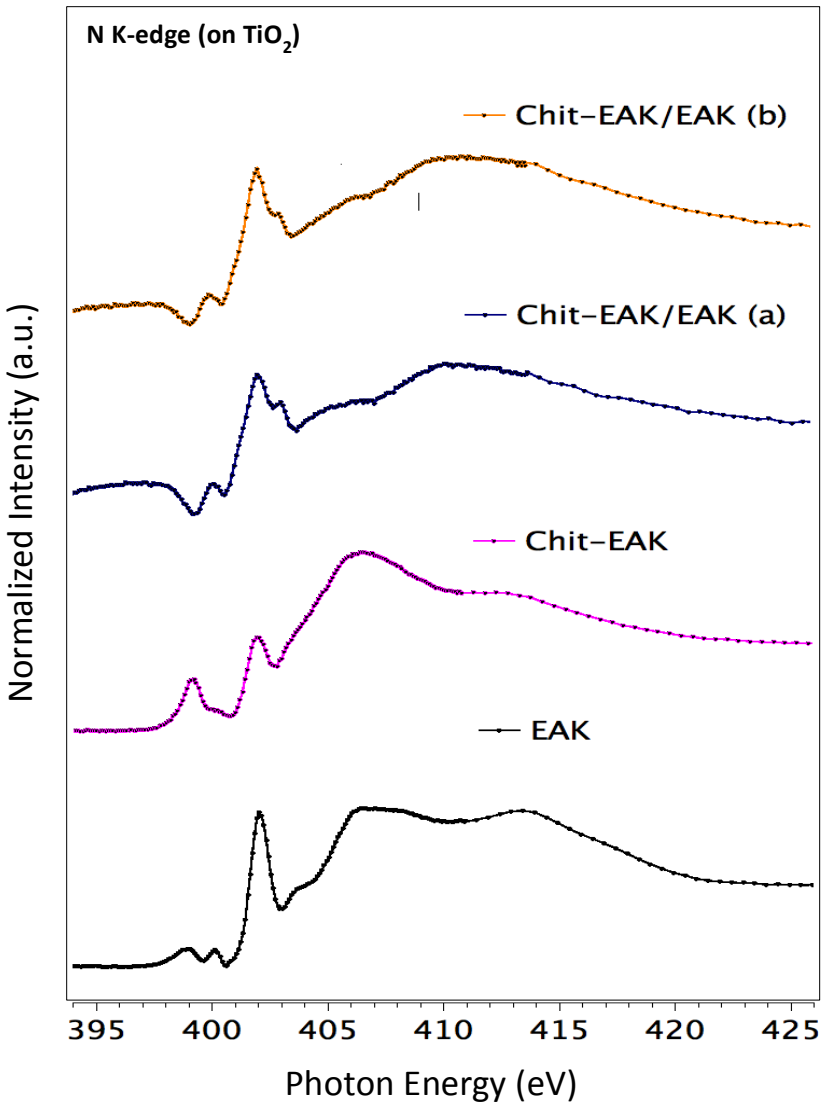

Figure 5. N K-edge spectra of Chit, Chit-EAK and Chit-EAK/EAK monolayers on TiO_2.

Summing up the above considerations, a layer-by-layer structure for Chit-EAK and Chit-EAK/EAK (a) and (b) films on TiO_2 can be envisaged, as schematically depicted in Schemes1 A) and B). In our interpretation, a first layer of chitosan is anchored to the titania surface through a C-O-Ti bridge; then, a first layer of EAK chains covalently anchored to the chitosan molecules appears in Chit-EAK; finally, in Chit-EAK/EAK

samples, the layer-by-layer structure is completed by the physisorbed oligopeptide in increasing amount going from sample Chit-EAK/EAK (a) to (b).

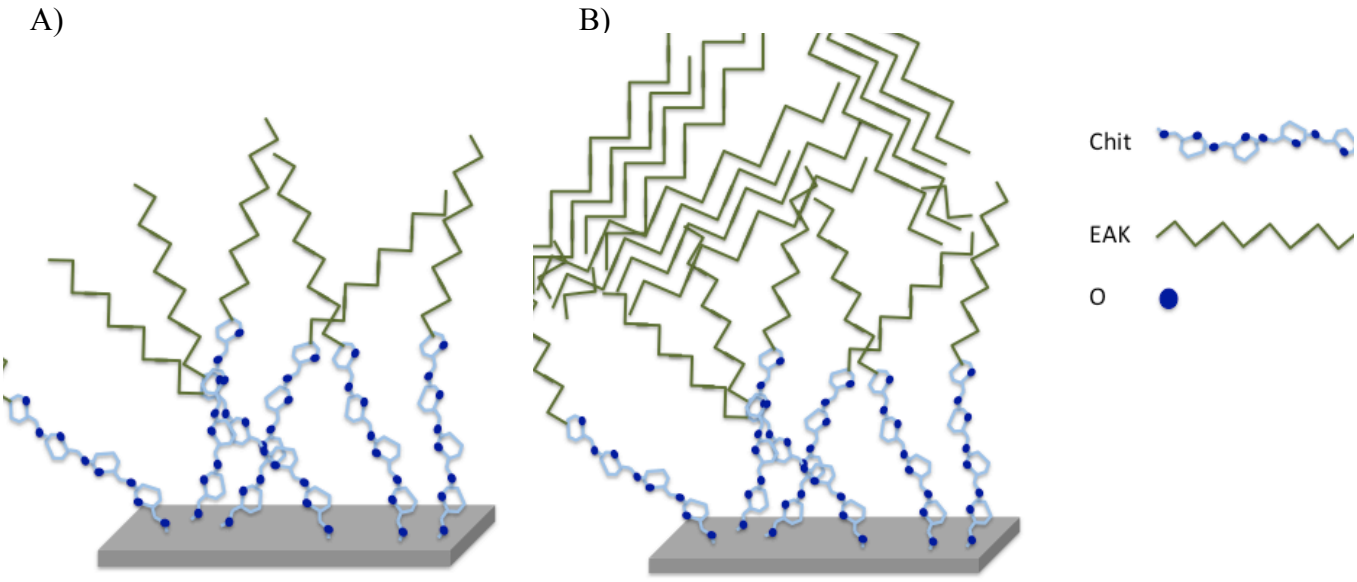

Scheme 1. Layer-by-layer arrangement hypothesized for A) Chit-EAK and B) Chit-EAK/EAK films on TiO_2.

To obtain a more accurate description of the layer-by-layer structure of Chit-EAK and Chit-EAK/EAK films anchored to titania substrates, all samples were also investigated by angular dependent NEXAFS measurements. To evaluate if a molecular preferential orientation occurs, NEXAFS measurements at the C and N K-edges were carried out as a function of the incidence angle of the impinging photons with respect to the sample surface. To evidence the most indicative dichroic effects, spectra collected at grazing (20°) and normal (90°) incidence angles at N K-edge, that is the most indicative for SAPs orientation investigation [[12]], were selected and compared. In the following Figure 6, angular dependent N K-edge spectra collected on EAK, Chit-EAK, Chit-EAK/EAK (a) and Chit-EAK/EAK (b) thin films anchored onto titania substrates are reported.

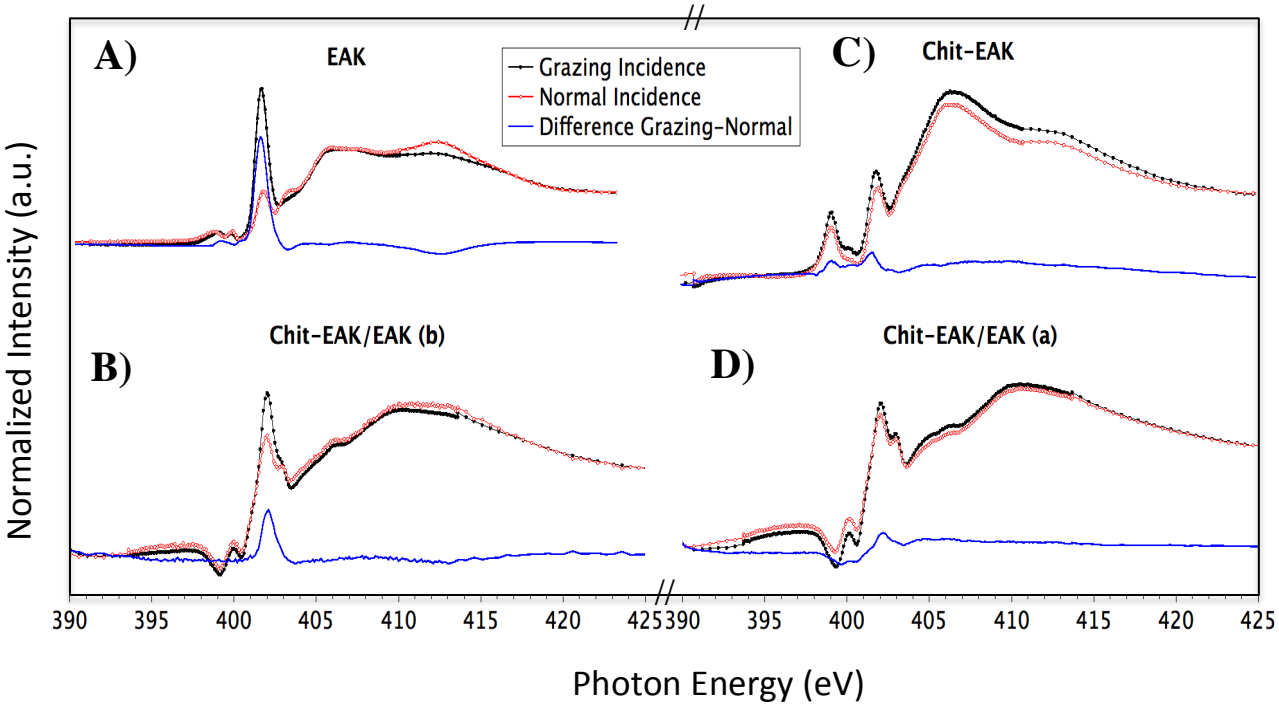

Figure 6. Angular dependent N K-edge NEXAFS spectra collected at Normal (90°) and Grazing (20°) incidence angles of the impinging x-ray beam on A) EAK; B) Chit-EAK/EAK (b); C) Chit-EAK; D) Chit-EAK/EAK (a) films anchored on TiO_2. The difference (Grazing - Normal) spectra, evidencing dichroic effects, are also shown (blue lines).

For EAK (Figure 6 A) and Chit-EAK/EAK (b) (Figure 6 B) deposited on gold and titanium, angular dependence of the π* is observed; The ratio between the peak intensities at normal (90°) and grazing (20°) incidence, determined for the selected resonance by peak fitting of the experimental data, can be used to calculate the average tilt angle between the π* vector orbital for the C=O bond and the normal to the surface, using the equation reported by Stöhr [34] for the three-fold or higher symmetry substrates, assuming the polarization factor P = 0.95. For Chit-EAK/EAK (b) deposited on gold and titanium the tilt angle of the peptide chains is of about 70°, as already evidence in [12] for the reference

sample (EAK) and re-calculated for the newly deposited pristine EAK analyzed in this work.

Interestingly, no dichroic effects or very small effects are observed for Chit-EAK (Figure 6 C) and Chit-EAK/EAK (a) (Figure 6 D) thin films, on both substrates. This experimental finding allows us to refine the hypothesized layer-by-layer arrangement scheme, as depicted in the following Scheme 2.

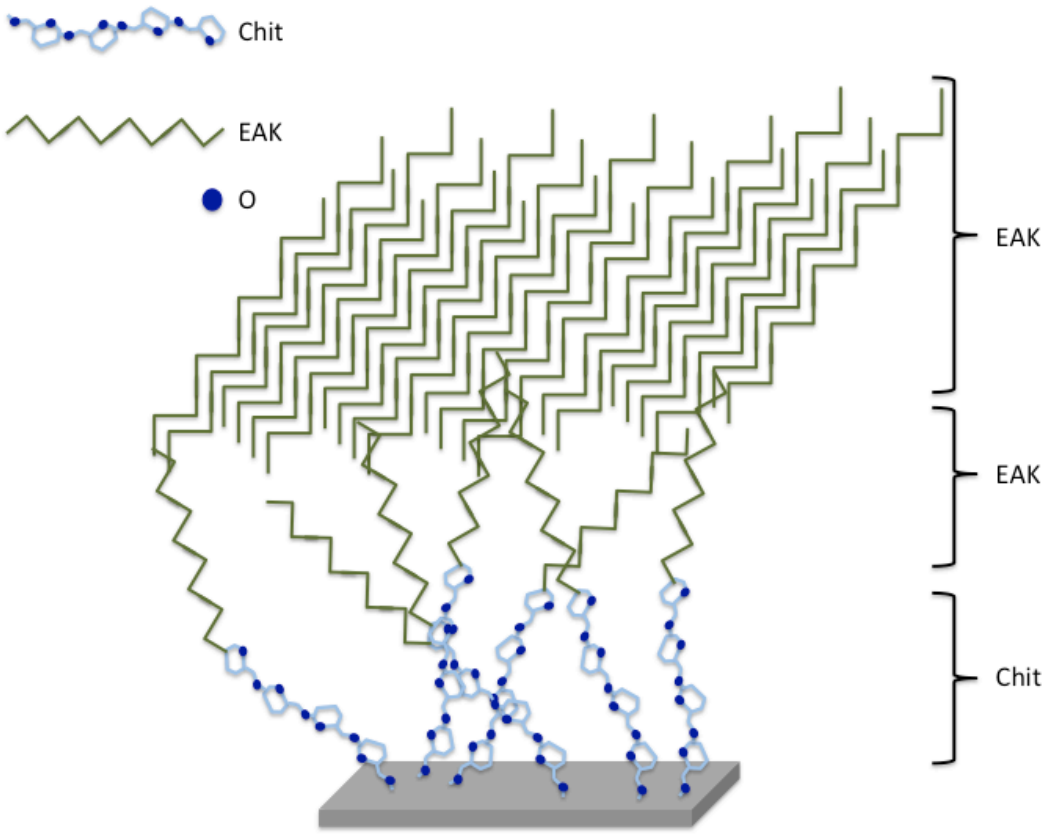

Scheme 2. Schematic representation of the layer-by-layer arrangement hypothesized for Chit-EAK/EAK (b) film on TiO_2.

SUMMARY AND CONCLUSIONS

Layer-by-layer structures of chitosan and the self-assembling peptide EAK16-II were successfully anchored onto titania surfaces, by following a simple deposition procedure from solution, that allows for easily obtaining films with different peptides amount. For comparison, the same procedure was applied to the preparation of mixed chitosan and EAK16-II films on polycristalline gold surfaces. The chemical stability of the biomolecules employed for the films construction was assessed by X-ray Photoemission Spectroscopy; RAIRS measurements evidenced the good chitosan coverage on the surface in Chit-EAK samples, a β-sheet secondary structure for EAK oligopeptide, and an increasing of the peptide-related features intensity when the peptide amount increases (either by physisorbing an EAK layer on the substrate/Chit-EAK system, either increasing the EAK solution concentration from 0.1 to 1.0 mM). Near Edge X-rays Absorption Fine Structure spectroscopy allowed to probe both the molecular structure of the systems and the molecular arrangement, when occurring, in the thin films. By comparing the complementary information provided by XPS, RAIRS and NEXAFS measurements, a coherent interpretation of the layer-by-layer structure organization attained by chitosan and EAK16-II biomolecules on the titania surfaces was envisaged, with the chitosan oligomers covalently bonding the titania surface through a Ti-O-C bridge, a first layer of EAK oligopeptides covalently bonded to the Chit chains, i.e. leading to an epitaxial layer on the Chit surface (already showing faible β-sheet secondary structures, as expected for this SAP peptide and proved by IRRAS), and then a last compact layer of physisorbed EAK molecules, that constitute the external layer in Chit-EAK/EAK (a) and (b) samples, strongly oriented as revealed by the dichroic effects in the angular dependent NEXAFS N K-edge spectra.

This complex structure opens exciting perspectives for applications in the field of tissue engineering, for the developing of anti-biotic and bio-active innovative prosthetic materials.

AUTHOR INFORMATION

Corresponding Author

*Dr. Valeria Secchi. *Department of Science, Roma Tre University of Rome Via della Vasca Navale 79, 00146 Rome, Italy; e-mail valeria.secchi@uniroma3.it

Author Contributions

The manuscript was written through contributions of all authors. All authors have given approval to the final version of the manuscript.

Funding Sources

The "Dipartimento di Scienze", Roma Tre University is gratefully acknowledged for partially funding this research.

ACKNOWLEDGMENT

The Grant of Excellence Departments, MIUR-Italy (ARTICOLO 1, COMMI 314 - 337 LEGGE 232/2016) is gratefully acknowledged.

The authors acknowledge the CERIC-ERIC Consortium for the access to experimental facilities and financial support, and the infrastructure project no. CZ.02.1.01/0.0/0.0/16_013/0001788 and LM2015057 for the support of the SPL– MSB facility.

ABBREVIATIONS

Chit, chitosan; EAK, EAK16-II oligopeptide; SR, Synchrotron Radiation; XPS, x-ray Photoelectron Spectroscopy; RAIRS, Reflection-Absorption InfraRed Spectroscopy, NEXAFS, Near Edge x-ray Absorption Fine Structure spectroscopy.

REFERENCES

(1) Romanò, C. L.; Scarponi, S.; Gallazzi, E.; Romanò, D.; Drago L.; Antibacterial coating of implants in orthopaedics and trauma: a classification proposal in an evolving panorama, *J. Orthop. Surg. Res.* **2015,** 10, 157. DOI 10.1186/s13018-015-0294-5.

(2) Gristina, A.G.; Naylor, P.; Myrvik, Q.; Infections from biomaterials and implants: a race for the surface, *Med. Prog. Technol*. **1988** 14, 205–24.

(3) Subbiahdoss, G.; Kuijer, R.; Grijpma, D.W.; van der Mei, H.C.; Busscher, H.J.; Microbial biofilm growth vs. tissue integration: "the race for the surface" experimentally studied**,** *Acta Biomater*. **2009**, 5, 1399–1404. DOI: 10.1016/j.actbio.2008.12.011.

(4) Costerton, W.; Veeh, R.; Shirtliff ,M.; Pasmore, M.; Post, C.; Ehrlich, G.; The application of biofilm science to the study and control of chronic bacterial infections, *J. Clin. Invest*. **2003**, 112, 1466–77. DOI:10.1172/JCI20365.

(5) Chen, Y.; Busscher, H.J.; van der Mei, H.C.; Norde, W.; Statistical analysis of long- and short-range forces involved in bacterial adhesion to substratum surfaces as measured using atomic force microscopy, *Appl. Environ. Microbiol*. **2011**, 77,5065–70. DOI: 10.1128/AEM.00502-11.

(6) Wang, Y.; Subbiahdoss, G.; de Vries, J.; Libera, M.; van der Mei, H.C.; Busscher, H.J.; Effect of adsorbed fibronectin on the differential adhesion of osteoblast-like cells and

Staphylococcus aureus with and without fibronectin-binding proteins, *Biofouling* **2012**, 28,1011–21. DOI:10.1080/08927014.2012.725471.

(7) Anderson, J.M.; Rodriguez, A.; Chang, D.T.; Foreign body reaction to biomaterials. *Semin. Immunol*. **2008**, 20,86–100. DOI:10.1016/j.smim.2007.11.004.

(8) Busscher, H.J.; van der Mei, H.C.; Subbiahdoss, G.; Jutte, P.C.; van den Dungen, J.J.; Zaat, S.A.; Schultz, M.J.; Grainger, D.W.; Biomaterial-associated infection: locating the finish line in therace for the surface, *Sci. Transl. Med*. **2012**, 4, 153. DOI:10.1126/scitranslmed.3004528.

(9) Zimmerli, W.; Lew, P.D.; Waldvogel, F.A.; Pathogenesis of foreign body infection. Evidence for a local granulocyte defect, *J. Clin. Invest*. **1984**, 73, 1191–200. DOI:10.1172/JCI111305.

(10) Engelsman, A.F.; Saldarriaga-Fernandez, I.C.; Nejadnik, M.R.; van Dam, G.M.; Francis, K.P.; Ploeg, R.J.; Busscher, H.J.; van der Mei, H.C.; The risk of biomaterial-associated infection after revisionsurgery due to an experimental primary implant infection. *Biofouling*, **2010**, 26, 761–7. DOI:10.1080/08927014.2010.515027.

(11) Khoo, X.; Hamilton, P.; O'Toole, G.A.; Snyder, B.D.; Kenan, D.J.; Grinstaff, M.J.; Directed assembly of PEGylated-peptide coatings for infection-resistant titanium metal, *J. Am. Chem. Soc*. **2009**, 131, 10992–10997. DOI: 10.1021/ja9020827.

(12) Polzonetti, G.; Battocchio, C.; Dettin, M.; Di Bello, C.; Iucci, G.; Carravetta, V.; Thin films of a self-assembling peptide on TiO_2 and Au studied by NEXAFS, XPS and IR spectroscopies, *Mater. Sci. Eng. C*. **2006**, 26, 929-234. DOI: 10.1016/j.msec.2005.09.062.

(13) Zhang, S.; Emerging biological materials through molecular self-assembly, *Biotech Adv.* **2002**, 20, 321-339; DOI: 10.1016/S0734-9750(02)00026-5

(14) Gelain, F.; Horii, A.; Zhang, S.; Designer self-assembling peptide scaffolds for 3-D tissue cell cultures and regenerative medicine, *Macromol. Biosci.* **2007**, 7, 544-551; DOI: 10.1002/mabi.200700033

(15) Goy, R.C.; de Britto, D.; Assis, O.B.G.; A review of the antimicrobial activity of chitosan, *Polímeros: Ciência e Tecnologia,* **2009**, 3(19), 241-247. DOI: 10.1590/S0104-14282009000300013.

(16) Costa, F.; Maia, S.; Gomes, P.; Martins, M.C.; Characterization of hLF1-11 immobilization onto chitosan ultrathin films and its effects on antimicrobial activity, *Acta Biomater*. **2014**, 8, 3513-3521. DOI:10.1016/j.actbio.2014.02.028.

(17) Grasshoff, K.; M. Ehrhardt, K. Kremling, Almgreen, T.; Methods of Seawater Analysis, Verlag Chemie, Weinheim, Verlag Chemie, Weinheim ; (2nd, rev. and extended ed). **(1983);** New York.

(18) Forte, G.; Messina, G.M.L.; Zamuner, A.; Dettin, M.; Grassi, A.; Marletta, G.; *Colloids and Surf B Biointerfaces.* **(2018),** 168, 148-155. DOI:10.1016/j.colsurfb.2018.01.016

(19) Moulder J.F., Stickle W.F., Sobol P.E., Bomben K.D., Handbook of X-ray Photoelectron Spectroscopy, Physical Electronics Inc., Minnesota, Eden Prairie (Ed.), (1996).

(20) Shirley, D.A.; High-resolution X-ray photoemission spectrum of the valence bands of gold, *Phys. Rev. B* **1972**, 12, 4709.

(21) Beamson G., Briggs D., High Resolution XPS of Organic Polymers, The Scienta ESCA 300 Database, John Wiley & Sons, Chichester (1992).

(22) Battocchio, C.; Concolato, S.; Fahlman, M.; Iucci, G.; Santi, M.; Sotgiu, G.; Orsini, M.; Grafting of chitosan on Titanium and Ti6Al4V alloy with carboxyl groups as anchoring points, *Mater. Sci. Eng. C* **2018**, submitted.

(23) Skwarczynska, A.; Kaminska, M.; Owczarz, P.; Bartoszek, N.; Walkowiak, B.; Modrzejewska, S. The structural (FTIR, XRD, and XPS) and biological studies of thermosensitive chitosan chloride gels with b-glycerophosphate disodium *J. Appl. Polym. Sci.* **2018** 46459

(24) Jumirska, J.; Czerwicka, M.; Kaczyński, Z.; Bychowska, A.; Brzozowski, K.; Thöming, J.; Stepnowski, P.; Application of Spectroscopic Methods for Structural Analysis of Chitin and Chitosan, *Mar. Drugs* **2010**, 8, 1567-1636.

(25) Battocchio, C.; Iucci, G.; Dettin, M.; Carravetta, V.; Monti, S.; Polzonetti G.; Self-assembling behaviour of self-complementary oligopeptides on biocompatible substrates, *Mater. Sci. Eng. C* **2010**,169, 36-42. DOI:10.1016/j.mseb.2009.12.051.

(26) Haris, P.I.; Chapman, D.; The conformational analysis of peptides using Fourier transform IR spectroscopy, *Biopolymers* (Peptide Science), **1995**, 37, 251-63.

(27) Castano, S.; Desbat, B.; Laguerre, M.; Jufourcq, J.; Structure, orientation and affinity for interfaces and lipids of ideally amphipathic lytic LiKj(i=2j) peptides, *Biochim. Biophys. Acta* **1999**, 1416, 176-94.

(28) Stöhr, J.; Sette, F.; Johnson, A.L.; Near Edge X-ray Absorption Fine Structure Studies of Chemisorbed Hydrocarbons: Bond Lengths with a Ruler, *Phys. Rev. Lett.* **1984**, 53, 1684 – 1687.

(29) Gainar, A.; Stevens, J.S.; Jaye, C.; Fischer, D.A.; Schroeder, S. L. M.; NEXAFS Sensitivity to Bond Lengths in Complex Molecular Materials: A Study of Crystalline Saccharides, *J. Phys. Chem. B* **2015**, 119, 14373–14381. DOI:10.1021/acs.jpcb.5b07159.

(30) Monti, S.; Carravetta, V.; Battocchio, C.; Iucci, G.; Polzonetti, G.; Peptide/TiO_2 Surface Interaction: A Theoretical and Experimental Study on the Structure of Adsorbed ALA-GLU and ALA-LYS, *Langmuir* **2008**, *24*, 7, 3205–3214. DOI: 10.1021/la702956t.

(31) Secchi, V.; Guizzardi, R.; Russo, L.; Pastori, V.; Lecchi, M.; Franchi, S.; Iucci, G.; Battocchio, C.; Cipolla, L.; Maltose conjugation to PCL: Advanced structural characterization and preliminary biological properties, *J. Mol. Struct.* **2018**, 1159, 74-78. DOI: 10.1016/j.molstruc.2018.01.051.

(32) Stewart-Ornstein, J.; Hitchcock, A.P.; Hernández Cruz, D.; Henklein, P.; Overhage, J.; Hilpert, K.; Hale, J.D.; Hancock, R.E.; Using intrinsic X-ray absorption spectral differences to identify and map peptides and proteins, *J. Phys. Chem. B* **2007**, 111, 26, 7691-7699. DOI: 10.1116/1.2956637.

(33) Iucci, G.; Battocchio, C.; Dettin, M.; Gambaretto, R.; Di Bello, C.; Bogatti, F.; Carravetta, V.; Monti, S.; Polzonetti, G.; Peptides adsorption on TiO2 and Au: Molecular organization investigated by NEXAFS, XPS and IR, *Surf. Sci.* **2007**, 601,3843-3849. DOI: 10.1016/j.susc.2007.04.024.

(34) Stöhr, J. NEXAFS Spectroscopy, Springer Series in Surface Sciences, R. Geomer (Ed.), Springer-Verlag, **1991**, Ch. 9.4.3.

Chapter 7

Maltose conjugation to PCL: Advanced structural characterization and preliminary biological properties

V. Secchi [a, *], R. Guizzardi [b], L. Russo [b], V. Pastori [b], M. Lecchi [b], S. Franchi [a], G. Iucci [a], C. Battocchio [a], L. Cipolla [b]

[a] Department of Science, Roma Tre University of Rome, Via della Vasca Navale 79, 00146, Rome, Italy;

[b] Department of Biotechnology and Biosciences, University of Milano-Bicocca, Piazza della Scienza 2, 20126, Milano, Italy

Journal of Molecular Structure 1159 (2018) 74e78

DOI:10.1016/j.molstruc.2018.01.051

7. Maltose conjugation to PCL: Advanced structural characterization and preliminary biological properties

Regenerative medicine is a branch of translational research in tissue engineering which deals with the *"process of replacing, engineering or regenerating human cells, tissues or organs to restore or establish normal function".* The emerging trends in regenerative medicine rely among others on biomaterial-based therapies, with the use of biomaterials as a central delivery system for biochemical and physical cues to manipulate transplanted or ingrowth cells and to orchestrate tissue regeneration. Cell adhesion properties of a biomaterial strongly depend on its surface characteristics. Among others poly(ε-caprolactone) (PCL) is a biocompatible and biodegradable material with low cytotoxicity that is widely adopted as synthetic polymer in several applications. However, it is hydrophobic, which limits its use in tissue engineering. In order to improve its hydrophilicity and cellular compatibility, PCL surface was grafted with maltose. I paid attentions on the characterization of the modified PCL surface using X-ray Photoelectron Spectroscopy (XPS) and Near Edge x-ray Absorption Fine Structure (NEXAFS) spectroscopies, with the aim to probe the chemical composition of the sample surface and to confirm the expected molecular modification.

Journal of Molecular Structure 1159 (2018) 74–78

Contents lists available at ScienceDirect

Journal of Molecular Structure

journal homepage: http://www.elsevier.com/locate/molstruc

Maltose conjugation to PCL: Advanced structural characterization and preliminary biological properties

Valeria Secchi [a, *, 1], Roberto Guizzardi [b, 1], Laura Russo [b], Valentina Pastori [b], Marzia Lecchi [b], Stefano Franchi [a], Giovanna Iucci [a], Chiara Battocchio [a], Laura Cipolla [b, **]

[a] Department of Sciences, University of Roma Tre, Via della Vasca Navale 79, 00146, Rome, Italy
[b] Department of Biotechnology and Biosciences, University of Milano-Bicocca, Piazza della Scienza 2, 20126, Milano, Italy

ARTICLE INFO

Article history:
Received 5 December 2017
Received in revised form
16 January 2018
Accepted 19 January 2018

Keywords:
Bioactivated PCL
Small carbohydrates epitopes
Surface chemical structure
Tissue engineering
Regenerative medicine

ABSTRACT

The emerging trends in regenerative medicine rely among others on biomaterial-based therapies, with the use of biomaterials as a central delivery system for biochemical and physical cues to manipulate transplanted or ingrowth cells and to orchestrate tissue regeneration. Cell adhesion properties of a biomaterial strongly depend on its surface characteristics.

Among others poly(ε-caprolactone) (PCL) is a biocompatible and biodegradable material with low cytotoxicity that is widely adopted as synthetic polymer in several applications. However, it is hydrophobic, which limits its use in tissue engineering. In order to improve its hydrophilicity and cellular compatibility, PCL surface was grafted with maltose through a two-step procedure in which controlled aminolysis of PCL ester bonds by hexanediamine was followed by reductive amination with the carbohydrate reducing end. The modified PCL surface was then characterized in detail by x-ray Photoelectron Spectroscopy (XPS) and Near Edge x-ray Absorption Fine Structure (NEXAFS) spectroscopies. In addition, the biocompatibility of the proposed biomaterial was investigated in preliminary biological assays.

1. Introduction

In the field of regenerative medicine, the design of innovative materials for tissue engineering applications usually requires the fabrication of a biocompatible and biodegradable scaffold, able to promote cell adhesion and growth [1,2]. A crucial point for the realization of such bioactive materials is their chemical characterization, since the specific nature of a material's surface, both from a chemical and physical point of view, determines its biological properties such as cell adhesion and proliferation.

In this context, poly(ε-caprolactone) (PCL) is a well known biocompatible and biodegradable [3,4] material with low cytotoxicity that is widely adopted as synthetic polymer for medical applications [5–9], due to its several desirable features, such as good stability under ambient conditions and ease of processability with different techniques and morphologies. However, PCL is a hydrophobic polymer, limiting its suitability for cell adhesion and growth. In order to improve hydrophilicity and cellular compatibility, PCL surface can be modified with appropriates chemical groups, biomolecules, or by physical treatments, improving hydrophilicity and/or eliciting a desired cellular response. For example several techniques can be exploited, such as laser [10] or plasma treatments [11], followed by covalent immobilization of collagen or other Extracellular Matrix (ECM) proteins such as gelatin, and laminin [12–14]. At the same time different bioconjugation strategies have been developed in order to graft material surface with a specific bioactive compound. Several authors describe how heparin, proteoglycans [15] or specific Arginylglycylaspartic acid (RGD) peptides improve cellular adhesion on synthetic material surface [16]. The RGD sequences are present in many ECM proteins and promote the interaction between integrin receptors triggering an integrin-mediated cell adhesion process influencing cell behaviour on the scaffold, including differentiation, apoptosis, and migration [17]. The covalent grafting of selected (bio)molecules on PCL can be obtained by controlled polyester hydrolysis using NaOH or aminolysis, promoting the generation of specific functional groups on the scaffolds, useful for subsequent functionalization [18].

* Corresponding author.
** Corresponding author.
E-mail addresses: valeria.secchi@uniroma3.it (V. Secchi), laura.cipolla@unimib.it (L. Cipolla).
[1] These authors contributed equally to the work.

https://doi.org/10.1016/j.molstruc.2018.01.051
0022-2860/

Up to now, covalent functionalization of PCL scaffold with small carbohydrates epitopes has been rarely explored, despite the observation that “glyco-epitopes” improve hydrophilicity [19,20], while inducing specific cellular responses [21–23]. In fact, carbohydrates located on cell membranes play important roles in biological communication, and are responsible for cell/cell, and cell/matrix interactions in cellular aggregates or multicellular organs, through signal proteins such as lectins [24]. In addition, carbohydrates are inherently compatible with the metabolic system and have high potential for biological and biomimetic effect [25]. Saccharides have indeed several advantages, whose combination makes them unique candidates for applications in the field of regenerative medicine [26].

We present herein the functionalization of PCL scaffolds with α-glucoside residues and their surface investigation by X-ray Photoelectron Spectroscopy (XPS) and Near Edge X-Ray Absorption Fine Structure (NEXAFS).

The PCL functionalization is achieved by a two-step procedure as highlighted in Scheme 1. Controlled aminolysis of PCL ester bonds by 1,6-hexanediamine, followed by reductive amination with commercially available maltose, allows the exposition of α-glucoside residues on PCL surface, with a controlled spatial orientation of the carbohydrate moiety. The surface-modified PCL has been characterized in details by XPS and NEXAFS measurements to probe the chemical composition of the sample surface and to confirm the expected molecular modification. In addition, the biocompatibility of the proposed material was investigated in preliminary biological assays, evaluating the behaviour of a neuroblastoma cell line. The choice of the cell line and of the carbohydrate residues for PCL functionalization was based on a previous result obtained by our group: we observed that F11 cell lines cultured on maltose-functionalised collagen through the same chemistry didn't proliferate, but on the contrary were able to differentiate into active neurons, without the addition of any differentiation agent in the culture medium [22]. On this basis, we wanted to explore the possibility that the same carbohydrate moiety exposed on a PCL surface instead of collagen could act in a similar way.

2. Experimental methods

All reagents and solvents were purchased from Sigma-Aldrich and used without any further purification.

2.1. Synthesis

2.1.1. Scaffold preparation

PCL scaffolds were prepared through a solvent casting method using PCL (M_w = 65 000 - Sigma Aldrich) pellets. Briefly, PCL pellets were dissolved in chloroform (0.1 g/mL), under stirring for 4 h at r.t. After complete dissolution, 1.2 mL of the solution was poured into 3 cm diameter teflon jars, the solvent evaporated in the fumehood (2 days), and finally thoroughly washed first with 3 mL of ethanol for 10 min and then three times with 20 mL of milliQ water for 15 min.

The PCL scaffolds were obtained as small thin discs (60 mg), 2 cm in diameter.

2.1.2. Amine grafting

PCL discs were immersed in a 20% (w/w) solution of 1,6-hexandiamine in *i*-propanol at 37 °C as previously described [18]. After the treatment, the specimens were extensively washed with ethanol and air-dried.

2.1.3. PCL neoglycosylation

Aminated discs were immersed in citrate buffer (pH = 6.00, 5 ml). Subsequently 1.046 g of maltose (final concentration 0.6 M) and 95 mg of $NaBH_3CN$ (0.3 M) were added and reacted overnight. The dishes were rinsed extensively with deionized water.

2.2. Spectroscopic techniques

2.2.1. XPS analysis

X-Ray Photoelectron Spectroscopy (XPS) analyses were performed using an instrument of our own design and construction consisting of a preparation and analysis UHV chamber, equipped with a 150 mm mean radius hemispherical electron analyzer with a four element lens system with a 16-channel detector giving a total instrument resolution of 1.0 eV as measured at the Ag $3d_{5/2}$ core level. MgKα non-monochromatized X-ray radiation (hν = 1253.6 eV) was used for acquiring core level spectra for all samples (C1s, N1s and O1s). The spectra were energy referenced to the C1s signal of aliphatic C atoms having a binding energy BE = 285.00 eV. Atomic ratios were calculated from peak intensities by using Scofield's cross section values and calculated λ factors. Curve-fitting analysis of the C1s, N1s and O1s spectra were performed using Gaussian profiles as fitting functions, after

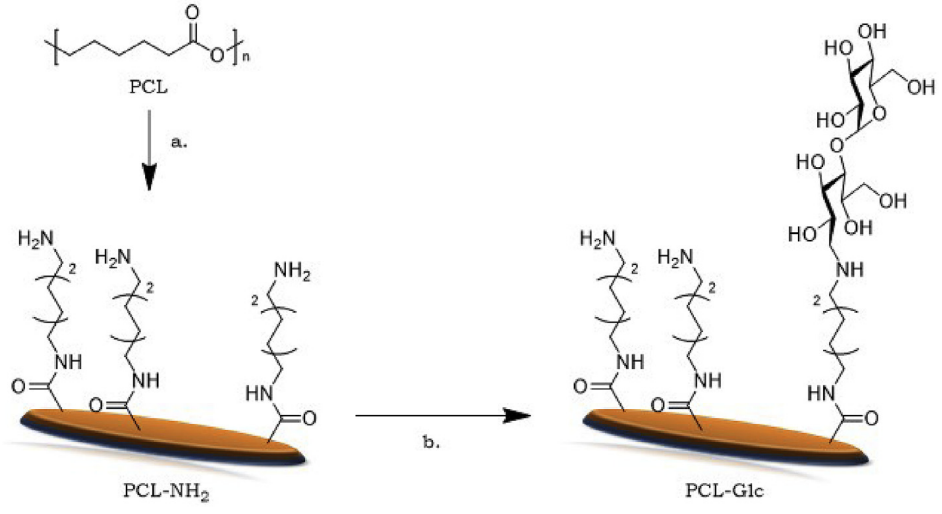

Scheme 1. a. 20% (w/w) 1,6-hexanediamine/*i*-propanol, b. Maltose (0.6 M) $NaCNBH_3$ (0.3 M) citrate buffer (pH = 6).

subtraction of a Shirley-type background [27]. Atomic ratios were calculated from peak intensities using Scofield's cross-section values and calculated λ factors [28].

2.2.2. NEXAFS analysis

Synchrotron-induced NEXAFS experiments were performed at the ELETTRA storage ring at the bending magnet for emission absorption and reflectivity (BEAR) beamline, installed at the left exit of the 8.1 bending magnet exit. O k-edge and C k-edge spectra were collected at normal (90°), grazing (20°) and magic (54.7°) incidence angles of the polarized photon beam with respect to the sample surface. The photon energy and the resolution were calibrated at the K absorption edges of Ar, N_2 and Ne. The spectra were normalized subtracting a straight line that fits the part of the spectrum below the edge and assessing to 1, the value at 550.00 eV for O K-edge and 320.00 eV for C K-edge.

2.3. Biological assays

Neuroblastoma F11 cells (a fusion product of mouse neuroblastoma N18TG-2 cell line and rat dorsal root ganglion) were used as cellular model to investigate material biocompatibility. Cells were seeded at density 12 000 cells in 24-multiwell plates in which PCL disks completely covered the well surface, and were maintained without splitting until the day of the experiment. They were cultured in Dulbecco's modified Eagle's medium (Sigma-Aldrich), 2 mM glutamine (Sigma-Aldrich), 10% of foetal bovine serum (Sigma-Aldrich) and incubated at 37 °C in a humidified atmosphere with 5% CO_2. Cells received fresh medium twice per week. After 7 days, they were mechanically detached from the substrate and counted by a Burker chamber for proliferation analysis. 2 wells per 4 independent experiments were analyzed for each material. Data are presented as mean ± SEM. Significance evaluation was obtained using the Student's t statistic.

3. Results and discussion

3.1. Sample preparation

Previous works have already evidenced that aminolysis by diamines represents an easy and friendly way to efficiently graft PCL surface with primary amine. Thus, PCL scaffolds have been functionalised with amine groups as previously reported [29].

In order to covalent graft carbohydrate moieties on material surfaces, different chemoselective conjugation reactions can be used [30,31]. Generally, carbohydrate conjugation is frequently obtained *via* multi-step procedures involving tedious protection/deprotection steps and suitable modifications of the carbohydrate in order to introduce reactive functionalities for coupling. Among them, reductive amination is one of the most straightforward strategies for glyconjugation (Scheme 2). In fact, the haemiacetal form of the reducing end is in equilibrium with the aldehyde form, when in solution; this equilibrium makes available carbonyl groups for the condensation with primary amines, affording Schiff's base that can be reduced to chemically stable secondary amines. This approach results in a direct coupling of carbohydrate toward several substrates in aqueous conditions in a single step avoiding any multi-step carbohydrate modification. Furthermore, this coupling strategy ensures a chemoselective exposure of glycosyl epitopes [32]. If the carbohydrate contains at least two monosaccharides, the reducing end results "sacrified" as spacer, while the reimaining sugars maintain their cyclic forms, suitable for receptor recognition. Thus, reductive amination of PCL-NH_2 with maltose affords PCL surface exposing to cell receptors α-glucosides (PCL-Glc).

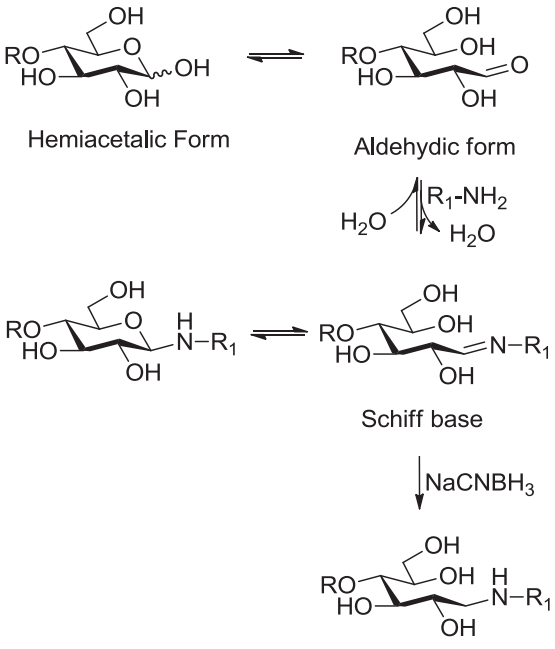

Scheme 2. Reductive amination of a reducing saccharide (R = α-glucose in case of maltose).

3.2. PCL-surface investigation

XPS measurements were carried out at C1s, O1s and N1s core level signals on PCL, aminated PCL (namely PCL-NH_2) and functionalised PCL with maltose (namely PCL-Glc) scaffolds with the aim to assess the chemical composition of the samples surface and to confirm the structure expected at the three functionalization steps (all Binding Energy (B. E.), Full Width Half Maxima (FWHM), experimental atomic ratio values and assignments are reported in Table S1 in the Supporting Information; for completeness of information, C1s and N1s XPS spectra, that will not be discussed in detail here, are reported in the supporting information as Fig. S1 and Fig. S2 respectively). The most significant signal probing the functionalization effectiveness is the O1s and specifically the peak contributions, identified by curve fitting, associated with C═O and C—OH functional groups. Therefore the O1s XPS data of PCL, PCL-NH_2, and PCL-Glc will be discussed here in detail and are reported in Fig. 1. All spectra show a complex structure and the contributions arising from the chemically different O atoms were individuated by applying a peak-fitting procedure. The spectra of all the samples show the presence of three Gaussian components attributed to the carbonyl bond (O═C B. E. = 531.04), to carbon atoms bonded to the hydroxyl groups and single-bonded to oxygen in PCL (O—C B.E. = 532.69) [33], and to physisorbed water (B. E. = 534.30) [34], in excellent agreement with the expected chemical structure of the samples.

The two main components in pristine PCL O1s spectrum reported in Fig. 1a, attributed to O═C and O—C, have very close intensities, as expected (experimental atomic ratio O═C/O—C = 0.9/1; theoretical atomic ratio O═C/O—C = 1/1; it is noteworthy that the statistic error in semiquantitative XPS analysis is of about 5% of the estimated value [35]).

As reported in Fig. 1b, the PCL-NH_2 sample shows an increase of the intensity of the signal attributed to the C═O group in respect to the PCL ((Fig. 1a), because of the formation of the amide group after the functionalization with 1,6-hexanediamine (experimental atomic ratio O═C/O—C = 1.5/1). What is more, in PCL-NH_2 sample a strong N1s signal appears (see Fig. S2 in the Supporting

Information) at about 399.5 eV BE, as expected for both amide and amine functional groups, confirming the effectiveness of PCL surface activation with diamines.

Remarkably, the PCL-Glc sample O1s spectrum (Fig. 1c) shows the increase of the intensity of the component attributed to the C—O groups due to the C—OH contribution, as a consequence of the maltose insertion on the sample surface (experimental atomic ratio O═C/O—C = 0.5/1).

NEXAFS O k-edge spectra of PCL, PCL-NH_2 and PCL-Glc samples recorded at the grazing incidence angle (54.7° of incidence of the x-ray radiation on the sample surface, ensuring no dichroic contributions arising by sample spatial orientation) are reported in Fig. 2.

Congruently with XPS data analysis, O K-edge NEXAFS spectra show resonances indicative for carbonyl bonds (O═C π* Photon Energy ≅ 532 eV) and carbon atoms bonded with the hydroxyl groups and single bonded C—O (O—C π* Photon Energy ≅536 eV; O—C σ* Photon Energy ≅ 534 eV; HO—C σ* Photon Energy ≅ 539 eV; 542 eV [36]), in agreement with the expected chemical structure. By comparing the reported spectra, it is noteworthy the increase of the intensity of the component attributed to the amide group of the PCL-NH_2 sample in respect to the same feature in pristine PCL, as well as the increase of the signal attributed to the O—H σ* after the functionalization with maltose.

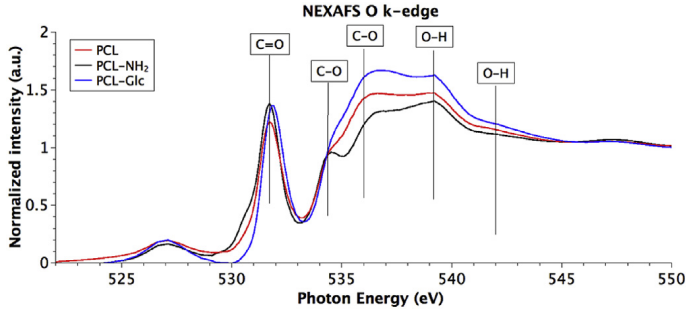

Fig. 2. O k-edge NEXAFS spectra collected on PCL, PCL-NH_2 and PCL-Glc recorded at grazing incidence.

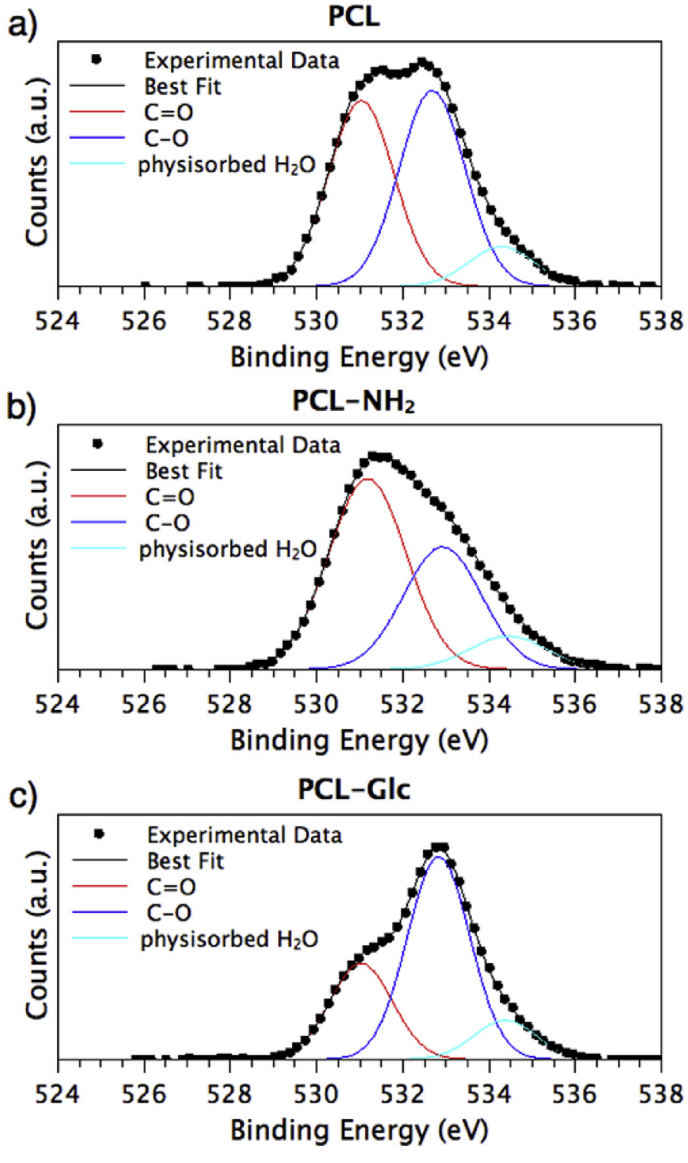

Fig. 1. O1s XPS spectra collected on PCL (a), PCL-NH_2 (b) and PCL-Glc (c); Spectral components are also reported as colored curves.

3.3. Biological studies

PCL is an interesting material for nervous tissue regeneration *in vitro* [37] or as biomaterial for synthetic nerve conduits [38]. For this reason we assayed material biocompatibility with F11 cell line, obtained by the fusion of mouse neuroblastoma with rat dorsal root ganglions. We compared the behaviour of neuroblastoma F11 cells plated on the different PCL samples with cells seeded on Petri dishes as control. PCL significantly reduced cellular growth of about 40% compared to the dish (0.62 ± 0.08 fold *versus* 1.03 ± 0.06 fold, p = 0.0008), whereas both PCL-NH_2 and PCL-Glu significantly increased proliferation (1.27 ± 0.09 fold, p = 0.035, and 1.30 ± 0.08 fold, p = 0.016, respectively) (Fig. 3). These results suggest that —NH_2 increased the biocompatibility of the material (probably through the increase of hydrophilicity), favouring cellular replication, and that glycosylation improved the significance (lower p-value) of the difference in proliferation between PCL and PCL-NH_2.

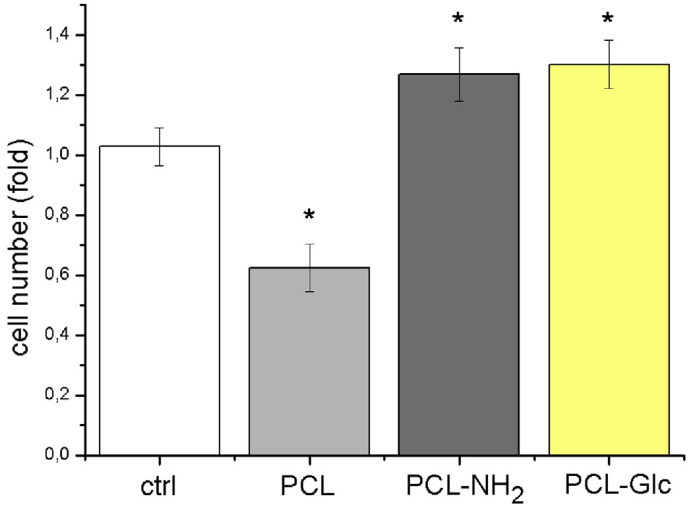

Fig. 3. F11 cell proliferation on Petri dishes (ctrl), on ε-Polycaprolactone (PCL), on ε-Polycaprolactone-linker (PCL-NH_2), and on functionalised PCL (PCL-Glc). Proliferation analysis was performed 7 days after cell deposition on the materials. Significantly lower values were observed for PCL (p = 0.0008) *versus* Petri dish. On the contrary, values were significantly increased for PCL-NH_2 (p = 0.035) and for PCL-Glc (p = 0.016).

4. Conclusions

We presented the functionalization of PCL with saccharides through a straightforward two-step procedure. Physico-chemical characterization carried out with surface sensitive techniques evidenced the successfulness of biomaterial functionalization and the chemical integrity of the bioactive moiety. Moreover, biological tests showed that PCL functionalised with maltose results in a slight improvement of cell proliferation, thus demonstrating that carbohydrate may positively influence biocompatibility of PCL surfaces.

Appendix A. Supplementary data

Supplementary data related to this article can be found at https://doi.org/10.1016/j.molstruc.2018.01.051.

References

[1] M. Tang, M. Purcell, J.A.M. Steele, K.-Y. Lee, S. McCullen, K.M. Shakesheff, A. Bismarck, M.M. Stevens, A.M. Howdle, C.K. Williams, Porous copolymers of ε-caprolactone as scaffolds for tissue engineering, Macromolecules 46 (2013) 8136–8143.

[2] S.J. Hollister, Porous scaffold design for tissue engineering, Nat. Mater. 4 (7) (2005) 518–524.

[3] R. Chandra, R. Rustgi, Recent advances in the synthesis, degradation and stabilization of poly (phenylene oxides), Prog. Polym. Sci. 23 (1998) 1273–1335.

[4] J. Pena, T. Corrales, I. Izquierdo-Barba, A.L. Doadrio, M. Vallet-Regi, Long term degradation of poly (ε-caprolactone) films in biologically related fluids, Polym. Degrad. Stab. 91 (2006) 1424–1432.

[5] A. Lancuski, F. Bossard, S. Fort, Carbohydrate-decorated PCL fibers for specific protein adhesion, Biomacromolecules 14 (6) (2013) 1877–1884.

[6] J. Xie, P.L. Michael, S. Zhong, B. Ma, M.R. MacEwan, C.T.J. Lim, Mussel inspired protein-mediated surface modification to electrospun fibers and their potential biomedical applications, Biomed. Mater. Res. 100A (2012) 929–938.

[7] A.S. Chung, H.S. Hwang, D. Das, P. Zuk, D.R. McAllister, B.M.J. Wu, Lamellar stack formation and degradative behaviors of hydrolytically degraded poly (ε-caprolactone) and poly (glycolide-ε-caprolactone) blended fibers, Biomed. Mater. Res. Part B. 100B (2012) 274–284.

[8] W. Yuan, C. Li, C. Zhao, C. Sui, W.-T. Yang, F.-J. Xu, M. Jie, Facilitation of gene transfection and cell adhesion by gelatin-functionalized PCL film surfaces, Adv. Funct. Mater. 22 (2012) 1835–1842.

[9] D. Mondal, M. Griffith, S.S. Venkatraman, Polycaprolactone-based biomaterials for tissue engineering and drug delivery: current scenario and challenges, Int. J. Polym. Mater. Polym. Biomater. 65 (2016) 255–265.

[10] A. Kurella, N.B. Dahotre, Surface modification for bioimplants: the role of laser surface engineering, J. Biomater. Appl. 20 (2005) 5–50.

[11] F. Taraballi, S. Zanini, C. Lupo, S. Panseri, C. Cunha, C. Riccardi, M. Marcacci, M. Campione, L. Cipolla, Amino and carboxyl plasma functionalization of collagen films for tissue engineering applications, J. Colloid Interface Sci. 394 (2013) 590–597.

[12] M. Abedalwafa, F. Wang, L. Wang, C. Li, Biodegradable poly-epsilon-caprolactone (PCL) for tissue engineering applications: a review, Rev. Adv. Mater. Sci. 34 (2) (2013) 123–140.

[13] M.P. Prabhakaran, J. Venugopal, C.K. Chan, S. Ramakrishna, Surface modified electrospun nanofibrous scaffolds for nerve tissue engineering, Nanotechnology 19 (45) (2008) 455102.

[14] F. Chen, C.N. Lee, S.H. Teoh, Nanofibrous modification on ultra-thin poly (e-caprolactone) membrane via electrospinning, Mater. Sci. Eng. C (2007) 325–332. C 27.2.

[15] R. Donzelli, F. Maiuri, G.A. Piscopo, M. De Notaris, A. Colella, E. Divitiis, Role of extracellular matrix components in facial nerve regeneration: an experimental study, Neurol. Res. 28 (8) (2006) 794–801.

[16] F. Causa, E. Battista, R. Della Moglie, D. Guarnieri, M. Iannone, P.A. Netti, Surface investigation on biomimetic materials to control cell adhesion: the case of RGD conjugation on PCL, Langmuir 26 (12) (2010) 9875–9884.

[17] M. Gabriel, G.P. van Nieuw Amerongen, V.W. van Hinsbergh, A.V. van Nieuw Amerongen, A. Zentner, Direct grafting of RGD-motif-containing peptide on the surface of polycaprolactone films, J. Biomater. Sci. Polym. Ed. 17 (5) (2006) 567–577.

[18] H.S. Yoo, T.G. Kim, T.G. Park, Surface-functionalized electrospun nanofibers for tissue engineering and drug delivery, Adv. Drug Deliv. Rev. 61 (12) (2009) 1033–1042.

[19] E.S. Place, N.D. Evans, M.M. Stevens, Complexity in biomaterials for tissue engineering, Nature Mater. 8 (2009) 457–470.

[20] L. Russo, T. Russo, C. Battocchio, F. Taraballi, A. Gloria, U. D'Amora, R. De Santis, G. Polzonetti, F. Nicotra, L. Ambrosio, L. Cipolla, Galactose grafting on poly (ε-caprolactone) substrates for tissue engineering: a preliminary study, Carbohydr. Res. 405 (2015) 39–46.

[21] L. Russo, C. Battocchio, V. Secchi, E. Magnano, S. Nappini, F. Taraballi, L. Gabrielli, F. Comelli, A. Papagni, B. Costa, G. Polzonetti, F. Nicotra, A. Natalello, S.M. Doglia, L. Cipolla, Thiol–ene mediated neoglycosylation of collagen patches: a preliminary study, Langmuir 30 (5) (2014) 1336–1342.

[22] L. Russo, A. Sgambato, M. Lecchi, V. Pastori, M. Raspanti, A. Natalello, S.M. Doglia, F. Nicotra, L. Cipolla, Neoglucosylated collagen matrices drive neuronal cells to differentiate, ACS Chem. Neurosci. 5 (4) (2014) 261.

[23] A. Sgambato, L. Russo, M. Montesi, S. Panseri, M. Marcacci, E. Carava, M. Raspanti, L. Cipolla, Different sialoside epitopes on collagen film surfaces direct mesenchymal stem cell fate, ACS App. Mater. Interfaces 8 (24) (2015) 14952–14957.

[24] G.Y. Wiederschain, Essentials of glycobiology, Biochemistry (Mosc.) 74 (9) (2009) 1056, 1056.

[25] L. Cipolla, B. La Ferla, C. Airoldi, C. Zona, A. Orsato, N. Shaikh, L. Russo, F. Nicotra, Carbohydrate mimetics and scaffolds: sweet spots in medicinal chemistry, Future Med. Chem. 2 (4) (2010) 587–599.

[26] L. Russo, L. Cipolla, Glycomics: new challenges and opportunities in regenerative medicine, Chem. Euro. J 22 (38) (2016) 13380–13388.

[27] D.A. Shirley, High-resolution X-ray photoemission spectrum of the valence bands of gold, Phy. Rev. B 5 (12) (1972) 4709–4714.

[28] P. Swift, D. Shuttleworth, M.P. Seah, in: D. Briggs, M.P. Seah (Eds.), Practical Surface Analysis by Auger and X-ray Photoelectron Spectroscopy, J. Wiley & Sons, Chichester, 1983 (chapter 5) and appendix 3.

[29] Z.G. Tang, R.A. Black, J.M. Curran, J.A. Hunt, N.P. Rhodes, D.F. Williams, Surface properties and biocompatibility of solvent-cast poly [ε-caprolactone] films, Biomaterials 25 (19) (2004) 4741–4748.

[30] F. Peri, L. Cipolla, B. La Ferla, F. Nicotra, Glycoconjugate and oligosaccharide mimetics by chemoselective ligation, C.R. Chim. 6 (7) (2003) 635–644.

[31] D. Bini, L. Russo, C. Battocchio, A. Natalello, G. Polzonetti, S.M. Doglia, F. Nicotra, L. Cipolla, Dendron synthesis and carbohydrate immobilization on a biomaterial surface by a double-click reaction, Org. Lett. 16 (5) (2014) 1298–1301.

[32] D.S. Dalpathado, H. Jiang, M.A. Kater, H. Desaire, Reductive amination of carbohydrates using NaBH (OAc) 3, Anal. Bioanal. Chem. 381 (6) (2005) 1130–1137.

[33] NIST X-ray Photoelectron Spectroscopy Database National Insititute of Standards and Technology, Gaithersburg, 2012. https://www.nist.gov/pml/x-ray-mass-attenuation-coefficients.

[34] S. Hiromoto, T. Hanawa, K. Asami, Composition of surface oxide film of titanium with culturing murine fibroblasts L929, Biomaterials 25 (2004) 979.

[35] J.E. Castle, in: D. Briggs, M.P. Seah (Eds.), Practical Surface Analysis by Auger and X-ray Photoelectron Spectroscopy, John Wiley and Sons Ltd, Chichester, 1984, p. 302, https://doi.org/10.1002/sia.740060611, 1983, 533 pp., Surf. Interface Anal. 6.

[36] V. Feyer, O. Plekan, R. Richter, M. Coreno, K.C. Prince, V. Carravetta, Photoemission and photoabsorption spectroscopy of glycyl-glycine in the gas phase, J. Phys. Chem. A 113 (40) (2009) 10726–10733.

[37] M. Barbarisi, G. Marino, E. Armenia, Q. Vincenzo, F. Rosso, M. Porcelli, A. Barbarisi, Use of polycaprolactone(PCL) as scaffolds for the regeneration of nerve tissue, J. Biomed. Mater. Res.A 103A (2015) 1755–1760.

[38] A.J. Reid, A.C. de Luca, A. Faronia, S. Downes, M. Sun, G. Terenghi, P.J. Kingham, Long term peripheral nerve regeneration using a novel PCL nerve conduit, Neurosci. Lett. 544 (2013) 125–130.

Chapter 8

Concluding Remarks

8. Concluding Remarks

The final objective of my thesis was to study different types of biomaterials for tissue engineering applications.

Broadly speaking, the bioactive material surface characteristics are strongly influenced by the method of surface preparation, handling and storage. During preparation of the implant, the outmost layers of the material are subjected to various chemical processes that will leave residues at the surface. The close connection between surface preparation and resulting characteristics implies that in order to manufacture implants with reproducible structured surfaces, all aspects of the production process and ensuing logistics need to be carefully controlled. Preparation of an ordered and homogeneous layer is mandatory in order to enhance biocompatibility and cells adhesion [[1]].

The physico-chemical characterization carried out with surface sensitive techniques as SR-XPS (Synchrotron Radiation induced X-Ray Photoelectron Spectroscopy) and NEXAFS (Near-Edge X-Ray Absorption Fine Structure) is important in order to evidence the successfulness of biomaterial functionalization and the chemical integrity of the bioactive moiety.

At first, I focused my attention to a model sample made by a metal surface grafted with SAP with a cysteine (Cys) introduced as a terminal residue. The Cys thiol functional group is able to covalently graft metal surfaces, inducing the formation of a stable and well-organized coverage on the metal substrate, preserving at the same time the ability of the SAP to self-assemble in antiparallel β-sheet structures. This study opens wide perspectives for efficient chemical modification of surfaces with biomolecules to include bioactive motifs and/or to add nanometric fibrous patterns and in the light of the interesting properties observed for the functionalized surface, the proposed functionalization scheme involving the Cys side chain and Au surface can be extended, with some modification, for different metals used as biomaterials.

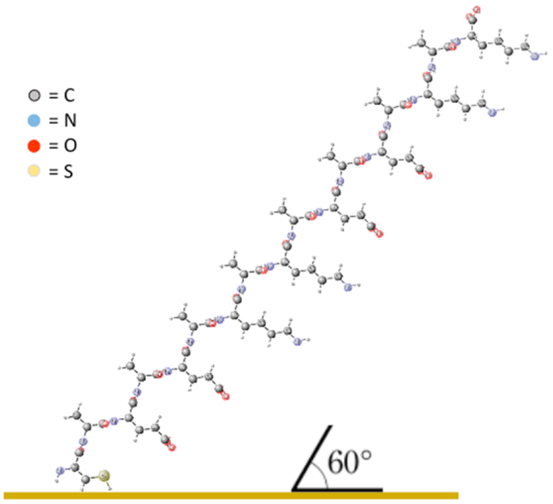

Figure 1.6.: Schematic Representation of the EAK-Cys Molecular Orientation on the Gold Surface as Deduced by AD-NEXAFS Measurements

In the second part of my PhD project, I focused my attention on the SAP immobilization on titania and Ti25Nb10Zr alloy surfaces as a function of pH and Ionic Strength of the mother solution with the aim of determining the best experimental conditions for the peptide adhesion on both substrates. Preparation of an ordered and homogeneous SAP layer is mandatory in order to enhance biocompatibility and osteoblasts adhesion; the experimental findings of this work revealed that the SAP molecular orientation can be considered constant in a rather wide pH range, while the SAP immobilization on the TiO_2 and Ti25Nb10Zr alloy surfaces is enhanced in acidic pH conditions. At all the investigated pH values, increase in the Ionic Strength of the peptide solution results in an increase of the peptide overlayer thickness.

The next step of the design of a biomaterial based on titanium starts with the considerations that infections are one of the most important reasons for implant's failure [2]. This is of utmost importance especially in patients with underlying compromised immunity or in those patients undergoing revision surgery, in which the relative risk of infection is multiplied [3]. As suggested in the literature by Gristina, a biomaterial surface needs to be modified in order to prevent bacterial adhesion and proliferation into surrounding tissues and promote osteointegration at the same time [4]. For this reason, in the last part of my PhD project I studied a complex biomaterial based on titanium and biofunctionalized with two different biomolecules: SAP and chitosan. Layer-by-layer structures of chitosan covalently functionalized with SAP,

were successfully anchored onto TiO_2 surfaces, by following a simple deposition procedure from solution that allowed for easily obtaining films with different peptides amount. For comparison, the same procedure was applied to the preparation of mixed chitosan and oligopeptide films on polycristalline gold surfaces. By comparing the complementary information provided by the surface-sensitive XPS, RAIRS and NEXAFS spectroscopic techniques, a coherent interpretation of the layer-by-layer structure organization attained by chitosan and SAP biomolecules on the TiO_2 surfaces was envisaged, with the chitosan oligomers covalently bonding the TiO_2 surface through a Ti-O-C bridge, a first layer of oligopeptides covalently bonded to the chitosan chains, i.e. leading to an epitaxial layer on the chitosan surface (already showing faible β-sheet secondary structures, as expected for this SAP peptide and proved by IRRAS), and then a last compact layer of physisorbed SAP molecules, strongly oriented as revealed by the dichroic effects in the angular dependent NEXAFS N K-edge spectra.

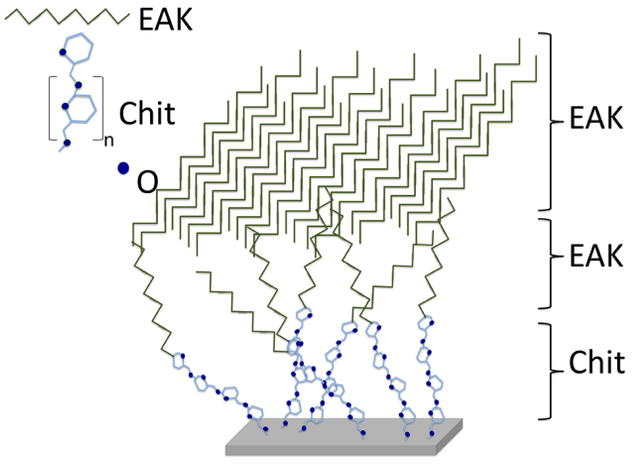

Figure 1.7.: schematic representation of the layer-by-layer arrangement hypothesized for Chit-EAK/EAK (b) film on TiO_2

This complex structure opens exciting perspectives for applications in the field of tissue engineering, for the developing of anti-biotic and bio-active innovative biomaterials.

In the last part of this thesis I focused my attention to a biomaterial conceived for regenerative medicine applications, a branch of translational research in tissue engineering and molecular biology which deals with the "process of replacing, engineering or regenerating human cells, tissues or organs to restore or establish normal function". A crucial point for the realization of this kind of bioactive materials is the chemical characterization, since the specific nature of a material's surface, both from a chemical and physical point of view, determines its biological properties such as cell adhesion and proliferation. In this context I presented the functionalization of PCL with saccharides through a straightforward two-step procedure. The physico-chemical characterization carried out with surface sensitive techniques evidenced the successfulness of biomaterial functionalization and the chemical integrity of the bioactive moiety.

In conclusion, this interdisciplinary research work was focused on the selection and evaluation of the most suitable biomaterial that is able to stimulate the response of the cells in order to restore damaged tissues. It is noteworthy that, as reported in the here presented papers, identifying and selecting the favourite biomaterial is a fundamental step in order to proceed from the biomedical research to the clinical application.

References

[1] Bakacova L., Filova E., Parizek M., Ruml, T., Svorcik V., Modulation of cell adhesion, proliferation and differentiation on materials designed for body implants, *Biotechnology Advances* (**2011)**; 29: 739–767.
DOI:10.1016/j.biotechadv. 2011.06.004.

[2] Romanò C. L., Scarponi S., Gallazzi E., Romanò D., Drago L., Antibacterial coating of implants in orthopaedics and trauma: a classification proposal in an evolving panorama, *Journal of Orthopedical Surgery and Research* (**2015);** 10: 157.
DOI 10.1186/s13018-015-0294-5.

[3] Engelsman A.F., Saldarriaga-Fernandez I.C., Nejadnik M.R., van Dam G.M., Francis K.P., Ploeg R.J., Busscher H.J., van der Mei H.C., The risk of biomaterial-associated infection after revision surgery due to an experimental primary implant infection. *Biofouling* (**2010**); 26: 761–7.
DOI:10.1080/08927014.2010.515027.

[4] Busscher H.J., van der Mei H.C., Subbiahdoss G., Jutte P.C., van den Dungen J.J., Zaat S.A., Schultz M.J., Grainger D.W., Biomaterial-associated infection: locating the finish line in the race for the surface, *Science Translational Medicine* (**2012**); 4: 153.
DOI:10.1126/scitranslmed.3004528.

List of publications

- ✓ V. Secchi, B. Bochicchio, A. Bracalello, A. Pepe, R. Mastrantonio, T. Persichini, G. Iucci, C. Battocchio, Chimeric Resilin/Elastin-like engineered polypeptide: structural characterization and biological properties, *in preparation*

- ✓ V. Secchi, S. Franchi, D. Ciccarelli, M. Dettin, A. Zamuner, G. Iucci, C. Battocchio, Biofunctionalization of TiO_2 Surfaces with Self-Assembling Layers of Oligopeptides Covalently Grafted to Chitosan, s*ubmitted*

- ✓ S. Franchi, V. Secchi, M. Santi, M. Dettin, A. Zamuner, C. Battocchio, G. Iucci, Biofunctionalization of TiO_2 surfaces with self-assembling oligopeptides in different pH and Ionic Strength conditions: Charge effects and molecular organization, *Material Science and Engineering: C,* 2018, 90: 651-656
  DOI: 10.1016/j.msec.2018.05.006

- ✓ V. Secchi, S. Franchi, M. Santi, M. Dettin, A. Zamuner, G. Iucci, and C. Battocchio, Self-Assembling Behavior of Cysteine-Modified Oligopeptides: an XPS and NEXAFS Study*, Journal of Physical. Chemistry C*, 2018, 122; 11: 6236-6239
  DOI: 10.1021/acs.jpcc.8b00794

- ✓ V. Secchi, S. Franchi, M. Santi, A. Vladescu, M. Braic, T. Skála, J. Lavkova, M. Dettin, A. Zamuner, G. Iucci, C. Battocchio, Biocompatible Materials Based on Self-Assembling Peptides on Ti25Nb10Zr Alloy: Molecular Structure and Organization Investigated by Synchrotron Radiation Induced Techniques*, Nanomaterials*, 2018, *8*(3), 148;
  DOI:10.3390/nano8030148

- ✓ V. Secchi, R. Guizzardi, L. Russo, V. Pastori, M. Lecchi, S. Franchi, G. Iucci, C. Battocchio, L. Cipolla, Maltose conjugation to PCL: Advanced Structural Characterization and preliminary Biological Properties*, Journal of Molecular Structure*, 2018, 1159 C: 74-78
  DOI:10.1016/j.molstruc.2018.01.051

- ✓ V. Secchi, S. Franchi, B. Bochicchio, A. Pepe, M. Fioramonti, G. Polzonetti, C. Battocchio, Nanofibers of Human Tropoelastin-inspired Peptides: Structural Characterization and Biological Properties; *Material Science and Engineering C,* 2017, 1;77: 927-934
  DOI: 10.1016/j.msec.2017.04.019

- ✓ L. Russo, C. Battocchio, V.Secchi, E. Magnano, Thiol−ene Mediated Neoglycosylation of Collagen Patches: A Preliminary Study*, Langmuir*, 2014, 30:1336−1342;
  DOI: 10.1021/la404310p

ACKNOWLEDGMENTS

Firstly, I would like to express my sincere gratitude to my supervisor Prof. Chiara Battocchio, for encouraging my research and for allowing me to grow as a scientist. Thank for giving me the opportunity to take this challenge, to travel, get in touch and being fascinated with worlds different from mine. I could not have imagined having a better Mentor during this incredible experience. Thank you!

Thank to professor Giovanna Iucci, for the precious support and help.

Thank to Stefano for sharing with me much of my PhD work…and food: the lubjanska in Basovizza, the awful breakfast and the "romantic dinner" in Prague, the lunch by the sea in Salonicco!

Thank to all the people of LaChim who make it such a funny place to work and live: nano-Chiaretta :D , Carlini, Francesco, Marta, Davide, Dr. Iole Venditti, Dr. Guido Infante and of course to all of "my" adopted students!

Thank to professor Tiziana Persichini, Roberta and Veronica for the hospitality in lab 3.8!

Thank to all my friends: my person Mary, my life-long friends from Nuoro (and Orani), Franci & Ancelle, my PhD-mate Vale, Giulia, Marti, Flavio, Marcolino, Biky and many others..!

Special mention to my Family-in-Rome: Chiara, Domi and Sara!

Lastly and mostly, thank to Mum, Dad, Bobby and my Extended-Family for their constant love, support and encouragement!